การพัฒนาฟิล์มกรองแสงจากพอลิเมอร์ที่เกิดรอยจากการเหนี่ยวนำด้วยนิวตรอน

นางสาว เสาวนีย์ อัศวผาติบุญ

วิทยานิพนธ์นี้เป็นส่วนหนึ่งของการศึกษาตามหลักสูตรปริญญาวิศวกรรมศาสตรดุษฎีบัณฑิต
สาขาวิชาวิศวกรรมนิวเคลียร์   ภาควิชานิวเคลียร์เทคโนโลยี
คณะวิศวกรรมศาสตร์ จุฬาลงกรณ์มหาวิทยาลัย
ปีการศึกษา 2553

DEVELOPMENT OF LIGHT FILTER FILM FROM NEUTRON INDUCED

TRACK- ETCH POLYMER

Miss Sawwanee Asavaphatiboon

A Dissertation Submitted in Partial Fulfillment of the Requirements

for the Degree of Doctor of Engineering Program in Nuclear Engineering

Department of Nuclear Technology

Faculty of Engineering

Chulalongkorn University

Academic Year 2010

Thesis Title	DEVELOPMENT OF LIGHT FILTER FILM FROM NEUTRON INDUCED TRACK- ETCH POLYMER
By	Miss Sawwanee Asavaphatiboon
Field of Study	Nuclear Engineering
Thesis Advisor	Associate Professor Nares Chankow, M.Eng.
Thesis Co-advisor	Assistant Professor Doonyapong Wongsawaeng, Ph.D.

Accepted by the Faculty of Engineering, Chulalongkorn University in Partial Fulfillment of the Requirements for the Doctoral Degree

.... Dean of the Faculty of Engineering
(Associate Professor Boonsom Lerdhirunwong, Dr. Ing.)

THESIS COMMITTEE

.... Chairman
(Associate Professor Supitcha Chanyotha, Ph.D.)

.... Thesis Advisor
(Associate Professor Nares Chankow, M.Eng.)

.... Thesis Co-advisor
(Assistant Professor Doonyapong Wongsawaeng, Ph.D.)

.... Examiner
(Associate Professor Sunchai Nilsuwankosit, Ph.D)

.... Examiner
(Phongphaeth Pengvanich, Ph.D.)

.... External Examiner
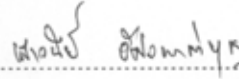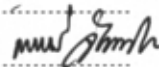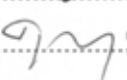(Associate Professor Tripob Bhongsuwan, Ph.D.)

เสาวนีย์ อัศวผาติบุญ : การพัฒนาฟิล์มกรองแสงจากพอลิเมอร์ที่เกิดรอยจากการ เหนี่ยวนำด้วยนิวตรอน. (DEVELOPMENT OF LIGHT FILTER FILM FROM NEUTRON INDUCED TRACK-ETCH POLYMER) อ. ที่ปรึกษาวิทยานิพนธ์หลัก: รศ. นเรศร์ จันทน์ขาว, อ. ที่ปรึกษาวิทยานิพนธ์ร่วม : ผศ.ดร. ดุลยพงศ์ วงศ์แสวง, 108 หน้า.

งานวิจัยนี้เป็นการพัฒนาฟิล์มกรองแสงจากพอลิเมอร์ที่เกิดรอยจากการเหนี่ยวนำด้วย นิวตรอน การทดลองได้นำแผ่นพลาสติกพอลิคาร์บอเนตที่ใช้ในอุตสาหกรรมแผ่นกันสาด มาอาบ นิวตรอนที่ได้จากต้นกัมมันตรังสีแคลิฟอร์เนียม-252 (^{252}Cf) นิวตรอนทำอันตรกิริยากับอะตอมของ ไฮโดรเจนที่เป็นโครงสร้างโมเลกุลของพอลิเมอร์ ทำให้เกิดรอยแฝงของโปรตอน ซึ่งสามารถทำให้เห็น รอยโปรตอนเหล่านี้ได้ โดยการนำมาล้างกัดรอยด้วยสารละลายที่เป็นด่าง ในการวิจัยนี้ใช้สารลาย PEW ซึ่งมีส่วนผสมของโพแทสเซียมไฮดรอกไซด์ ร้อยละ 15 เอทานอล ร้อยละ 40 และน้ำร้อยละ 45 จากนั้นนำพอลิเมอร์ที่มีรอยโปรตอนมาวิเคราะห์หาค่าความหนาแน่นของรอยและขนาดของ เส้นผ่าศูนย์กลางของรอย จากนั้นทดสอบคุณสมบัติการผ่านของแสงสามย่าน คือ แสงอุลตราไวโอ เลต แสงที่มองเห็นด้วยตา และแสงอินฟราเรด ด้วยเครื่องวัด SD2400 เพื่อศึกษาคุณสมบัติการ กรองและการกระจายแสง นอกจากนั้นยังได้ทำการศึกษาการเปลี่ยนแปลงการกระจายตัวของขนาด เส้นผ่าศูนย์กลางของรอยโปรตอน โดยทำการเปลี่ยนแปลงอุณหภูมิและเวลาที่ใช้ในการล้างกัดรอย

ผลจากการพัฒนาฟิล์มกรองแสงจากพอลิเมอร์ที่เกิดรอยจากการเหนี่ยวนำด้วยนิวตรอน เทียบกับแผ่นพลาสติกพอลิคาร์บอเนตปกติ พบว่า ประสิทธิภาพการกรองแสงที่มองเห็นได้ มีค่า เพิ่มขึ้นร้อยละ 5-15 และประสิทธิภาพการกรองแสงอินฟราเรด มีค่าเพิ่มขึ้นร้อยละ 1-12 สำหรับ แผ่นพลาสติกพอลิคาร์บอเนตที่มีความหนาแน่นของรอยโปรตอนในช่วง 3.04 x10^5– 1.11 x10^6 รอยต่อตารางเซนติเมตร สำหรับประสิทธิภาพในการกรองแสงอุลตราไวโอเลต พบว่าสามารถกรอง ได้ร้อยละ 100 เนื่องจากคุณสมบัติของแผ่นพลาสติกพอลิคาร์บอเนตเอง และจากการศึกษา คุณสมบัติการแพร่กระจายของลำแสงอินฟราเรดจากเลเซอร์พอยน์เตอร์ พบว่า การแพร่กระจายของ แสงอินฟราเรดเพิ่มขึ้น 1 - 3 เท่า

จากการศึกษา สรุปได้ว่าแผ่นพอลิคาร์บอเนตที่มีรอยอนุภาคโปรตอนเหมาะที่จะนำไปใช้ เป็นตัวแพร่กระจายแสง

ภาควิชา	นิวเคลียร์เทคโนโลยี	ลายมือชื่อนิสิต
สาขาวิชา	วิศวกรรมนิวเคลียร์	ลายมือชื่อ อ.ที่ปรึกษาวิทยานิพนธ์หลัก
ปีการศึกษา	2553	ลายมือชื่อ อ.ที่ปรึกษาวิทยานิพนธ์ร่วม

4971837621   : MAJOR NUCLEAR ENGINEERING

KEYWORDS : NUCLEAR TRACK ETCH / PROTON TRACK / POLYCARBONATE / Cf ^{252} / LIGHT TRANSMISSION / POLYMER

SAWWANEE ASAVAPHATIBOON: DEVELOPMENT OF LIGHT FILTER FILM FROM NEUTRON INDUCED TRACK-ETCH POLYMER. ADVISOR: ASSOC. PROF. NARES CHANKOW, CO-ADVISOR: ASST. PROF. DOONYAPONG WONGSAWAENG, Ph.D., 108 PP.

This research work aimed to develop the light filter film from neutron induced track-etch polymer. Locally-available polycarbonate plastic sheets for sunshade were irradiated with neutrons from radioisotope source, Californium-252 (^{252}Cf). Neutrons interacted with hydrogen atoms in polymer molecules and induced a latent of proton tracks in the polymer. The tracks can be made visible upon etching in a basic solution. This study used a PEW solution which composed of 15% KOH, 40% ethanol and 45% water. The polymer containing proton tracks was analyzed for track density and track diameter. Light transmission properties in three regions, i.e. ultraviolet, visible light and infrared, were tested using SD2400 apparatus in order to evaluate filtering and diffusing properties. Additionally, variations in etching temperature and etching time were studied in order to evaluate proton track diameter distribution.

Results showed that the filtering efficiency of track-etched polycarbonate film with track density of about $3.04 \times 10^{5} - 1.11 \times 10^{6}$ tracks/cm^{2} increased by 5 - 15 % in the visible light region and 1 - 12 % in the infrared region compared with normal polycarbonate sheet. Furthermore, the filtering efficiency in the ultraviolet region was 100% due to the inherent property of polycarbonate sheet. Finally, study of infrared light diffusion property using a laser pointer beam revealed 1 - 3 folds increase in infrared light diffusion.

It can be concluded that the proton track-etched polycarbonate plastic sheets were suitable to be used as a light diffuser.

Department : _____Nuclear Technology_____   Student's Signature _____Sawwanee Asavaphatiboon_____

Field of Study : ____Nuclear Engineering_____   Advisor's Signature _____Nares Chankow_____

Academic Year : _2010_____   Co-advisor's Signature _____

Acknowledgments

Contents

Page

Chapter

List of Tables

List of Figures

CHAPTER I

INTRODUCTION

1.1 Background on problems of interest

Nuclear tracks or ion tracks was first observed by D.A.Young in 1958 [1]. He found microscopic track formations in the surface of a lithium fluoride crystal that had been irradiated with fission fragments and etched in a mixture of hydrofluoric and acetic acids. One year later, Silk and Barnes observed with the electron microscope damaged regions in mica which marked the paths of heavy charged particles such as those from fission fragments or cosmic rays. Since 1962 particle tracks in solids have been the subject of intensive research. In 1975, Fleischer, Price and Walker published an extensive and definitive text on "Nuclear Tracks in Solids" [2].

The passage of heavily ionizing, nuclear particles through most insulating solids creates narrow paths of intense damage on an atomic scale. These damage tracks may be revealed and made visible in an ordinary optical microscope by treatment with a properly chosen chemical reagent that rapidly and preferentially attacks the damaged material. It less rapidly removes the surrounding undamaged matrix in such a manner as to enlarge the etched holes that mark and characterize the sites of the original, individual, damaged regions [3].

The applications of nuclear tracks have been developed and applied in a wide variety of technical fields such as nuclear fusion, cosmic rays, molecular identification with nanopores, imaging X-ray astronomy, magnetic studies with nanowires, polymeric nanowires, radon and neutron dosimetry, and thermochronology [4]. D. Nikezic and K.N. Yu mentioned in their paper "Analyses of light scattered from etched alpha-particle tracks in PADC" that there were only a few references in the literature on scattering of light from etched tracks in SSNTDs [5]. In most of the cases, scattered light was used to measure track densities from experiments related to neutron dosimetry by Harvey and Weeks, 1987; Popov and Pressyanov, 1997; Meyer et al., 1997 and Groetz et al., 1999. Groetz et al. (1998) developed a model for laser light scattering by nuclear tracks in CR-39 detectors. Nikezic et al., 2005; Yu et al., 2007 studied the optical characteristics of etched tracks in PADC films using the *ray tracing method* were performed (Nikezic et

al., 2005; Yu et al., 2007). Based on geometrical optics, a computer program called TRACK_VISION 1.0 (Nikezic and Yu, 2008) was used.

In this research, the light filter from neutron induced track-etched polymer was developed. The aim of this study was to create proton tracks in thin sheet of polymer to be used as light filter or light diffuser. This is based on light scattering by nuclear tracks which are dependent mainly upon track density and track size. The track density is directly proportional to number of neutrons falling on the plastic sheet while the track size is dependent upon type and energy of charged particles as well as the etching condition.

1.2 Thesis objectives

The objectives of the dissertation are:

1.2.1   To prepare track-etch polymer films by neutron irradiation.

1.2.2   To investigate properties of track-etch polymer films on transmission and scattering of visible light, ultraviolet (UV) and infrared (IR).

1.2.3   To investigate experimentally and theoretically the effects of track density and sizes on transmission and scattering of visible light, ultraviolet (UV) and infrared (IR).

1.2.4 To develop a track-etch polymer film preparation method for industrial production.

1.3 Scope of work

1.3.1   Track formation process on films uses neutrons from radioisotope source via $^1H(n,n)^1H$ and $^1H(n,n')^1H$ reactions.

1.3.2   Investigate properties of track-etch polymer films on transmission of visible light, ultraviolet (UV) and infrared (IR).

1.3.3   Investigate experimentally and theoretically the effects of track density and sizes on transmission of visible light, ultraviolet (UV) and infrared (IR).

      1.3.4 Design and develop a track-etch polymer film preparation method for industrial production.

1.4 Expected benefit

      The developed track-etch polymer film from neutron irradiation can be used as UV, visible light and Infrared filter or diffuser.

1.5 Research Methodology

      1.5.1   Select the polymer film materials such as Polystyrene, Polycarbonate, or Polyethylene etc.

      1.5.2   Design and conduct experiment to produce proton tracks on polymer of different track densities at different etching conditions

      1.5.3   Investigate properties of track-etch polymer films on transmission and scattering of visible light, ultraviolet (UV) and infrared (IR)

      1.5.4   Test physical properties of track-etch polymer film

      1.5.5   Research conclusion and discussion

1.6 Organization and chapter contents

      This dissertation consists of five chapters. The chapters are organized principally to focus on the development of light filter or diffuser using proton track etch polymer by neutron induction from radioisotope source.

      Chapter 1 deals with background and problem of interest, objective, scope, expected benefits and research methodology of the study.

      Chapter 2 mentions the principles and applications of track etched detector, neutron interaction, theory of light, the review literature including previous work.

      Chapter 3 describes the design and construction of the equipment. Parameters that might affect density, size distribution and shape of track and the measurement of light transmission have been evaluated.

      Chapter 4 describes the experimental result of the relationship of the track density and track size distribution to temperature of etchant, transmission of light in three ranges: Ultraviolet, Visible light and Infrared.

Finally in Chapter 5, the overall findings of the studies are concluded and discussed.

CHAPTER II

THEORY AND LITERATURE REVIEW

This chapter describes the theoretical and application aspects of track etched detector, neutron interaction, theory of light as well as literature review.

2.1 Principles of Track etched detector

2.1.1 Mechanism of Track formation

A complete satisfactory model of track registration and formation mechanisms does not yet exist. There are many models to explain the process of track formation. The "**Ion Explosion spike model**" [3] is so for the most reasonable theory (Figure 2.1). According to this model a positively charged energetic particle passing through a medium knocks out the orbital electrons of atoms lying in and around the vicinity of its passage. The dominant process is the ionization of K or L shell electrons. Due to this knock out of electrons a cylindrical region full of positive ions (holes) is produced. Due to Coulomb repulsion between positive charged ions some of them are ejected into the interstitial positions leaving behind a vacancy rich and a few microns long (40-80 A°) cylindrical core. In view of this model track formation mechanism depends upon a variety of parameters, such as mass, ionization state and velocity of the incident ion and ionization potential of the absorbing material. In the case of electrical conductors and good semi-conductors the electrons around this region neutralize the cylindrical region of positive holes so that such media are not able to register the passage of incoming ions. While in crystalline solids these positive ions thereupon repel one another violently, thus disturbing and distorting the regular lattice in crystal produce a more or less cylindrical region (30 A°) under a high strain[6].
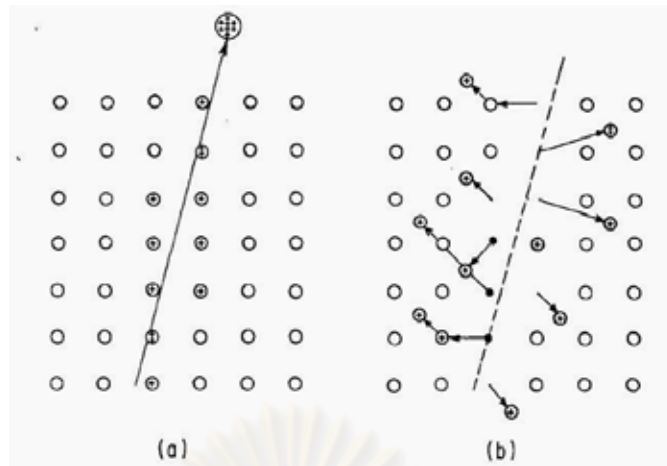
Figure 2.1 The ion explosion spike mechanism for track formation in inorganic solids. The original ionization left by passage of a charged particle (a) is unstable and ejects ions into the solid, creating vacancies and interstitials (b). [3]

The ion explosion spike model requires the following conditions for track formation.

a) The electrostatic stress must be greater than the bonding strength of the crystal. This shows the material of low mechanical strength or low dielectric constant is more likely to store etchable tracks.

b) There must be at least one ionization event per atomic place for the track formation to be automatically continuous.

c) The free electron density of the track storing material must not be greater than a permissible maximum value. This condition restricts track formation in good insulators alone and thus metals do not store tracks.

d) The hole mobility of material must not be high because this results into neutralization of the core atoms which in turn will prevent the formation of track. Thus semi-conductors like silicon and germanium having high hole mobility will not form tracks.

In organic polymers the traversing ion breaks the long molecular chains and produces relatively stable free radicals, small gas inclusion and other products of chemical radiation damage, by ionization and excitation of primary particles and δ-ray, shown as Figure 2.2. Broken chains ends & free radicals are produced in this region. The density of the absorbing material is reduced in this region, which has been directly

observed by low energy neutron scattering. These new region are latent damaged trails and can be seen at very high magnification (30,000x) under a transmission electron microscope [7].
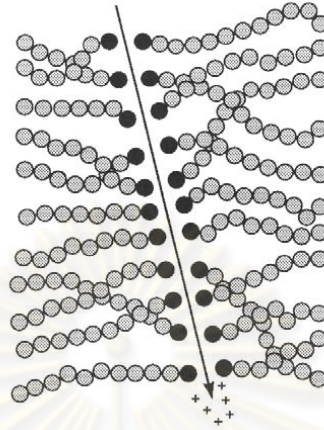
Figure 2.2 Schematic illustration of a chain scission in polymers caused by the passage of heavily charged particles. [8]

2.1.2 Restricted energy loss [1, 9]

The primary process of charged-particle interaction with the detector material is ionization and excitation of the molecules in the detector. The initial charged particle loses its energy through the many interaction processes. Theoretically, it interacts through Coulomb force with charged particles (electrons and nuclei) in the material. Of course, distal interactions may be neglected and we focus on the particle interactions with atoms and molecules that are close to its path. The majority of the interactions occur with electrons and only a small number of interactions are with nuclei. Since the initial heavy charged particle (only such particles can produce tracks) is much heavier than electrons, the direction of the particle effectively does not change and the path is almost completely a straight line. This may not be true if the particle interacts with a nucleus, where a significant deviation from the initial direction may occur. However, such interactions are relatively rare. Some deviations from the straight line can happen close to the end of the particle range, when the energy of a particle becomes very low.

The particle loses its energy in many small interaction processes, so the energy loss each time is usually very small when compared to its energy. For example, ionization of one molecule in air on average needs about 32 eV, which is 10^{-5} to 10^{-6} of the particle energy (assuming that the particle energy is in the MeV region). As a result of these many

small interaction processes, the particle will continuously slow down in the detector material. The physical quantity that describes the slowing down of charged particles in mater is the stopping power -dE/dx (or the stopping force used by some authors), where dE is the energy lost in the distance dx. Stopping power is given in J/m or in keV/mm. The energy lost by a particle in the distance dx is the energy transferred to the material so this quantity is also called the linear energy transfer (LET).

Stopping power is proportional to the square of the charge of the incoming particle, Z_1^2, and it is inversely proportional to its velocity; thus the stopping power increases as the particle velocity is decreased.

The classical formula that describes the specific energy loss is known as the Bethe-Bloch Formula, which is valid for all types of heavy charged particles with velocities that are large compared to orbital electron velocities.

The Bethe-Bloch formula has different forms for heavy and light particles:

- For heavy charged particles (α particles and protons):

$$-\frac{dE}{dx} = \frac{4\pi Z^2 e^4}{m_e \upsilon^2} NB$$

$$B = Z\left[\ln\frac{2m_e\upsilon^2}{I} - \ln\left(1 - \frac{\upsilon^2}{c^2}\right) - \frac{\upsilon^2}{c^2}\right] \tag{2.1}$$

where υ is velocity of the charged particle

Ze is charge of the charged particle

N is number density of the target

M_e is rest mass of the electron

I is experimentally evaluated average excitation and ionization potential

B is stopping number

- For light charged particles (electrons and positrons)

$$-\frac{dE}{dx} = \frac{2\pi e^4}{m_e \upsilon^2} NB$$

$$B = \left[\ln\frac{m_e\upsilon^2 E}{2I^2(1-\beta^2)} - (\ln 2)\left(\sqrt{1-\beta^2} - 1 + \beta^2\right) + 1 - \beta^2 + \frac{1}{8}\left(1 - \sqrt{1-\beta^2}\right)^2\right] \tag{2.2}$$

$\beta = \upsilon/c$

For the charged particles with $\upsilon \ll c$ (non-relativistic particles) only the first term in the stopping number (B) equation is necessary. Equations 2.1 and 2.2 show that B varies slowly with particle energy and is proportional to the atomic number (Z) of the absorber material. Thus the stopping power varies as $1/\upsilon^2$, or inversely with particle energy.

The Bethe-Bloch formula also shows that higher-Z materials have greater stopping powers. Table 2.1 demonstrated I values of various compounds.

Table 2.1 Mean ionization/ excitation potential I for various compounds [10]

Compound	I (eV)	Compound	I (eV)
Air (dry)	85.7	Lithium fluoride	94
Water (liquid)	75	Photographic emulsion	331
Water (vapor)	71.6	Sodium iodide	452
Muscle (skeletal)	75.3	Polystyrene	68.7
Bone (compact)	91.9	A-150 plastic	65.1

2.1.3 Range-Energy relationship [9]

The general expression for linear stopping power (linear energy loss) for a charged particle that is slowing down in a medium is the Bethe-Bloch formula. Since the energy loss is proportional to the square of the charge of the coming particle, an α particle is expected to stop much faster than a proton in a given medium.

Semi=empirical formulas express the range of charge particles as a function of kinetic energy.

For α particles, the range in air at a temperature of 15°C and 760 mm pressure is given by the equations

$$R_{air}\,(cm) = \begin{cases} 0.56\left(\dfrac{cm}{MeV}\right)E\,(MeV) & E \langle 4\,MeV \\ 1.24\left(\dfrac{cm}{MeV}\right)E\,(MeV) - 2.62\,(cm) & 4\,MeV \langle E \langle 8\,MeV \end{cases} \tag{2.3}$$

The range (expressed as density thickness) of an α particles in any other medium, R_m, is given by

$$R_m\,(cm) = \frac{0.00056\ A^{1/3}}{\rho_m}\,R_{air} \tag{2.4}$$

where A is the atomic mass number of the medium, R_{air} is the range of the α particles in air, and ρ_m is the density of the medium.

The proton range in air is defined as

$$R_{air}\left(m\right) = \left[\frac{E_p\left(MeV\right)}{9.3}\right]^{1.8} \quad for \quad E_p\left(few\ MeV - 200\ MeV\right) \tag{2.5}$$

The range of protons in aluminum is given by the semi-empirical formula

$$R_{Al}\left(\mu m\right) = \begin{cases} \dfrac{10.5E_p^2}{0.68 + 0.434\ \ln\left(E_p\right)} & 2.7\,MeV \leq E_p \leq 20\,MeV \\ 14.21E_p^{1.5874} & 1\,MeV \langle E_p \leq 2.7\,MeV \end{cases} \tag{2.6}$$

For example, estimate the range of proton 3 MeV in air

$$R_{air}\left(m\right) = \left[\frac{E_p\left(MeV\right)}{9.3}\right]^{1.8} = \left[\frac{3}{9.3}\right]^{1.8} = 0.130\ m$$

Nowadays, some computer software is available for the calculation of stopping power and range of charged particles in different media. The most well-known one is the *SRIM (Stopping and Range of Ions in Matter)* program developed by Ziegler et al.

A series of such measurements with different charged particles and different energies is used to define the registration properties of a substance (Fleischer et al., 1964a; 1967a). For example, Figure 2.3 gives theoretical curves of the relative damage caused by different ions as a function of their velocities. The figure indicates the wide variation response, which extends from cellulose nitrate, which will register low energy proton (Jones and Neidigh, 1967) to those of minerals so insensitive that they will not register argon even at its maximum ionization rate (Fleischer et al., 1966; 1967b) [3].
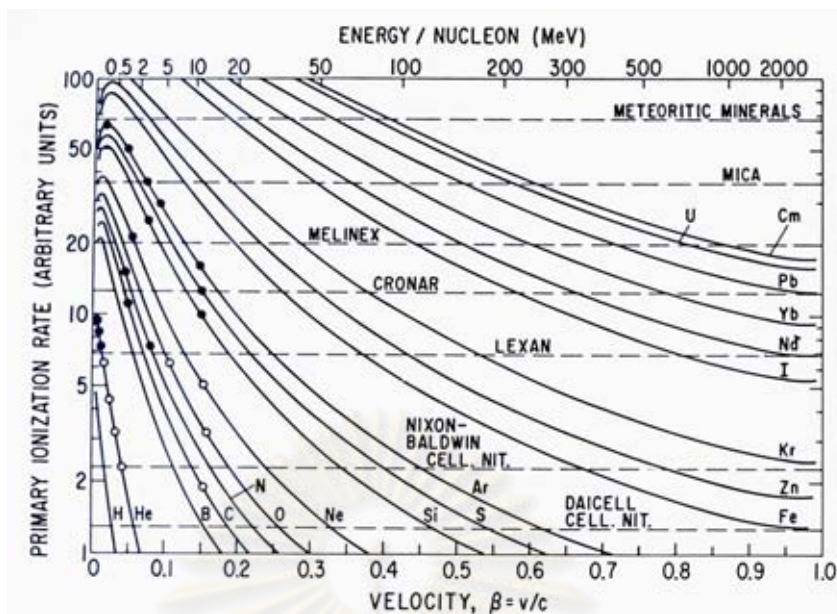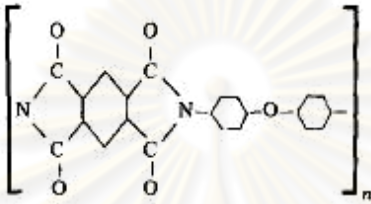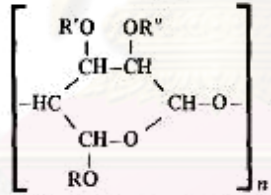
Figure 2.3 Damage vs. velocity for different charged particles. [3]

Each detector has a level below which no tracks are etched and one above which all particles create tracks. The experimental points for accelerator ions in Lexan polycarbonate are given as open circles for zero registration and as filled circles for 100% registration. Thresholds for other detectors are also indicated [3].

SSNTD materials can be ranked in order of sensitivity. Tables 2.2 and 2.3 are adapted from the compilation of Fleischer *et al.* [3]. They list a range of different materials and indicate for each the smallest ion that has been observed to form an etchable track, together with the energy of that ion. It is important to note that the data for polymers is often specific to a particular formulation and particles which form tracks in, say, one cellulose nitrate product may have no effect on a nominally similar polymer from a different manufacturer. In addition, registration behavior can be markedly influenced by etching conditions, for example, temperature, concentration, preconditioning by exposure to specific environments such as ultraviolet light and oxygen. Accordingly some overlap between closely ranked detector materials may occur when these experimental parameters are varied.

Table 2.2 Sensitivity order of track detector materials ranked in qualitative classes [2]

Organic SSNTDs (polymeric)

Material	Composition principal repeating unit(s)	Smallest ionizing ion detected (together with its energy where known)
Polyethylene	$[CH_2]_n$	
Polystyrene	$[CH_2\ CH.\ C_6\ H_5]_n$	Fragments from fission processes
Polyvinylchloride–vinylacetate co-polymer	$\left[\begin{array}{c}CH_2-C.H\\ \mid\\ Cl\end{array}\right]_n-\left[\begin{array}{c}CH_2\ CH\\ \mid\\ COOCH_3\end{array}\right]_m$	42 MeV ^{32}S
Polyvinylchloride–vinylidenechloride co-polymer	$\left[\begin{array}{c}CH_2-CH\\ \mid\\ Cl\end{array}\right]_n-\left[CH_2-C\ Cl_2\right]_m$	42 MeV ^{32}S
Polyethylene	$[OC-\bigcirc-COO(CH_2)_2O]_n$	
Polyimide		36 MeV ^{16}O
Polyoxymethylene	$[-CH_2O-]_n$	28 MeV ^{11}B
Polypropylene	$\left[\begin{array}{c}CH_2-CH\\ \mid\\ CH_3\end{array}\right]_n$	1 MeV ^{4}He
Polyvinylchloride	$\left[\begin{array}{c}CH_2-CH\\ \mid\\ Cl\end{array}\right]_n$	
Polymethylmethacrylate	$\left[\begin{array}{c}CH_2-C.CH_3\\ \mid\\ COOCH_3\end{array}\right]_n$	3 MeV ^{4}He
Cellulose esters	general structure	3 MeV ^{4}He
Cellulose acetate butyrate	where R = acetyl, R' = butyrate	
Cellulose triacetate	where R, R', R'' = acetyl	
Cellulose nitrate	where R = nitrate	0.55 MeV ^{1}H

Table 2.3 Inorganic SSNTDs (minerals, crystals, glasses) [2]

Material	Composition	Smallest ionizing ion detected and its energy
Diopside	$CaMg(SiO_3)_2$	170 MeV ^{54}Fe
Augite	$CaMg_3Fe_3Al_2Si_4O_{19}$	170 MeV ^{56}Fe
Hypersthene	$Mg_{1.5}Fe_{0.5}Si_2O_6$	100 MeV ^{56}Fe
Olivene	$MgFeSiO_4$	
Orthoclase	$KAlSi_3O_8$	100 MeV ^{40}Ar
Quartz	SiO_2	100 MeV ^{40}Ar
Soda-lime glass	$23SiO_2 : 5Na_2O : 5CaO : Al_2O_3$	20 MeV ^{20}Ne
Phosphate glass	$10P_2O_5 : 1.6BaO : Ag_2O : 2K_2O : 2Al_2O_3$	
Silica glass	SiO_2	16 MeV ^{40}Ar
Oligoclase	$Na_4CaAl_6Si_{14}O_{40}$	4 MeV ^{28}Si
Bytownite	$NaCa_6Al_9Si_{11}O_{40}$	4 MeV ^{28}Si
Phlogopite mica	$KMg_2Al_3Si_{10}O_{10}(OH)_2$	
Muscovite mica	$KAl_3Si_3O_{10}(OH)_2$	2 MeV ^{20}Ne
Labrodorite	$Na_2Ca_3Al_8Si_{12}O_{40}$	
Zircon	$ZrSiO_4$	
Bronzite	$Mg_{1.7}Fe_{0.3}Si_2O_6$	
Enstatite	$MgSiO_3$	
Flint glass	$18SiO_2 : 4PbO : 1.5Na_2O : K_2O$	2–4 MeV ^{20}Ne
Tektite glass (obsidian)	$22SiO_2 : 2Al_2O_3 : FeO$	

2.1.4 Categories of track-etched detector

Etchable tracks are formed in a variety of materials. All are electrical insulators, although some wide band gap semiconductors are also known to record tracks. The materials falls into two main categories: inorganic solids such as crystals and glasses, and organic solids, such as polymers. In the first category, the most popular materials are mica and flint glass, whereas polycarbonate and polyester films are the most common organic track-etch detectors. A list of the most useful materials is given in Table 2.4.

Table 2.4 The categories of track-etch detector [6]

Commonly Used track etch materials		
	Atomic Composition	Least Ionizing Ion Seen
Inorganic Materials		
Quartz	SiO_2	100 MeV ^{40}Ar
Phlogopite mica	$KMg_2Al_2Si_3O_{10}(OH)_2$	
Muscovite mica	$KAl_3Si_3O_{10}(OH)_2$	2 MeV ^{20}Ne
Silica glass	SiO_2	16 MeV ^{40}Ar
Flint glass	$18SiO_2:4PbO:1.5NaO_2:KO_2$	2-4 MeV ^{20}Ne
Organic Materials		
Polyethylene terephthalate (Cronar, Melinex)	$C_5H_4O_2$	36 MeV ^{16}O
Bisphenol A-polycarbonate (Lexan, Makrofol)	$C_{16}H_{14}O_3$	0.3 MeV ^4He
Polymethylmethacrylate (Plexiglass, Lucite, Perspex)	$C_5H_8O_2$	3 MeV ^4He
Cellulose triacetate (Cellit, Triafol-T.Kodacel TA-401 unplasticized)	$C_3H_4O_2$	
Cellulose nitrate (Daicell)	$C_6H_8O_9N_2$	0.55 MeV ^1H

Figure 2.4 demonstrated fission tracks from the same source ^{252}Cf in a variety of materials which can be viewed in a light microscope after chemical etching.
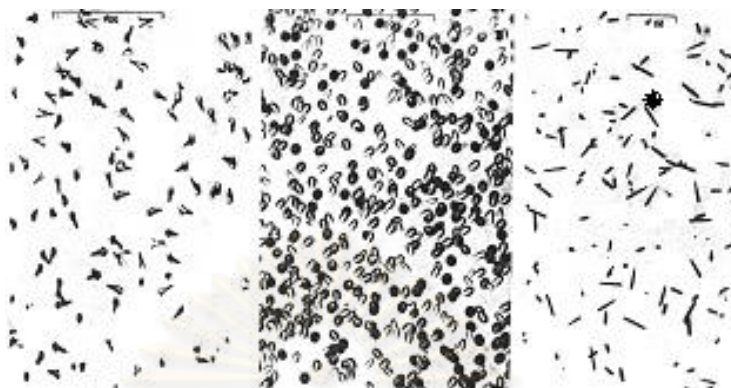
Figure 2.4 Drawings of etched fission tracks induced by the same source (^{252}Cf) in different materials: a) K feldspar; b) soda-lime glass; c) Lexan polycarbonate. [3]

2.2. Track etching

2.2.1. Track geometry [2]

The track can be made visible upon etching in a strong acid or base solution. The entire surface of the material is attacked, but those points at which particles tracks have entered are etched about 10 times faster. The tracks can thus be made to form pits on the surface that are large enough to be easily visible through an optic microscope.

The chemical action of the etch is characterized by the ratio V_T/V_G where V_T is the rate of dissolution along the track and V_G the bulk etch rate of the detector surface remote from any tracks (G ≡ general). In the simple instance of a particle penetrating a detector normal to its original surface as in Figure 2.4 and assuming that V_T is constant along the track and V_G is constant and isotropic, then V_T/V_G will be constant for short etching distances in isotropic non-crystalline solids. Both l and d are directly observable quantities from the competitive effects of V_G and V_T and become smaller as V_T approaches V_G and vice versa, i.e. both l and d decrease as V_T/V_G decreases. Hence, for the situation envisaged in Figure 2.5:

$$l = (V_T - V_G)t \qquad (2.2)$$

where t = etching time, and

$$d = 2V_G t \left[\frac{(V_T - V_G)}{(V_T + V_G)} \right]^{1/2} \tag{2.3}$$

It can be seen that when $V_T = V_G$, both l and d vanish, which is a required property of these equations. Also the cone angle, as defined in Figure 2.5 is given by Eq. 2.4:

$$\theta = \sin^{-1} \left(\frac{V_G}{V_T} \right) \tag{2.4}$$
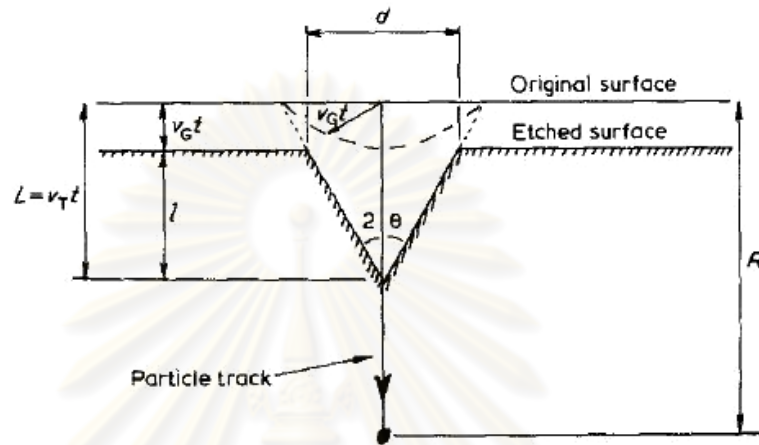
Figure 2.5 Track etching geometry with V_T and V_G constant for a vertically incident

particle. [3]

The geometry of the etched track becomes more complicated if V_T varies along the track length, and this more realistic situation has been treated by Fleischer *et al.* In general terms, an increasing V_T with depth will produce a cone of increasing sharpness, the surfaces being concave from without, while a decreasing V_T will give the opposite effect, although the cone point remains sharp until V_T has decreased virtually to the bulk etch velocity of V_G.

For the more general case of oblique particle incidence, the geometry is more complicated. If track inclined with the track obliquity angle, ϕ at less than the critical angle θ_c to a surface can be erased by the etching process. (Figure 2.6) Then the incidence angle must exceed a critical angle in order to avoid its disappearance due to the progressive etching of the normal surface.
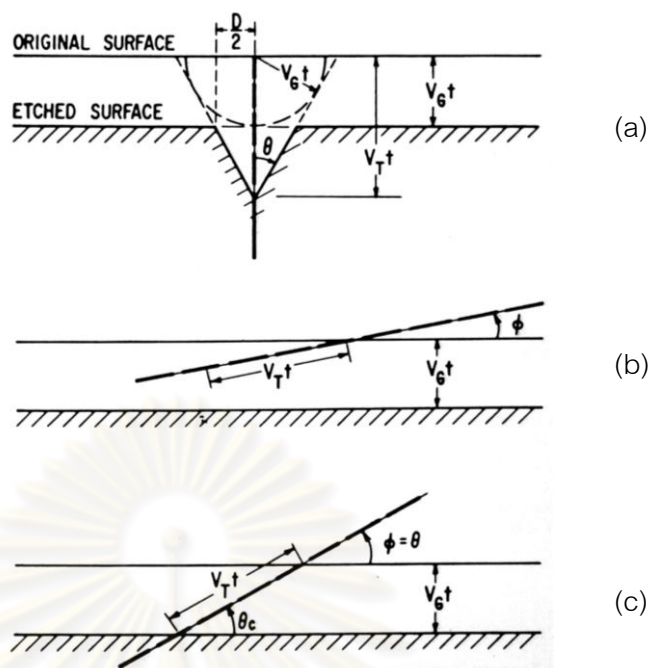
Figure 2.6 (a) Model of track etching in which the normal surface is removed at a velo-

city V_G and the damaged track at a velocity V_T, leading to a cone-shape pit.

(b) Tracks formed at an angle ϕ less than the critical angle θ_C are not revealed because the normal surface advances faster than the etch rate along the track.

(c) The case in which the particle enters at the critical angle θ_C. Tracks entering the surface at an angle greater than the critical angle will be visible after etching. [3]

2.2.2. Factors influencing etch rate

In principle, any chemical reagent will function as an etchant if it attacks a detector at an appropriate rate, and usually etching conditions are optimized empirically for each detector material. For minerals and glasses, many etchants are based on hydrofluoric acid and etchants for polymeric detectors are frequently solutions of alkali hydroxides.

The etch rate of nuclear track etch in certain SSNTD depends on the following;

a)   The nature, concentration, and temperature of the etchant used.

b)   The time of etching

c)   The environmental conditions existing before, during and after irradiation.

There have been many investigations to study the etching parameters for the more common polymeric detectors. These have elucidated the influence of composition of the etchants, its strength, its temperature and also degree of liquid agitation and various pre-etching treatments on the development of track pits. Figure 2.7 and 2.8 are examples of this extensive data. [2]
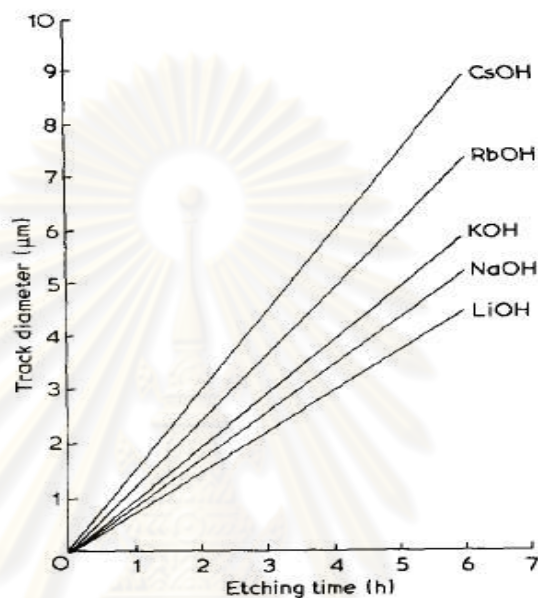
Figure 2.7 The effect of alkali hydroxide type on the track etching rate of a polycarbonate. 5N solution of 60°C. [2]
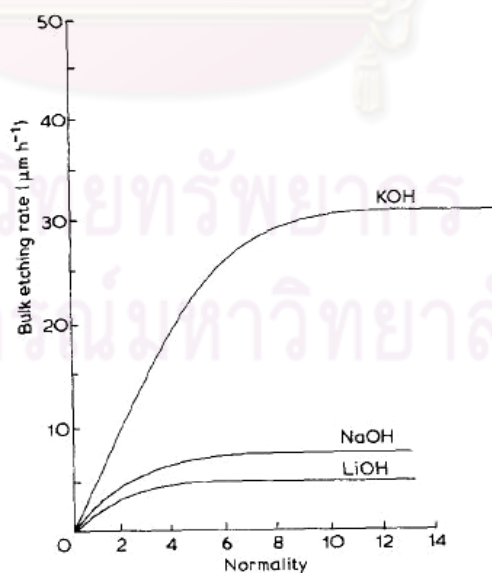
Figure 2.8 The effect of etchant concentration on the bulk etching rate of a cellulose nitrate detector (Daicell) at 50°C. [2]

Temperature and concentration of chemicals are variables that allow control of the attack rate so that etching occurs, but not too rapidly, as illustrated by Figure 2.9 [3].
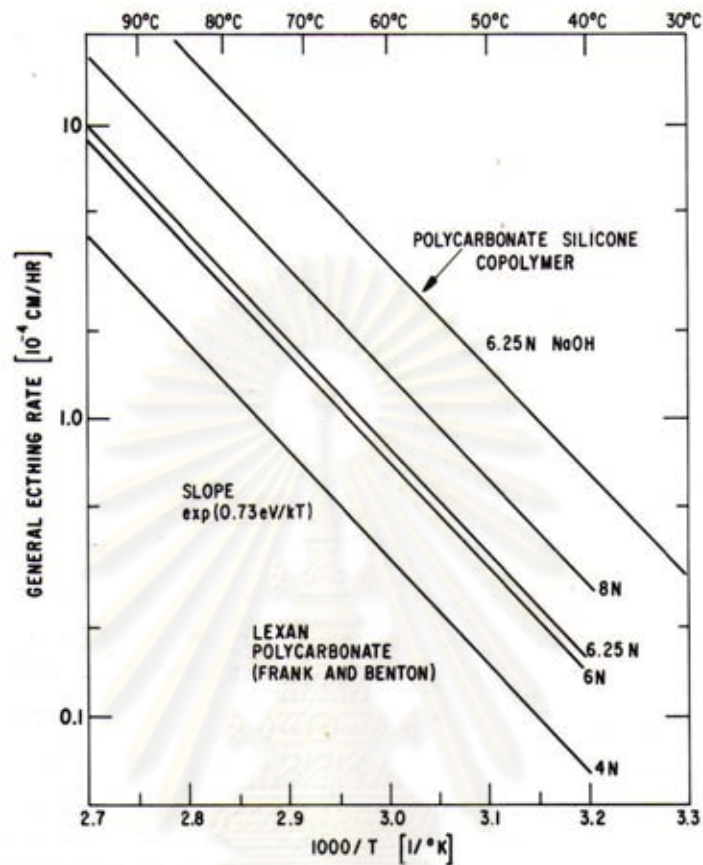
Figure 2.9 Etching rates are typically exponential functions of inverse temperature and increase with concentration. [3]

The shape of the track changes drastically with prolonged etching, going through three phases: conical, of transition, and spherical (see Figure 2.10). The final geometry of the etch pit profile depends, therefore, on the instant when the chemical etching is stopped. The conical phase lasts until the etching reaches the end of the damage trail. In this phase, the shape of the track is conical and its open surface is elliptical. When this phase finishes, the transition phase starts in which the bottom of the track is being rounded whereas the open surface is still elliptical. The etching rate is, then equal to the bulk etch rate in all directions. The spherical phase is reached when the shape of the track is spherical and its open surface circular [8].
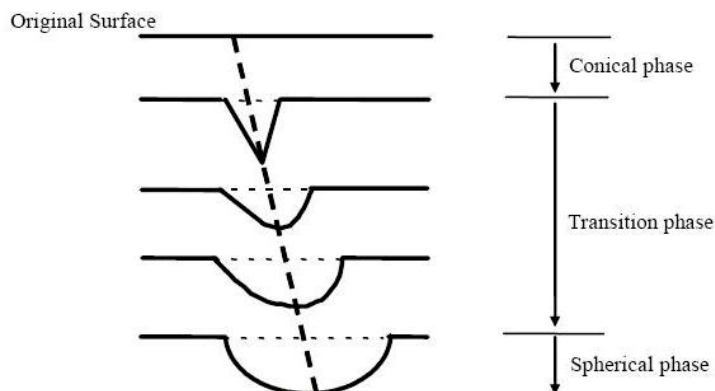
Fig. 2.10 The evolution of an etch pit profile with prolonged chemical etching. [8]

Polymer surfaces on exposure to photo-radiation undergo various changes, either alone or in combination, usually of oxidative, ozonolysis, or thermal character which causes chain scission and/or crosslinking. Such effects lead to either localized or bulk surface hardening, or softening, dependent on the dominant reaction in any specific instance. Surface "hardening", often caused by heating or ageing, is usually associated with a decrease in etching rate, while "softening" can cause a substantial increase. "Softening" agents observed, in addition to ultraviolet light have been O_3, H_2O_2 , NO. The moisture content of some detectors, as indicated by their storage humidity conditions, can also affect the etching rates of a water-sensitive polymer, e.g. cellulose nitrate can be made to double its etching rate. It has also been reported that the storage of polycarbonate in liquid nitrogen prior to etching increases its sensitivity to a particles.

A neutral environment of vacuum or nitrogen atmosphere decreases the track etching rate, possibly by oxygen exclusion. It is useful to note that the detector cellulose triacetate irradiated in a vacuum will not display alpha particle tracks on etching but can be sensitized after exposure to oxygen at high pressure (~ 100 atm).

Cellulose nitrates, polycarbonates, polyethylene terephthalate all show increased track etching rates on exposure to O_2, NO, H_2O_2 + ultraviolet light. Exceptionally, N_2O+ ultraviolet decreases track etching rates.

The experimental consequences of these facts are that polycarbonates, after irradiation, need protection from ultraviolet light sources such as sunlight and fluorescent lights if it is important that their track etching properties be standardized. Cellulosics after

irradiation need oxygen aeration, atmospheric pressure being satisfactory followed by either prompt processing, or refrigeration, to suspend any chemical changes as in this instance the etch rate slowly decreases with time and gradual polymer decomposition occurs.

The various additives, anti-degradients, plasticizers, etc., used in formulating polymer materials often considerably change their etching characteristics, rate variations of 1 to 35 have been reported. In particular, the presence of an ultraviolet stabilizer is recognized as suppressing the track-etching properties of polymeric detectors by conferring opacity to ultraviolet light.

In the case of crystalline materials, high doses of lightly ionizing radiation have so far failed to alter measurable etching parameters. However, weathering, specific annealing, and other thermal effects, do play influential roles in the etching of tracks in inorganic detectors [2].

Examples of some commonly used solid state nuclear track detectors are given in Table 2.5 [8]. A list of chemical etchants generally used along with the etching conditions for different detectors, particle sensitivity and the critical angle of etching are also given in Table.

Table 2.5 Examples of etching condition of SSNTDs. [11]

Category	Detector Material	General Etching Conditions	Lightest Detectable Particle	Critical Angle Q_c
Minerals/ Crystals	Olivine	KOH Soln., 160°C, 6 min; 10 % HF, 23°C, 30 sec.	Fe	
	Zircon	85 % H_3PO_4, 500°C, 1 min.	Ca	
	Quartz	KOH Soln., 210°C, 10 min.	Ar (100 MeV)	
	Mica	48 % HF, 23°C, 3 Sec- 40 min.	Ne(20 MeV)	4° 30'
Glasses	Sodalime glass	48 % HF, 23°C, 3 Sec.	Ne(20 MeV)	~ 50°
	Phosphate glass	48 % HF, 23°C, 3 Sec.	F (20 MeV)	1-5°
Plastics	Polycarbonate Plastics (Lexan, Makrafol, Milar)	6 N NaOH, 60°C, 60 min.	He (0.3 MeV)	~ 2-3°
	Cellulose Nitrate (Daicell, LR-115, CA-80-15)	3-6N NaOH, 50°C, 40 min.	H (0.5 MeV)	~ 4-8°
	Allyldiglycol Polycarbonate (CR-39)	6 N NaOH, 70°C, 1-4 hrs.	H (1.0 MeV)	~ 10°

For a clear concept and practical use of the track formation phenomena one must predict that at how much energy particles will produce etchable tracks under certain fixed experimental conditions. Various scientists have suggested that track formation should be related to number of different parameters. For an exact and precise analysis of track formation phenomena, some of the important parameter taken into account is the following

i)   Charge, mass and velocity of the traversing ion.

ii)   The typical critical angle θ with respect to surface of the detector.

iii)   Types of the detector material.

iv)   Nature, concentration, and temperature of the etchant

v)   Etching time

vi)   Environmental conditions existing before, during and after irradiation.

2.3. Applications of Track-etched detectors

The areas of potential applications of Solid State Nuclear Track Detectors are growing rapidly. In 2006, P. Buford Price [4] had brief reviews of applications of the nuclear track technique to nuclear fusion, cosmic rays, molecular identification with nanopores, imaging X-ray astronomy, magnetic studies with nanowires, polymeric nanowires, radon and neutron dosimetry, and thermochronology with ^{238}U and ^{244}Pu fission tracks. These are some applications of filtering from his reviews.

2.3.1 Research and technology with nanopores in track-etch films

DeBlois and Bean (1970) and co-workers (DeBlois and Wesley, 1977; DeBlois et al., 1977), who used a single track-etched pore in a polycarbonate film to detect and measure sizes of viruses down to ~40 nm.

In 1991 David Deamer (U. C. Santa Cruz) and Daniel Branton (Harvard) initiated research on nanopore sequencing of single-stranded nucleic acids. They and their colleagues hit upon the idea of using a cage-like molecule, α-hemolysin, containing a pore with an internal diameter of ~2.2 nm and a limiting aperture of 1.5 nm diameter. This pore can be embedded in a lipid bilayer and an electrical field used to drive a single strand of a charged DNA fragment through the pore. Although such membranes have been successful in measuring long stretches of the same nucleotides, such as 30

adenines followed by 70 cytosines (Kasianowicz et al., 1996; Akeson et al., 1999), current research is aimed at identifying each nucleotide as it passes through the pore. One of Deamer's ideas is to use mica with a 6 nm single pore to support an α-hemolysin pore and to slow the rate of passage of nucleic acid fragments to ~10^{-3} sec per base in order to avoid blurring of signals. There is now considerable effort, especially among those who use the Unilac heavy ion facility at Darmstadt, Germany, to develop synthetic nanopores small enough to compete with α- hemolysin. Mara et al. (2004) have made a good start, using asymmetric pores 2 to 4 nm in diameter in a polyimide film to distinguish double-strand DNA fragments in the size range from ~290 to ~4000 base pairs. Heins et al. (2005) have recently shown that a conically shaped polyimide film with a single 4.5 nm nanopore is able to detect single porphyrin molecules of diameter ~2 nm.

2.3.2 Ion track filters for imaging X-ray astronomy

Mitrofanov and Apel (2006) have developed a blocking cut-off filter that rejects UV and visible light from the sun while allowing soft X-rays to penetrate the film. Three identical filters capable of rejecting the 10^{8}-times larger flux of solar UV and visible light have been installed in the SPIRIT telescope assembly, which includes a Herschel telescope-coronagraph and a Ritchey- Chrétien telescope that have been operating on board the Coronas-F satellite since 2001. The filter used is an 8.5-μm-thick PET foil with a density of 1.4 x 10^{7} cm^{-2} etched tracks of diameter 1.5 μm and with two-layer thin Al films on each surface. It was optimized for detection of 13.5 to 30.4 nm X-rays. The UV and visible light is cut off by diffraction and absorption on the pore walls.

2.4 Neutron Interactions [12, 13]

Since neutrons are electrically neutral, they are not affected by the electrons in an atom or by the positive charge of nucleus. As a consequence, neutron passes through the atomic electron cloud and interacts directly with the nucleus. In short, neutrons collide with nuclei, not with atoms. A neutron can have many types of interactions with a nucleus. Figure 2.11 shows the types of interactions.
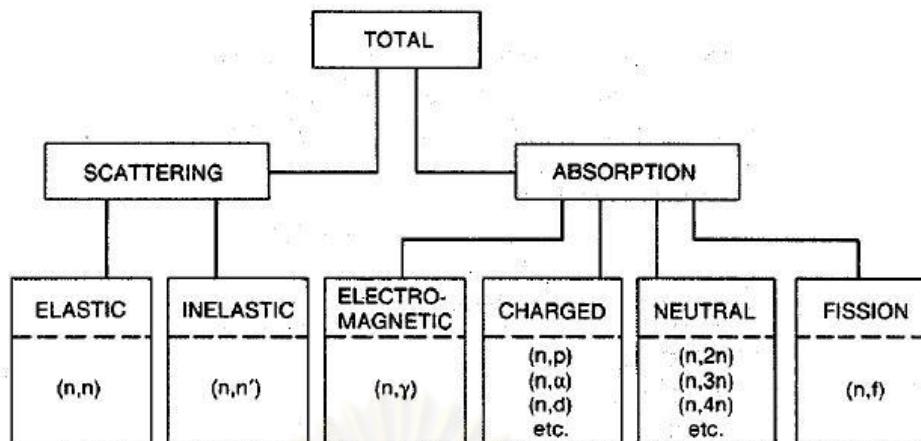
Figure 2.11 Various categories of neutron interactions. The letters separated by commas in the parentheses show the incoming and outgoing particles. [13]

An interaction may be one of two major types scattering or absorption. When a neutron is scattered by a nucleus, its speed and direction change but the nucleus is left with the same number of protons and neutrons it had before the interaction. The nucleus will have some recoil velocity and it may be left in an excited state that will lead to the eventual release of radiation. When a neutron is absorbed by a nucleus, a wide range of radiations can be emitted or fission can be induced.

2.4.1 Elastic scattering

In this process, the neutron strikes the nucleus, which is almost always in its ground state, the neutron reappears, and the nucleus is left in its ground state. The neutron in this case is said to have been elastically scattered by the nucleus. In the notation of nuclear reactions, this interaction is abbreviated by the symbol (n,n).

2.4.2 Inelastic scattering

This process is identical to elastic scattering except that the nucleus is left in an excited state. Because energy is retained by the nucleus, this is clearly an endothermic interaction. Inelastic scattering is denoted by the symbol (n,n').

2.4.3 Electromagnetic or Radiative Capture

Here the neutron is captured by the nucleus, and one or more γ rays – called capture γ rays- are emitted. This is an exothermic interaction and is denoted by (n,γ). Since the original neutron is absorbed, this process is an example of a class of interactions known as absorption reactions.

2.4.4 Charged Particle Reaction

Neutrons may also disappear as the result of absorption reactions of the type (n,α) and (n,p). Such reactions may be either exothermic or endothermic.

2.4.5 Neutron producing reactions

Reactions of the type $(n,2n)$ and $(n,3n)$ occur with energetic neutrons. These reactions are clearly endothermic since in the $(n,2n)$ reaction one neutron and in the $(n,3n)$ reaction 2 neutrons are extracted from the struck nucleus.

2.4.6 Fission

Neutrons colliding with certain nuclei may cause the nucleus to split apart- to undergo fission.

2.5 Theory of Light [14]

Light is just one portion of the various electromagnetic waves (Figure 2.12). The electromagnetic spectrum covers an extremely broad range, from radio waves with wavelengths of a meter or more, down to x-rays with wavelengths of less than a billionth of a meter. Optical radiation lies between radio waves and x-rays on the spectrum, exhibiting a unique mix of ray, wave, and quantum properties.
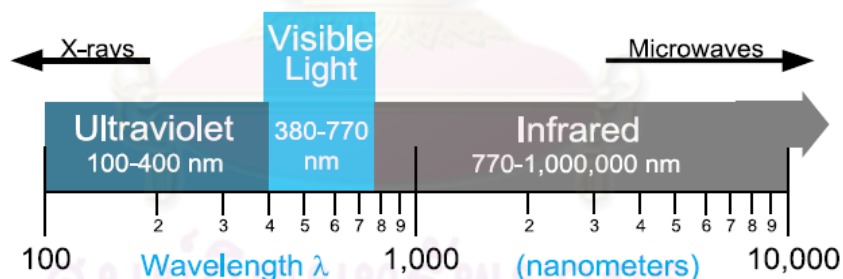
Figure 2.12 The optical portion of the electromagnetic spectrum. [14]

Like all electromagnetic waves, light waves can interfere with each other, become directionally polarized, and bend slightly when passing an edge. These properties allow light to be filtered by wavelength or amplified coherently as in a laser.

In radiometry, light's propagating wavefront is modeled as a ray traveling in a straight line. Lenses and mirrors redirect these rays along predictable paths. Wave effects are insignificant in an incoherent, large scale optical system because the light waves are randomly distributed and there are plenty of photons.

2.5.1 Ultraviolet Light

Short wavelength UV light exhibits more quantum properties than its visible and infrared counterparts. Ultraviolet light is arbitrarily broken down into three bands, according to its anecdotal effects (Figure 2.13). UV-A is the least harmful and most commonly found type of UV light, because it has the least energy. UV-A light is often called black light, and is used for its relative harmlessness and its ability to cause fluorescent materials to emit visible light - thus appearing to glow in the dark. Most phototherapy and tanning booths use UV-A lamps.
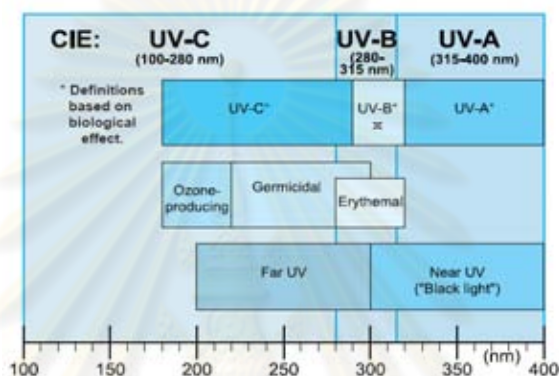
Figure 2.13 Common ultraviolet band designations. [14]

UV-B is typically the most destructive form of UV light, because it has enough energy to damage biological tissues, yet not quite enough to be completely absorbed by the atmosphere. UV-B is known to cause skin cancer. Since most of the extraterrestrial UV-B light is blocked by the atmosphere, a small change in the ozone layer could dramatically increase the danger of skin cancer. Short wavelength UV-C is almost completely absorbed in air within a few hundred meters. When UV-C photons collide with oxygen atoms, the energy exchange causes the formation of ozone. UV-C is almost never observed in nature, since it is absorbed so quickly. Germicidal UV-C lamps are often used to purify air and water, because of their ability to kill bacteria.

2.5.2 Visible Light

Visible light ranges in wavelength from approximately 400 nm to 700 nm. It is also known as the optical spectrum of light. The wavelength (which is related to frequency and energy) of the light determines the perceived color. The ranges of these different colors are listed in the Table 2.6 below. Some sources vary these ranges pretty drastically, and

the boundaries of them are somewhat approximate as they blend into each other. The edges of the visible light spectrum blend into the ultraviolet and infrared levels of radiation.

Table 2.6 The Visible light spectrum

The Visible light Spectrum	
Color	Wavelength (nm)
Red	625 - 740
Orange	590 - 625
Yellow	565 - 590
Green	520 - 565
Cyan	500 - 520
Blue	435 - 500
Violet	380 - 435

Most light that we interact with is in the form of *white light*, which contains many of these entire wavelength ranges within them. Shining white light through a prism causes the wavelengths to bend at slightly different angles due to optical refraction. The resulting light is, therefore, split across the visible color spectrum.

2.5.3 Infrared Light

Infrared light contains the least amount of energy per photon of any other band (Figure 2.14). Because of this, an infrared photon often lacks the energy required to pass the detection threshold of a quantum detector. Infrared is usually measured using a thermal detector such as a thermopile, which measures temperature change due to absorbed energy.
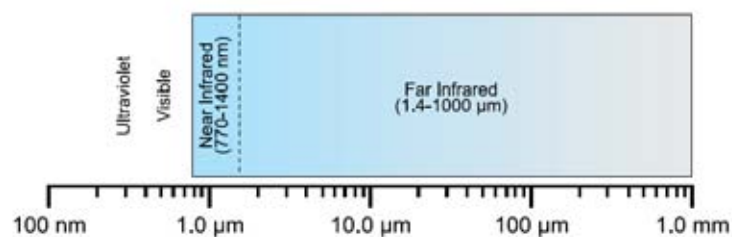
Figure 2.14 The infrared spectrum. [14]

While these thermal detectors have a very flat spectral responsivity, they suffer from temperature sensitivity, and usually must be artificially cooled. Another strategy employed by thermal detectors is to modulate incident light with a chopper. This allows the detector to measure differentially between the dark (zero) and light states.

Quantum type detectors are often used in the near infrared, especially below 1100 nm. Specialized detectors such as InGaAs offer excellent responsivity from 850 to 1700 nm. Typical silicon photodiodes are not sensitive above 1100 nm. These types of detectors are typically employed to measure a known artificial near-IR source without including long wavelength background ambient.

Since heat is a form of infrared light, far infrared detectors are sensitive to environmental changes - such as a person moving in the field of view. Night vision equipment takes advantage of this effect, amplifying infrared to distinguish people and machinery that are concealed in the darkness.

Infrared is unique in that it exhibits primarily wave properties. This can make it much more difficult to manipulate than ultraviolet and visible light, infrared is more difficult to focus with lenses, refracts less, diffracts more, and is difficult to diffuse. Most radiometric IR measurements are made without lenses, filters, or diffusers, relying on just the bare detector to measure incident irradiance.

2.5.4 Behavior of Light

The behavior of light pass through the matter can be divided to

2.5.4.1 Reflection

Reflection is the change in direction of a wavefront at an interface between two different media so that the wavefront returns into the medium from which it originated. Light reflecting off of a polished or mirrored surface obeys the law of reflection: the angle between the incident ray and the normal to the surface is equal to the angle between the reflected ray and the normal (Figure 2.15). When light obeys the law of reflection, it is termed a specular reflection. Most hard polished (shiny) surfaces are primarily specular in nature. Even transparent glass specularly reflects a portion of incoming light.

Many reflections are a combination of both diffuse and specular components. One manifestation of this is a spread reflection, which has a dominant directional component that is partially diffused by surface irregularities (Figure 2.16).
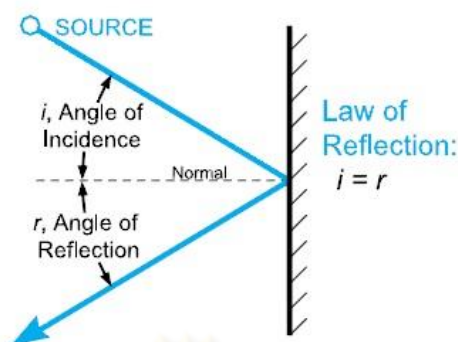
Figure 2.15 Law of reflection. [14]
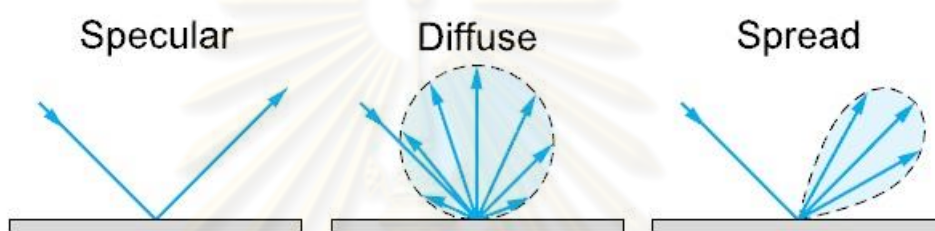
Figure 2.16 Specular, diffuse, and spread reflection from a surface. [14]

2.5.4.2 Refraction

When light passes between dissimilar materials, the rays bend and change velocity slightly, an effect called refraction (Figure 2.17). Refraction is dependent on two factors: the incident angle, θ_1, and the refractive index, n of the material, as given by Snell's law of refraction:

$$n_1 \sin (\theta_1) = n_2 \sin (\theta_2) \qquad (2.6)$$

where: n_1 is the refractive index of the medium the light is leaving,

θ_1 is the incident angle between the light ray and the normal to the medium to medium interface,

n_2 is the refractive index of the medium the light is entering,

θ_2 is the refractive angle between the light ray and the normal to the medium to medium interface
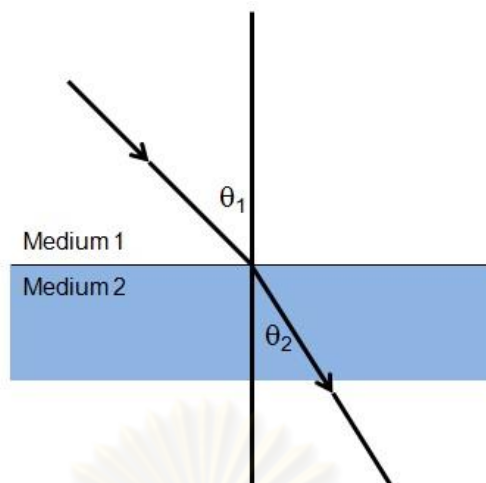
Figure 2.17 Refraction of light.

2.5.4.3 Diffraction

Diffraction is another wave phenomenon that is dependent on wavelength. Light waves bend as they pass by the edge of a narrow aperture or slit (Figure 2.18). This effect is approximated by:

$$\theta = \lambda / D \qquad (2.7)$$

where θ is the diffraction angle, λ the wavelength of radiant energy, and D the aperture diameter. This effect is negligible in most optical systems, but is exploited in monochromators. A diffraction grating uses the interference of waves caused by diffraction to separate light angularly by wavelength. Narrow slits then select the portion of the spectrum to be measured. The narrower the slit, the narrower the bandwidth that can be measured. However, diffraction in the slit itself limits the resolution that can ultimately be achieved.
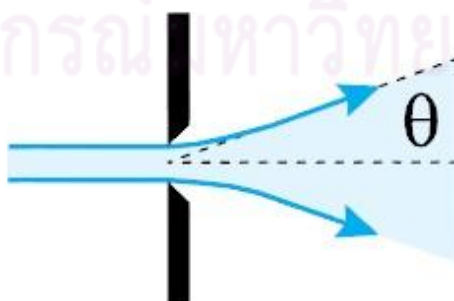
Figure 2.18 Diffraction of light. [14]

2.5.4.4 Transmission

When a beam monochromatic light passes through a transparent medium, part of the light is absorbed and the transmitted beam has a lower intensity than the intensity of the incident beam. The light that does not get through is said to be absorbed by the medium through which it passes.

Absorption by a filter glass varies with wavelength and filter thickness. Bouger's law states the logarithmic relationship between internal transmission at a given wavelength and thickness.

$$Log_{10}(\tau_1) / d_1 = log_{10}(\tau_2) / d_2 \tag{2.8}$$

Internal transmittance, τ_1, is defined as the transmission through a filter glass after the initial reflection losses are accounted for by dividing external transmission, τ_2 by the reflection factor Pd.

$$\tau_1 = T / Pd \tag{2.9}$$

When light passes through the rough material, it is often necessary to diffuse light, either through transmission or reflection (Figure 2.15). Diffuse transmission can be accomplished by transmitting light through roughened quartz, flashed opal, or polytetrafluoroethylene (PTFE, Teflon). Diffusion can vary with wavelength. Teflon is a poor IR diffuser, but makes an excellent visible/UV diffuser. Quartz is required for UV diffusion. Integrating spheres are coated with $BaSO_4$ or PTFE, which offer >97% reflectance over a broad spectral range with near perfect diffusion. These coatings are, however, quite expensive and fragile. It is often necessary to diffuse light, either through transmission or reflection.
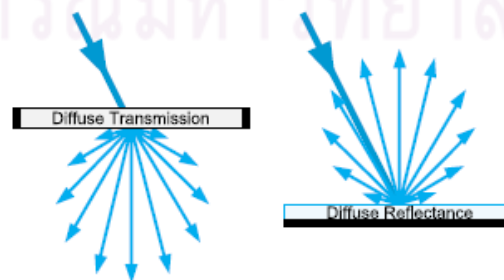
Figure 2.19 Diffuse transmission and reflectance. [14]

In 2007, Ali Mostofizadeh, Xiudong Sun and Mohammad Reza Kardan [15] reviewed paper to summarize some advanced theoretical and experimental methods applied in modern optics to develop some technical skills used in nuclear track studies. One of his reviews mentioned that some researcher using optical model about light transmission and light scattering phenomenon to describe the optical properties on nuclear track. Grietz et al., 1998 explained about light scattering phenomenon by conical and oblique etched track has been schematically shown in figure   2.16 and 2.17
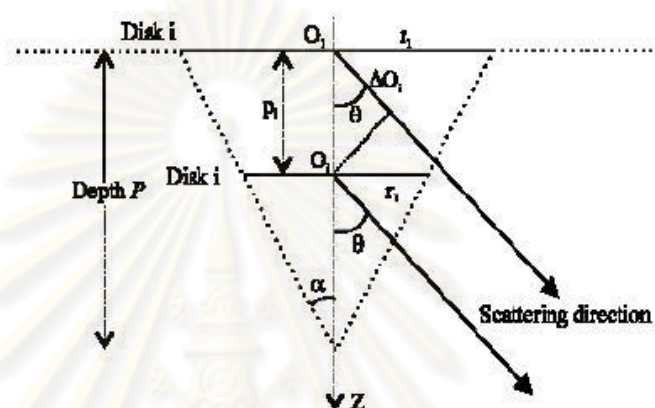
Figure 2.20 Geometry of a conical. [15]
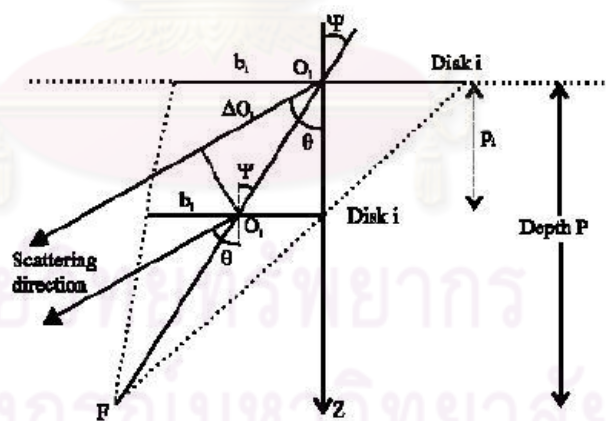
Figure 2.21 Geometry of an oblique tracks. [15]

His reviews mentioned about neutron and alpha particles etched tracks evaluation using He-Ne laser. Al-Saad et al. (2001) attempted to apply He-Ne laser light to investigate nuclear tracks of ^{241}Am alpha particles and Am-Be neutrons, registered by 250 μm CR-39 and 100 μm CN-85 foils. They used a photodiode as a light detector at the

distance 10 cm from the SSNTDs for measuring light scattered by track apertures. Figure 2.18 and showed the behavior of light transmission through the CR-39 and CN-85 foils irradiated by alpha particles and neutron in the normal incidence case (0°) versus chemical etching time, respectively.
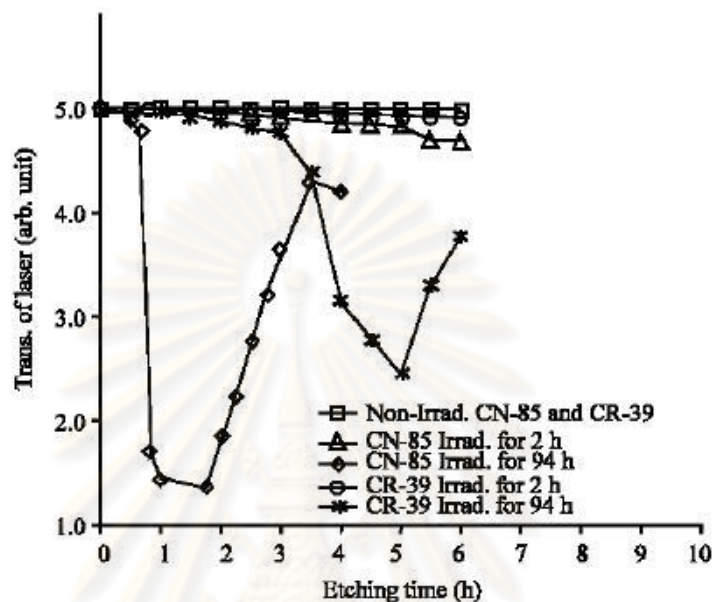
Figure 2.22 Transmission of laser light through the SSNTD's irradiated by α particle. [15]
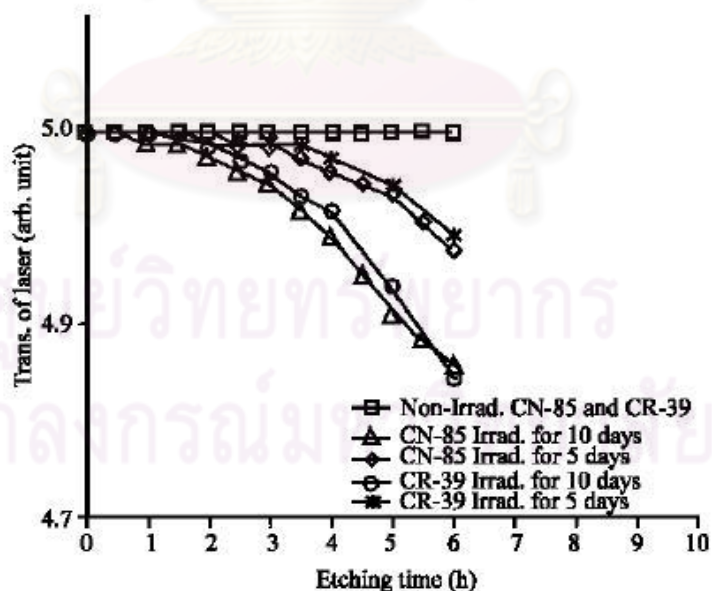
Figure 2.23 Transmission of laser light through the SSNTD's irradiated by neutron. [15]

The pattern of transmission of laser light through the SSNTD' irradiated by neutron is different from SSNTD' irradiated by alpha particle. They stated that the different

mechanism to generate fast-neutron-induced tracks in polymers can cause a different feature for mention curves. Since nuclear tracks are in fact the particular damages in polymeric structure of SSNTDs that are created by charge particles, neutrons (as electrical neutral particles) cannot directly be able to create primary latent tracks. Nonetheless, tracks are indirectly induced by neutrons based on creating of charged induced recoil-particles in the polymeric structure. On the other hand, the productive reactions of recoil-particles can occur anywhere inside the polymer volume along the neutrons trajectory, so there is no necessarily that the related polymeric destruction begins from the surface of polymer. Therefore, new tracks are likely to be created due to increase of etching time.

In this study, random and asymmetric track-etch pores in polymer used as light filter or diffuser films are generated by neutron induced track-etch. Neutrons from radioisotope source interact with hydrogen or nitrogen atoms of polymer via ^{1}H $(n,n)^{1}H$ and ^{1}H $(n,n')^{1}H$. Proton tracks will be created on polymer. Their pore size and shape can be varied in controllable manner which involve the temperature, the concentration of the etchant, and the etching duration.

2.6 Literature review

In 1975, Nares Chankow [16] used Cellulose nitrate (CN) to register radon alpha particles which diffused from uranium ore. In this study, he also varied the etching condition. He found that the optimum etching conditions used were 10% solution of NaOH, $60°C$ and 40 minutes etching time. And the alpha track densities on the films were proportional to the amount of uranium and radium in the ore.

In 1981, Stephens, Richard B. [17] patented about low reflectivity surfaces which are formed by particle track etching of a dielectric material such that the horizontal scale of surface texture is less than the wavelength of incident radiation and the depth of texture is equal to or greater than said wavelength. As a consequence, the reflection coefficient is thereby reduced by a factor of at least two, and light is more efficiently transmitted into the material. For solar cells encapsulated in transparent material, efficiency of absorption of solar radiation may be improved by at least about two times per etched surface, or to less

than about 2% for the air/transparent material interface and to less than about 15% for the transparent material/solar cell interface.

In 1989, Hameed Ahmed Khan and Naeem Ahmed Khan [18] had a review article Solid State Nuclear Track detection (SSNTD): A useful scientific tool for basic and applied research. In this paper, very briefly, summarizes the useful contribution this technique has made in the past and is making at present. The state of the art of applications of Solid State Nuclear Track Detectors in fields like nuclear physics, geochronology, cosmology, biology, bird altimetry, seismology, elemental analysis, material science, lithography, etc. has been given.

In 1991, Michael A. Gruntman [19] reviewed a novel of the filtering of EUV radiation for laboratory and space applications. The relevant theoretical considerations as well as available experimental data are presented. Foils perforated by a set of parallel channels with submicron diameters serve as wavelength dependent filters. Each channel passes photons when the wavelength is much smaller than the channel diameter. The transmission of the channel drops dramatically, however, when the wavelength becomes comparable to or larger than the channel diameter. Several different ways to manufacture such kind of filters are outlined, including nuclear track filters, anodized metal films, and microchannel plate technology. Advantages and disadvantages of each technique are discussed.

In 1996, P. C. Popov and D. S. Pressyanov [20] exposed Kodak-Pathe' LR 115 type II, at 25 mm distance, to alpha particles of a spectrometric ^{238}Pu source. After that the detectors were etched in 10% NaOH at 60°C for 120 min. The estimation of track densities is within 103-105 cm^{-2} range. A modified SSNTD is placed in optical contact with a prism, so that sensitive surface of the detector faced the microscope, to assess the internal reflection of a laser beam. They concluded that it can be obstructed total internal reflection of a laser beam.

In 2001, Nares Chankow, et al. [21] developed a technique for viewing Track-Etch neutron radiographs using a desktop scanner with a nickel coated metal backing which was placed on the scanner. It was found to be practical in viewing track-etch neutron radiographs without any additional development or investment.

In 2006, A.V. Mitrofanov, P.Yu. Apel [22] applied ion track filters as blocking cut-off filters for solar telescopes in imaging X-ray astronomy. Ion track membranes (ITMs) were produced of polyethylene terephthalate (PET) foils with the thickness L of 5–25 μm. Specimens of the PET foils were irradiated with the 250 MeV Kr ions up to the track density N of 10^6– 10^8 cm^{-2} on the U-400 cyclotron of the Flerov Laboratory of Nuclear Reactions JINR. ITms of high-porosity constitute a randomly inhomogeneous medium with sub-micrometer or micrometer open pores which not only transmits X-ray or extreme ultra violet (EUV) radiation and blocks long-wavelength UV radiation, but also transfers a focused imaging pattern with high-quality for further registration by means of CCD or imaging detectors of other types. X-ray and EUV filters based on ITMs with cylindrical parallel pores were successfully used as detector filters in the solar X-ray telescopes designed and manufactured at the Lebedev Physical Institute of the Russian Academy of Sciences (LPI, Moscow).

In 2006, A. V. Mitrofanov, P. Yu. Apel, I. V. Blonskaya and O. L. Orelovitch [23] found experimentally that porous polyimide and poly (ethylene naphthalate) membranes made by chemical etching of ion tracks using a scanning beam of 253-MeV ^{84}Kr ions on the U-400 cyclotron (Flerov laboratory, Joint Institute of Nuclear Research) are promising for optical diffraction filters and supports of thin-film filters used in X-ray astronomy instruments and also for laboratory applications. A series of large-pore membranes was fabricated from PI and PEN films, and their parameters were measured. These membranes may be used as components of neutral-density optical filters in the soft X-ray and vacuum ultraviolet spectral ranges.

In 2007, Ali Mostofizadeh, Xiudong Sun and Mohammad Reza Kardan [13] reviewed to summarize some advanced theoretical and experimental methods applied in modern optics to develop some technical skills used in nuclear track studies. They also described the process of tracks appearance in solid state detectors, the theoretical principles of light transmission through the polymeric detectors, some features of Fourier optics, practical and experimental aspects of the subject including the applications of coherent light in nuclear track evaluations.

In 2007, D. Nikezic and K.N. Yu [5] used a computer program called TRACK_VISION 1.0 which was developed in their laboratory to simulate light propagation

through the tracks and to calculate the brightness of all grid elements in the track wall. Four different cases for light ray propagation through the etched track were studied in detail. The track profile, optical appearance and distribution of scattered light were given for three typical types of etched tracks. These laid the foundation for future automatic determination of properties of the alpha particles producing the tracks through the scattered light.

In 2008, D. Nikezic and K.N. Yu [24] continued their works about a computer program called Track_Vision for determining the optical appearances of tracks in nuclear track materials. Their programming steps were outlined. This paper described the program were given, including the built-in *V* functions for the commonly employed nuclear track material commercially known as CR-39 (polyallyldiglycol carbonate) irradiated by alpha particles.

CHAPTER III

EXPERIMENTAL PROCEDURE AND DEVELOPMENT

This chapter describes the design of experiments on producing proton tracks in polymer as well as related experiments and associated measurements to study the properties of track-tech polymer on light transmission. Parameters that might affect the density, shape and size of the tracks are also experimentally investigated.

3.1 Equipment design and construction

3.1.1 Polymer

It is important to note that polymer is often specific to a particular formulation and particles which form tracks in Table 2.4 in Chapter II shows examples of some commonly used solid state nuclear track detectors. A list of chemical etchants generally used along with the etching conditions for different detectors, particle sensitivity and the critical angle of etching are also given. Table 2.4 shows that polycarbonate plastics (Lexan, Makrofol, Mylar) are sensitive to alpha particles of energy $\leq$ 0.3 MeV while cellulose nitrate (Diacell, LR-115, CA-80-15) and allyldiglycol polycarbonate (CR-39) are sensitive to proton particle of energy $\leq$ 0.5 and 1.0 MeV, respectively.

Fleischer et al. mentioned that cellulose nitrate, cellulose acetate and UV-sensitized Lexan are sensitive to protons of energy up to ∼100 keV. The fraction of atoms that are hydrogen is 32 % in cellulose nitrate and 45 % in Lexan. In a neutron energy interval from perhaps 20 to 100 keV, tracks of recoiled protons produced in elastic collisions with hydrogen in the plastic would be detectable [3].

In this study, many types of polymer such as cellulose nitrate, CR-39, CR-39 optical lens and sunshade polycarbonate plastic were first tested by irradiating with neutrons from a Cf-252 source submerged in water to produce recoil proton tracks.The

Cf-252 source emitted neutrons at the rate of 4.54 x 10^7 n/s on 28th of June 2002 as showed in part I of appendix A. In June 2010, when the irradiation was conducted, the neutron emission rate was about 5 x 10^6 n/s. The result showed that after etching proton tracks could be seen in CR-39, CR-39 optical lens and sunshade polycarbonate plastic. Then a locally available polycarbonate plastic for sunshade, 1.5 mm thick was used as a commercial PC because it is inexpensive and easily available.

Polycarbonate (PC) plastic, known by the trademarked names Lexan, Makrolon, Makroclear and others, are a particular group of thermoplastic polymers. The main polycarbonate material is produced by the reaction of bisphenol A and Phosgene ($COCl_2$). The chemical structure is showed as Figure 3.1 and the physical and thermal properties are showed in Table 3.1 [25].
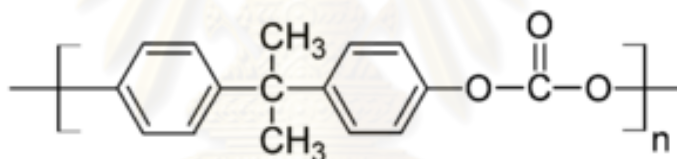
Figure 3,1 The structure of Polycarbonate polymer. [25]

Table 3.1 Physical and thermal properties of Polycarbonate

Property	
Density (ρ)	1.20-1.22 g/cm^3
Refractive index (n)	1.584-1.586
Melting temperature (Tm)	267°C

3.1.2 Neutron Irradiation

The scope of this study mentioned that track formation process on films used neutrons from radioisotope source via $^1H(n, n)^1H$ and $^1H(n, n')^1H$ reactions. The study was designed to use neutron radioisotope source because it was easy to operate when

compare to reactor and the maintenance cost is almost zero. The possible choices for radioisotope neutron source are much more limited and are based on either spontaneous fission or on nuclear reactions. The most common spontaneous fission source is ^{252}Cf. Its half life is 2.65 years is long enough to be reasonably convenient, and the isotope is one of the most widely produced of all the transuranics. The dominant decay mechanism is alpha decay, and the alpha emission rate is about 32 times that for spontaneous fission. The neutron yield is 0.116 n/s per Bq, where the activity is the combined alpha and spontaneous fission decay rate. On a unit mass basis, 2.30×10^6 n/s are produced per microgram of ^{252}Cf. The average neutron energy is about 2.1 MeV, and the predominant energy is about 0.7 MeV. The energy spectrum of the neutron is showed as Figure 3.2 [Appendix A].
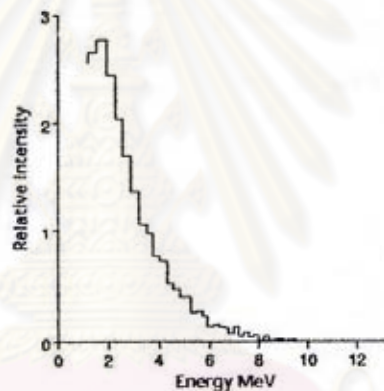
Figure 3.2 Neutron energy spectrums from the spontaneous fission of Cf-252.

Nuclear reaction radioisotope source generates neutron via (α, n) reaction. Because energetic alpha particles are available from the direct decay of a number of convenient radionuclides, it is possible to fabricate a small self-contained neutron source by mixing an alpha-emitting isotope with a suitable target material. Several different target materials can lead to (α, n) reactions for the alpha particle energies that are readily available in radioactive decay. The maximum neutron yield is obtained when beryllium is chosen as the target, and neutrons are produced through the reaction:

$$_2\alpha^4 + {}_4\text{Be}^9 \rightarrow {}_6\text{C}^{12} + {}_0\text{n}^1$$
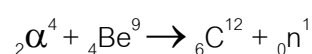
which has a Q-value of + 5.71 MeV.

Some of radioisotope (α, n) sources are [238]Pu-Be, [239]Pu-Be, [241]Am-Be, [244]Cm-Be, etc. The [239]Pu-Be source was the most widely used several years ago. However, because about 16 g of the material is required for 1 Ci (3.7 x 10^{10}Bq) of activity, sources of this type of a few centimeters in dimension are limited to about 10[7] n/s [6]. Nowadays, [241]Am-Be is most widely used. Half-life of [241]Am is 433 years. The energetic neutrons are generated following an interaction between the alpha particle and the target material's nucleus and possess energies up to 10 MeV, with an average value of ~4 MeV.

In this study, californium-252 (Cf-252) radioisotope source was used to be neutron source due to its high neutron emission rate and its average neutron energy was less than [241]Am-Be radioisotope source. Fleischer et al. mentioned that a neutron energy interval from perhaps 20 to 100 keV, tracks of recoiled protons produced in elastic collisions with hydrogen in the plastic would be detectable [3].

Cf-252 neutron source used in this research was originally 20 µg or 10.7 mCi on 28th of June 2002. The neutron emission rate was 4.54 x 10^{7} n/s [26]. Each of spontaneous fission emitted 3.76 neutrons. The calculated neutron emission on June 2010 was approximately 5 x 10^{6} n/s which gave the maximum neutron flux in water about 5 x 10^{4} n/cm[2].s. The specification of Cf-252 is showed in Appendix A. Figure 3.3 illustrates a drawing of Cf-252 source.
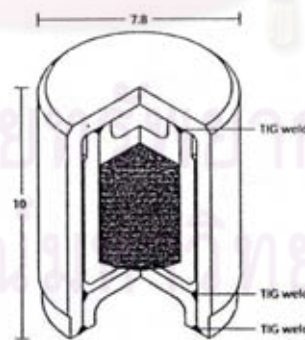
Figure 3.3 Illustration of Cf-252 neutron source.

In this study, the Cf-252 neutron source was placed at the end of L shape aluminum tube and sealed the end with aluminum plate. The diameter of tube was 0.8

cm, 0.2 cm thickness and 40 cm length. Inside of aluminum tube inserted with acrylic tube in order to fix Cf-252 source. (Shown as Figure 3.4)
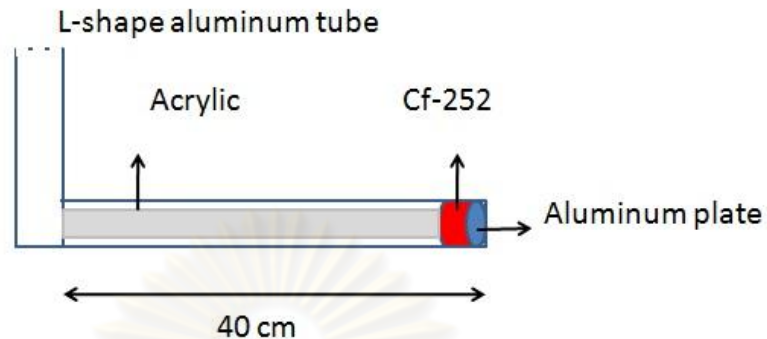
Figure 3.4 the designed envelop of Cf-252 source.
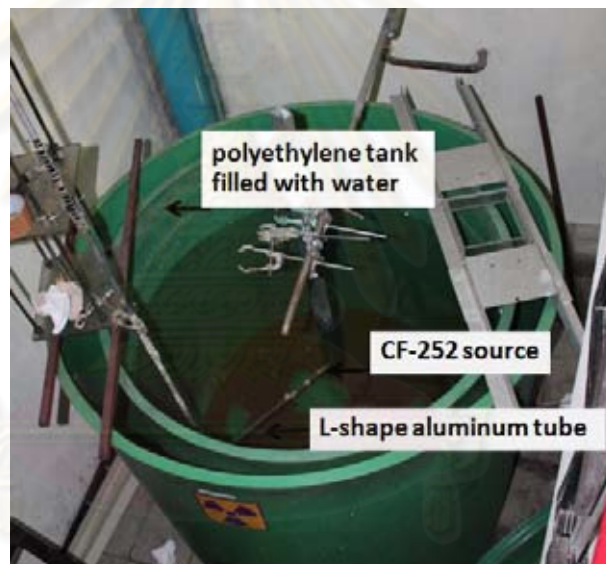
Figure 3.5 Showing Cf-252 source contained in an L shape aluminum tube submerged in a polyethylene tank filled with water.

The aluminum tube with Cf-252 source was placed under water in a polyethylene tank which was filled 1,000 liter of water. The diameter of inner tank was 105 cm and height was 105 cm (Figure 3.5). PC chip was put in an aluminum box and placed the box close to Cf-252 source in order to fix the distance of PC from the source. The proton track density in PC was varied by changing the irradiation time.

3.1.3 Etching conditions

After neutron irradiation, PC was etched to enlarge the latent tracks. From the literature review, Table 2.4 in Chapter II showed that the general etching condition of PC for alpha track is 6 N NaOH at 60°C, 60 min. Some researchers [25, 26, and 27] used PEW solution as the etchant for alpha track on PC. The PEW solution composed of 15% KOH, 40% ethanol and 45% H_2O.

The result from previous study [in part I, Appendix B] showed that the proper etchant for proton track on PC in this study was PEW solution. The etching time of PEW solution at 70°C was shorter than NaOH 6.25N at 60°C. The etching time for PEW and NaOH were 60 and 100 min, respectively.

The properties of track depend on the condition of etchant. In this study, the etching time and temperature were varied to create the different track sizes and shapes. Two etching conditions were studied:

3.1.3.1 The temperature of PEW solution was varied from 65, 70 and 75°C. The temperature of etchant was controlled with water bath (Figure 3.6)

Figure 3.6 Water bath with thermometer.

3.1.3.2 The etching time of PC was increased 15 minutes in each step from 15 to 90 minutes at the temperature 65, 70 and 75 $^\circ$C in order to investigate track shape and size.

3.1.4 Observation and measurement of proton tracks

Proton track on PC can be observed under an optical microscope equipped with Motic Image Plus version 2.0 digital microscopy software (User's Manual is showed in Appendix C). Figure 3.7 demonstrates the optical microscope equipped with Motic Image software. This software was used to capture the track image and saved in jpeg format. The magnification of optical microscope was approximately x100. Then the captured track image was used to characterize properties of the tracks by using the ImageJ software which was an image processing and analysis program (User's Manual showed in Appendix D). In this study, the parameter settings of the software in analysis of the tracks were showed in Figure 3.8. The range of particle size (μm^2) was 1 to infinity and circularity of track was 0.5 to 1.0.
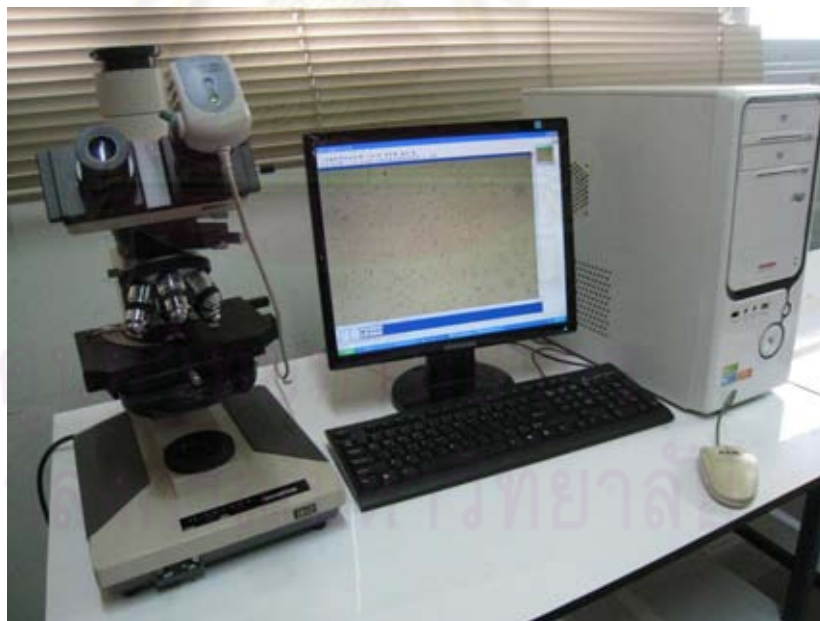
Figure 3.7 Microscope with Motic image capture software.

Figure 3.8 Parameter settings in analysis of proton tracks as seen on the screen
of the ImageJ software.

3.1.5 Light transmission measurement

Investigation of properties of track-etch polymer films on transmission of visible light, ultraviolet (UV) and infrared (IR) was conducted by using a SPECTRUM DETECTIVE Transmission Meter model SD2400. The transmission meter displays energy transmission values in three regions. The light sources used for the three regions have a peak response at the following wavelengths: UV 365 nm, visible light with full weighted spectrum and infrared 950 nm (Figure 3.9). The user's manual is showed in Appendix E.

Figure 3.9 SPECTRUM DETECTIVE Transmission Meter SD2400.

CHAPTER IV

EXPERIMENTS AND RESULTS

The experiments were conducted to form the proton tracks on PC under various conditions to estimate the correlation between the track density, average track size and the percentage of light transmission in three ranges i.e. ultraviolet, visible light and infrared. Track density was varied by varying irradiation time and track size and shape were controlled by etching temperature and etching time.

4.1 Formation of proton tracks using thermal neutrons from the Thai Research Reactor

This first step was to investigate proton track formation on PC, the effects of etching temperature and etching time. Four pieces of 2.5 cm x 5 cm PC chips were irradiated with neutrons from a beam tube designed for neutron radiography at the Thai Research Reactor TRR-1/M1 (Figure 4.1) for 1 hour. The neutron flux was approximately 1.26×10^6 n/cm^2.s with a cadmium ratio of greater than 200 [30]. PEW solution containing 15% potassium hydroxide (KOH), 40% ethyl alcohol (C_2H_5OH) and 45 % water (H_2O) was selected as the etchant. The neutron irradiated PC chips were then etched separately at different temperatures i.e. 65, 70, 75 and 80 $^\circ$C each for 60 minutes. The etched track images at different conditions were shown in Figures 4.2 - 4.3.
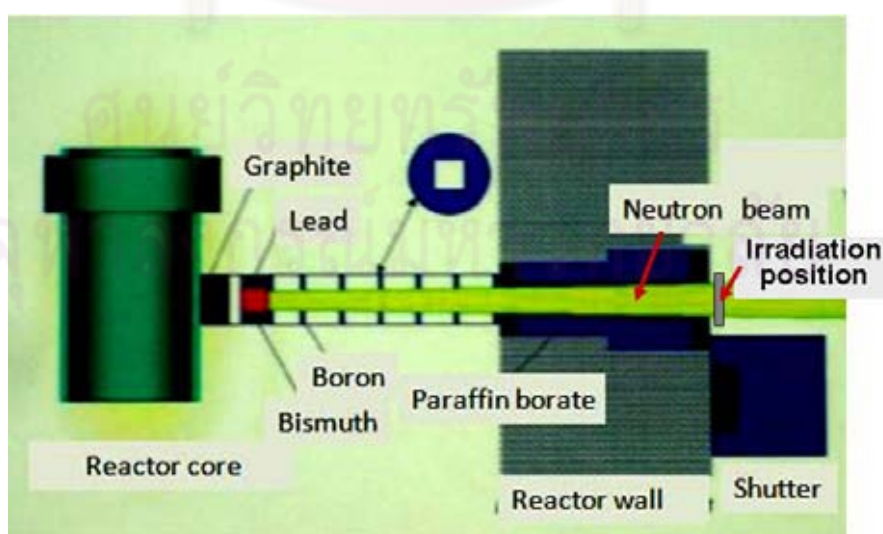
Figure 4.1 Diagram showing the thermal neutron beam for neutron radiography
at the Thai Research Reactor TRR1/M1.

(a) 65°C   (b) 70°C   (c) 75°C   (d) 80°C
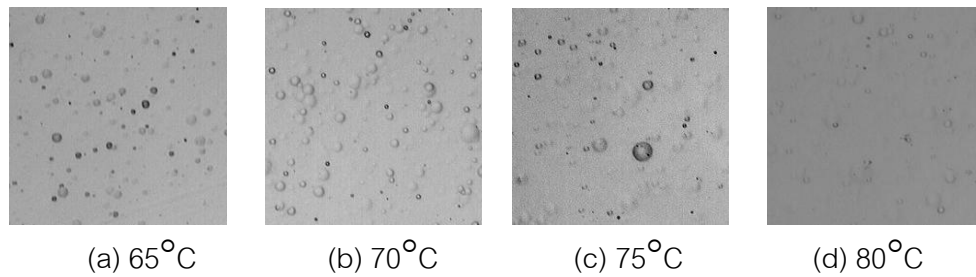
Figure 4.2 Proton track images on PC (x 100) at different etching temperatures.

(a) 65°C   (b) 70°C   (c) 75°C   (d) 80°C
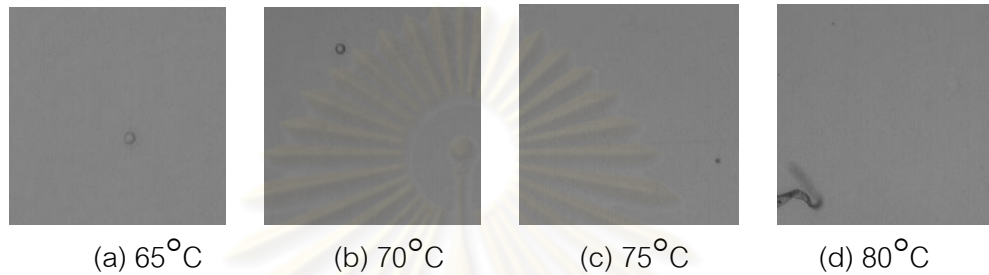
Figure 4.3 Unexposed PC images (x 100) after etching at different temperatures.

The track density of each etching temperature was shown in table 4.1. It showed that track density decreased with increasing of the etching temperature. This was because the etching rate at higher temperature was faster than at lower temperature. The etching time of 1 hour was too long for higher temperatures, thus some of proton tracks nearer to the surface were already removed as could be clearly seen in Figure 4.2 from (a) to (d). Distribution of track diameter at different etching temperatures i.e. 65, 70, 75 and 80°C was also shown in Table 4.2 and Figure 4.4 - 4.7.

Table 4.1 Track densities at the different temperatures

Etching Temperature	Track density (tracks/ cm^2)	Sensitivity in formation of proton tracks
65°C	1.68×10^5	3.70×10^{-5}
70°C	1.56×10^5	3.44×10^{-5}
75°C	1.55×10^5	3.41×10^{-5}
80°C	1.30×10^5	2.86×10^{-5}

For irradiation time of 1 hour, the neutron fluence or total neutrons at the irradiation position was approximately 1.26×10^6 n/cm^2.s $\times 3600$ s $= 4.54 \times 10^9$ n/cm^2. The sensitivity of PC to neutrons from the research reactor in formation of recoil proton tracks could then be calculated. For example at 65°C, the sensitivity was $(1.68 \times 10^5$ tracks/cm^2) $\div (4.54 \times 10^9$ n/cm^2) $= 3.70 \times 10^{-5}$.

Table 4.2 Distribution of track diameter at different temperatures

Track diameter (µm)	Number of track in percentage (%)			
	65°C	70°C	75°C	80°C
2	8	3	2	3
3	18	7	2	11
4	16	9	6	10
5	19	8	14	8
6	19	21	20	15
7	17	16	18	19
8	4	12	16	6
9	8	9	10	8
10	3	7	9	4
11	4	8	1	2
12	1	6	4	2
13	5	4	1	2
14	0	2	2	3
15	0	1	5	1
16	0	0	2	1
17	0	0	1	0
18	0	0	1	0
>19	0	0	1	0
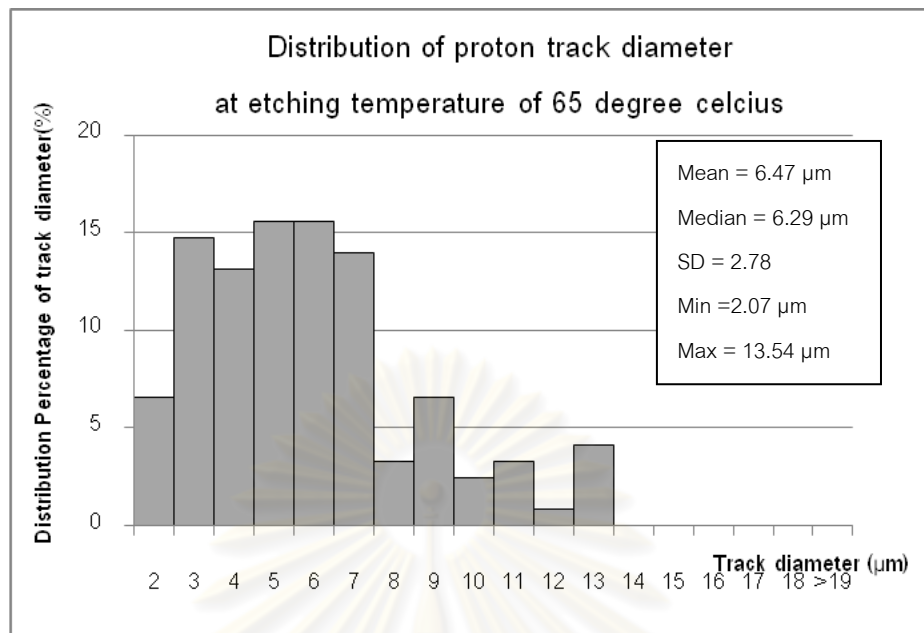
Figure 4.4 Distribution of track diameter at etching temperature 65°C.
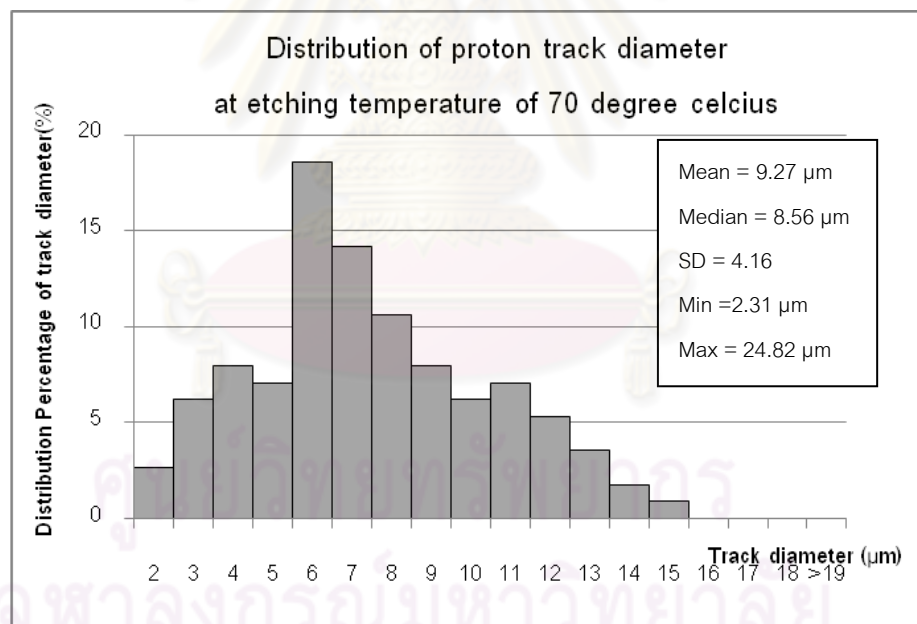
Figure 4.5 Distribution of track diameter at etching temperature 70°C.
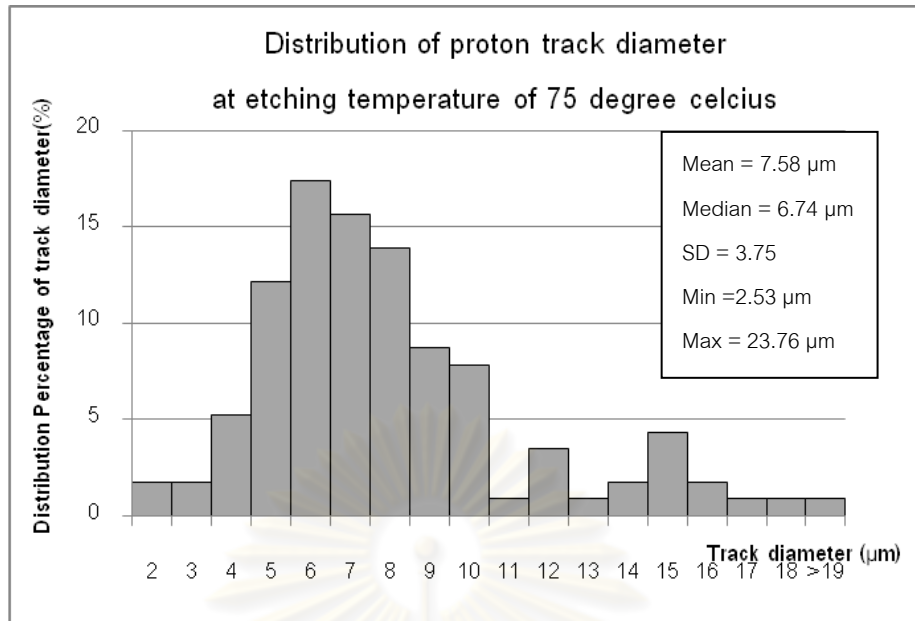
Figure 4.6 Distribuyion of track diameter at etching temperature 75°C.
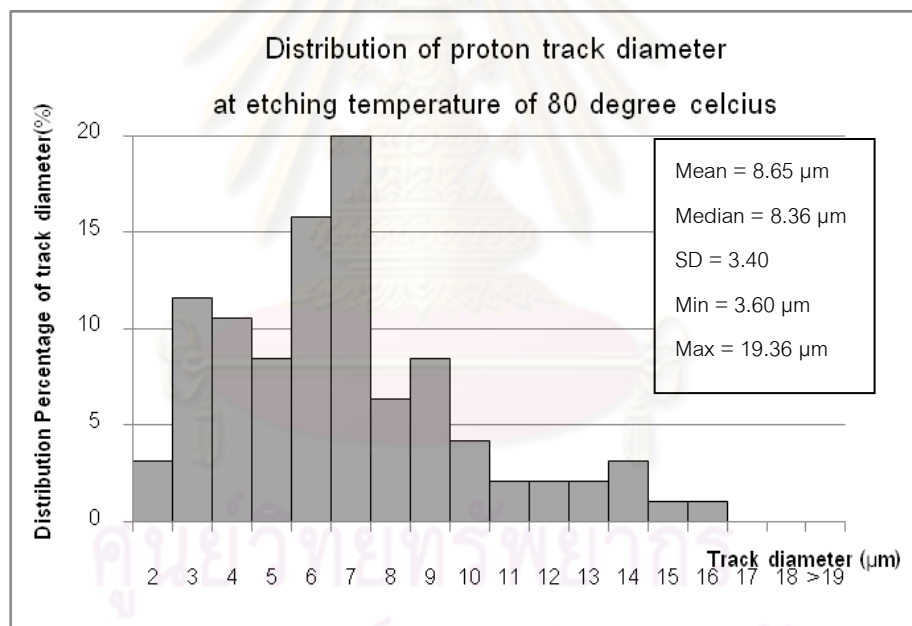
Figure 4.7 Distribution of track diameter at etching temperature 80°C.

Table 4.3 showed the mean, median, standard deviation (SD), minimum and maximum values of track diameter in each etching temperature.

Table 4.3 Track diameter statistics for each etching temperatures

Etching temperature	Track diameter (µm)				
	Mean	Median	SD	Minimum	Maximum
65°C	6.47	6.29	2.78	2.07	13.54
70 $^\circ$C	9.27	8.56	4.16	2.31	24.82
75 $^\circ$C	7.58	6.74	3.75	2.53	23.76
80 $^\circ$C	8.65	8.36	3.40	3.60	19.36

As illustrated in Figures 4.4 - 4.7, distribution of track diameter at the different etching temperatures was in similar pattern but different in track diameter particularly between 65°C and other etching temperatures. The track diameters at the 65°C were mainly in the range of 3 - 7 micrometers (µm) while the mean and median of track diameter were 6.47 µm and 6.29 µm respectively. There was no track with the diamerter greater than 15 µm. Distribution of track diameter at 70, 75 and 80 $^\circ$C etching temperatures was similar to at 65 $^\circ$C but the average track diameters were larger.

Light transmission through PC in three regions, i.e. ultraviolet (UV), visible light and infrared (IR), were carried out by using a SPECTRUM DETECTIVE Transmission Meter SD2400 the results are shown in Table 4.4.

Table 4.4 Percentage of light transmission at the different temperatures

Light region	Percentage of transmission						
	No PC (Blank)	$C_{no\ etch}$	C_{etch}	65 $^\circ$C	70 $^\circ$C	75 $^\circ$C	80 $^\circ$C
UV	100	0	0	0	0	0	0
Light	100	85	85	76	79	77	80
IR	100	91	92	83	84	83	87

Note : $C_{no\ etch}$= unexposed PC without etching

C_{etch} = unexposed PC etched at the 80°C for 1 hr

The results showed that PC itself could completely absorb UV while 85 % of visible light and 92 % of IR could transmit through the etched-unexposed PC. This was due to inherent property of PC. For etched PC having recoil proton tracks, percentage of visible light and IR transmission decreased in comparison to the PC with no tracks. at 65, 70 and 75 $^{\circ}$C were not different significantly. But the percentage of visible light transmission were different. Light transmited track-etched PC at 65 $^{\circ}$C less than the other conditions. The probably reason was the bigger number of track density.   The percentage of visible light and IR transmission of PC at 80 $^{\circ}$C was increased again due to some of tracks on the surface were removed.

4.2 Formation of proton tracks using neutrons from a Cf-252 source

Californium-251 (^{252}Cf) is a small sealed neutron source normally used for neutron activation analysis (NAA), neutron-induced prompt gamma-ray analysis, neutron radiography, moisture measurement, etc. It gives high neutron output, approximately 2.3×10^{6} neutrons/second per microgram, from spontaneous fission with a half-life of 2.6 years and the average neutron energy of 2 MeV [Appendix A]. It is most practical for use in producing track-etched PC as light filter and/or diffuser. This study is, therefore, focused on using a Cf-252 source. The source at the time of this investigation (June, 2010) had the neutron output of approximately 5×10^{6} n/s which gave maximum thermal neutron flux of about 5×10^{4} n/cm^{2}.s in water from the source. Neutron flux at other distances is shown in Figure 3, Appendix A. Neutrons irradiation was carried out by placing 4 pieces of PC chips under water at a desired position. The neutron irradiated PC chips were then etched under various conditions and tested as in the previous experiment.

4.2.1 Effects of etching temperature and etching time

Theoretically, formation of recoil proton tracks is dependent on neutron energy spectrum. As mentioned earlier, the cadmium ratio was about 200 for thermal neutrons from the neutron radiography tube at the nuclear reactor. For the Cf-252 source, it has been reported that the cadmium ratio was 10 – 20 [26] which was about 10 – 20 times lower. This means the average thermal neutron energy in water from the Cf-252 was higher. Formation of proton tracks and effects of etching temperature and etching time

may be in different degrees. Therefore, the experiment had to be repeated to investigate effects of etching temperature and etching time as well as to determine the sensitivity of PC to neutrons.

Proton tracks on PC were created by irradiating with neutrons from the Cf-252 for 1 day. The maximum thermal neutron flux of about 5×10^4 n/cm^2.s in water from the source. Twenty four pieces of PC chips were put into an aluminum box and placed 1 cm from the Cf-252 source in order to obtain the maximum neutron flux (as illustrated in Figure 4.8). The selected etchant was still PEW solution using etching temperatures varied from 65, 70 and 75°C and etching times varied from 15, 30, 45, 60 and 90 minute (min). After etching, the recoil proton tracks were observed under an optical microscope with magnification of X100. The track density and track diameter were then analyzed by using the ImageJ software. Finally, light transmission through the track-etched PC was measured by using the SPECTRUM DETECTIVE Transmission Meter SD2400. The results are shown in Table 4.4. The results indicated that at etching temperature 80°C, track density decreased and track size increased due to too high temperature.
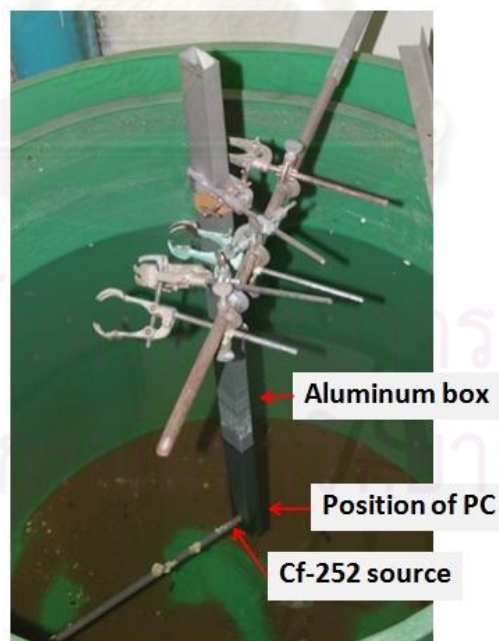
Figure 4.8 Cf-252 neutron irradiation facility.

Figures 4.9 - 4.10 illustrate the images of proton tracks on PC chips at different etching times at 65°C etching temperature. Figure 4.9 shows track images on the front

side of the PC chips (closer to Cf-252 source) while Figure 4.10 shows track images on the reverse side.

(a) 15 min.   (b) 30 min.   (c) 45 min.

(d) 60 min.   (e) 75 min.   (f) 90 min.
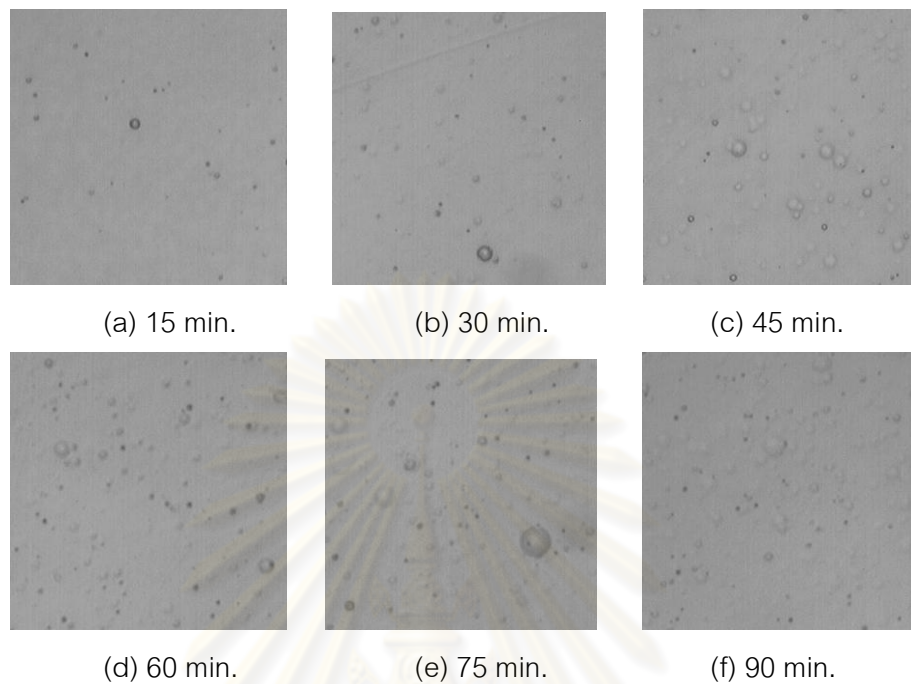
Figure 4.9 Track images (x100) on the front side of PC at different etching times and etching temperature 65°C.

(a) 15 min.   (b) 30 min.   (c) 45 min.

(d) 60 min.   (e) 75 min.   (f) 90 min.
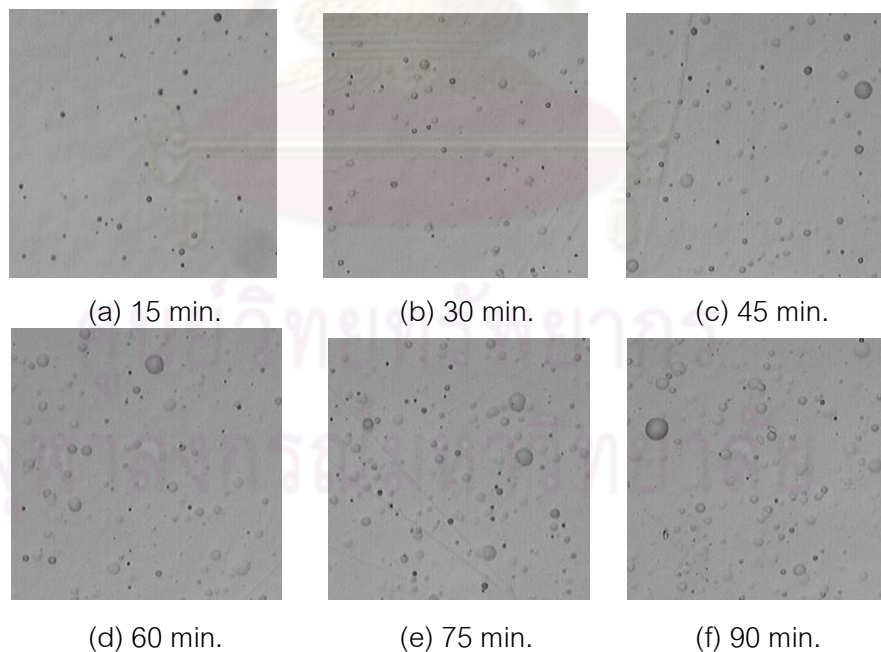
Figure 4.10 Track images (x100) on the reverse side of PC at different etching times and etching temperature 65°C.

Figures 4.11 - 4.12 illustrate the images of proton tracks on PC chips at different etching times at 70°C etching temperature. Figure 4.11 shows track images on the front side of the PC chips (closer to Cf-252 source) while Figure 4.12 shows track images on the reverse side.

| (a) 15 min. | (b) 30 min. | (c) 45 min. |
| (d) 60 min. | (e) 75 min. | (f) 90 min. |
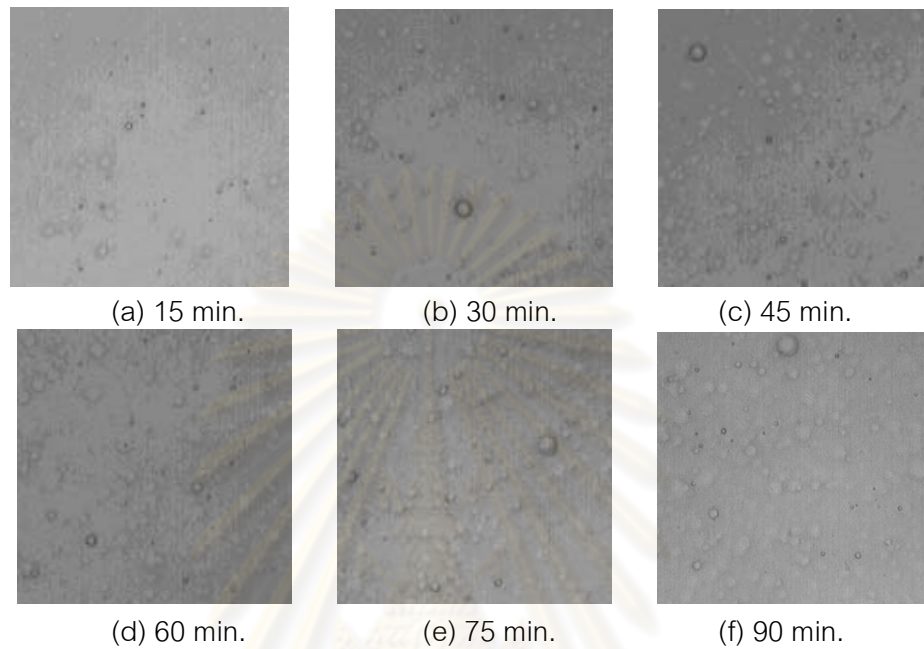
Figure 4.11   Track images (x100) on the front side of PC at different etching times and etching temperature 70°C.

| (a) 15 min. | (b) 30 min. | (c) 45 min. |
| (d) 60 min | (e) 75 min. | (f) 90 min. |
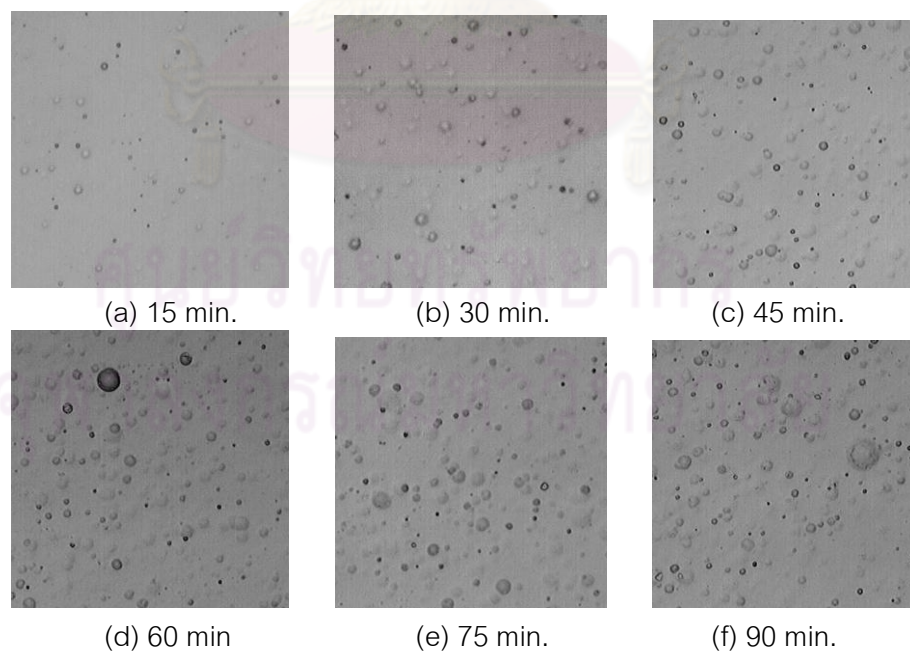
Figure 4.12 Track images (x100) on the reverse side of PC at different etching times and etching temperature 70°C.

Figures 4.13 - 4.14 illustrate the images of proton tracks on PC chips at different etching times at 75°C etching temperature. Figure 4.13 shows track images on the front side of the PC chips (closer to Cf-252 source) while Figure 4.14 shows track images on the reverse side.

| (a) 15 min. | (b) 30 min. | (c) 45 min. |
| (d) 60 min. | (e) 75 min. | (f) 90 min. |
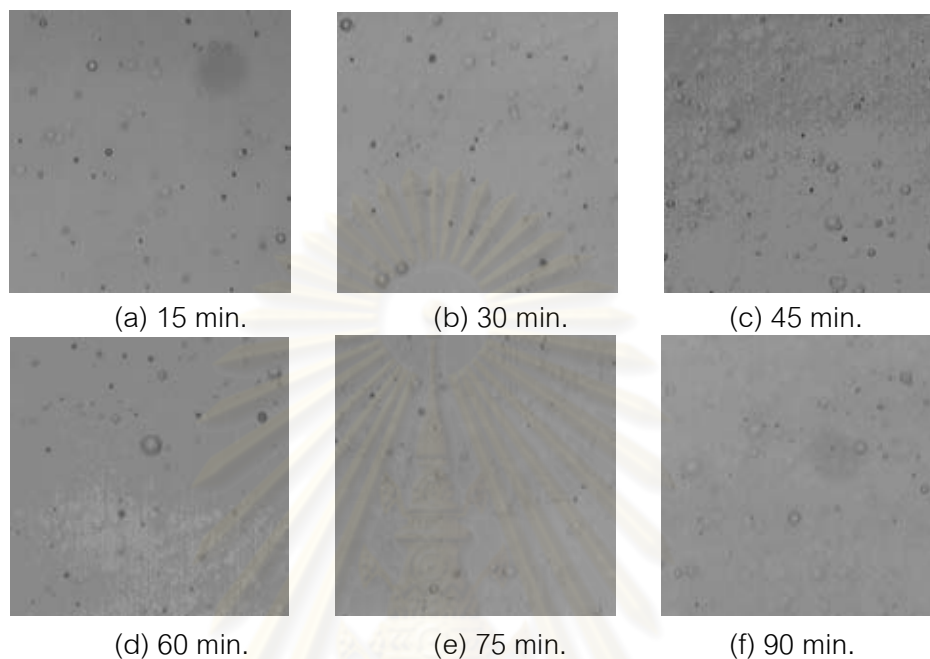
Figure 4.13   Track images (x100) on the front side of PC at different etching times and etching temperature 75°C.

| (a) 15 min | (b) 30 min | (c) 45 min |
| (d) 60 min | (e) 75 min | (f) 90 min |
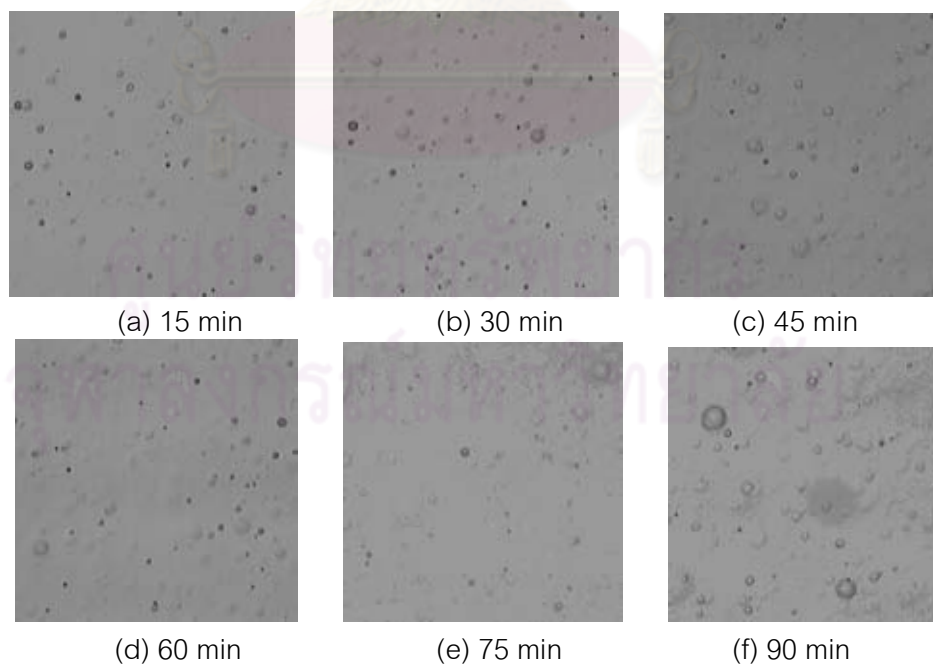
Figure 4.14   Track images (x100) on the reverse side of PC at different etching times and etching temperature 75°C.

Track densities were observed and counted on both sides of each PC chip. The track densities shown in Table 4.5 and Figure 4.15 are the total track density on both sides of the chip.

Table 4.5 Track density at different etching times and etching temperatures

Etching time	Track density (tracks/ cm^2)		
	65°C	70°C	75°C
15	1.52 x 10^5	2.44 x 10^5	2.86 x 10^5
30	2.31 x 10^5	3.26 x 10^5	3.60 x 10^5
45	3.08 x 10^5	3.84 x 10^5	4.12 x 10^5
60	3.41 x 10^5	4.21 x 10^5	3.01 x 10^5
75	3.85 x 10^5	2.77 x 10^5	2.37 x 10^5
90	3.87 x 10^5	3.24 x 10^5	2.57 x 10^5

Figure 4.15   Relationship between track density and etching time at different

temperatures: 65, 70 and 75°C.

The results showed that the optimum etching times for the maximum track densities at etching temperatures 65, 70 and 75°C were 75, 60 and 45 minutes respectively. At etching temperature of 70 and 75°C, the track densities increase with increasing of the etching time up to the maximum values then level off. For prolong etching time, the tracks on the surface were gradually removed resulting in decrease in track density.

Tables 4.6 - 4.8 shows distribution of track diameter at etching temperatures 65, 70 and 75 $^\circ$C respectively.

Table 4.6 Distribution of track diameter at etching temperature 65 $^\circ$C

Track size (µm)	Number of track in percentage					
	15 min	30 min	45 min	60 min	75 min	90 min
1	3.92	5.77	2.38	0.00	0.76	2.61
2	21.57	15.38	11.90	12.93	10.98	8.96
3	31.37	17.95	13.33	16.38	19.32	9.33
4	18.63	16.03	14.76	18.53	17.42	18.66
5	12.75	10.90	16.19	15.95	13.26	13.06
6	8.82	10.26	15.24	12.93	12.12	9.70
7	1.96	8.33	6.67	9.05	6.82	7.09
8	0.00	5.77	6.67	6.03	8.33	9.33
9	0.98	6.41	2.86	3.45	4.55	7.09
10	0.00	1.92	2.86	0.43	3.03	3.73
11	0.00	0.00	3.33	1.72	0.38	3.36
12	0.00	0.64	0.95	0.43	0.76	2.24
13	0.00	0.00	1.43	0.86	0.38	1.87
14	0.00	0.00	0.48	0.43	0.00	0.37
15	0.00	0.00	0.48	0.00	0.38	0.75
16	0.00	0.00	0.00	0.43	0.00	0.00
17	0.00	0.00	0.00	0.00	0.76	0.75
18	0.00	0.64	0.48	0.43	0.76	1.12
>19	3.92	5.77	2.38	0.00	0.76	2.61

Table 4.7 Distribution of track diameter at etching temperature 70 $^{\circ}$C

Track size	Number of track in percentage					
(μm)	15 min	30 min	45 min	60 min	75 min	90 min
1	0.00	0.00	0.00	0.00	0.50	0.00
2	6.10	3.96	4.17	6.78	2.51	4.66
3	19.51	10.13	12.88	13.22	9.55	14.83
4	12.20	10.57	10.23	13.90	13.07	13.14
5	18.90	13.66	12.12	10.85	7.54	13.56
6	10.37	9.69	7.20	11.86	15.58	10.17
7	10.98	10.57	10.23	7.46	9.55	7.20
8	10.98	9.25	9.09	7.12	8.04	9.75
9	3.05	6.17	11.36	7.80	7.54	5.08
10	3.66	7.05	6.06	5.42	9.05	5.51
11	3.66	4.85	4.92	3.39	2.51	2.54
12	0.61	3.96	5.30	4.07	5.03	2.97
13	0.00	4.41	3.03	2.03	2.51	1.69
14	0.00	2.20	1.14	2.03	0.50	1.27
15	0.00	1.32	0.76	1.02	2.51	0.85
16	0.00	0.88	0.38	1.02	0.50	0.85
17	0.00	0.88	0.76	0.68	0.50	1.27
18	0.00	0.44	0.00	0.00	1.51	0.42
19	0.00	0.00	0.38	0.34	0.00	0.85
>20	0.00	0.00	0.00	1.02	1.51	3.39

Table 4.8 Distribution of track diameter at etching temperature 75 °C

Track size	Number of track in percentage					
(µm)	15 min	30 min	45 min	60 min	75 min	90 min
1	0.00	0.81	0.00	0.00	0.00	0.00
2	2.60	8.54	8.13	1.46	4.42	2.67
3	24.48	17.89	21.55	20.87	17.13	6.95
4	14.06	14.23	13.43	20.39	9.39	7.49
5	10.42	15.85	6.71	13.59	4.97	8.56
6	19.27	11.79	7.42	6.80	4.42	13.37
7	10.94	8.13	10.25	10.19	2.76	8.02
8	7.81	6.91	10.95	7.28	9.39	11.76
9	5.21	3.66	3.89	4.37	6.63	8.02
10	3.65	2.85	3.53	5.83	5.52	3.74
11	1.04	3.25	4.24	3.40	8.84	4.81
12	0.52	3.25	1.41	1.94	6.08	4.81
13	0.00	0.81	1.77	0.49	6.63	5.35
14	0.00	0.41	4.59	1.46	1.66	6.95
15	0.00	0.81	1.06	0.00	2.76	3.21
16	0.00	0.00	0.35	0.49	1.10	0.53
17	0.00	0.41	0.00	0.49	1.66	1.60
18	0.00	0.00	0.35	0.49	0.55	1.07
19	0.00	0.00	0.35	0.00	2.21	0.53
>20	0.00	0.41	0.00	0.49	3.87	0.53

Figures 4.16 - 4.18 illustrate distribution track diameter in percentage at different etching times and etching temperatures of 65, 70 and 75 °C, respectively.
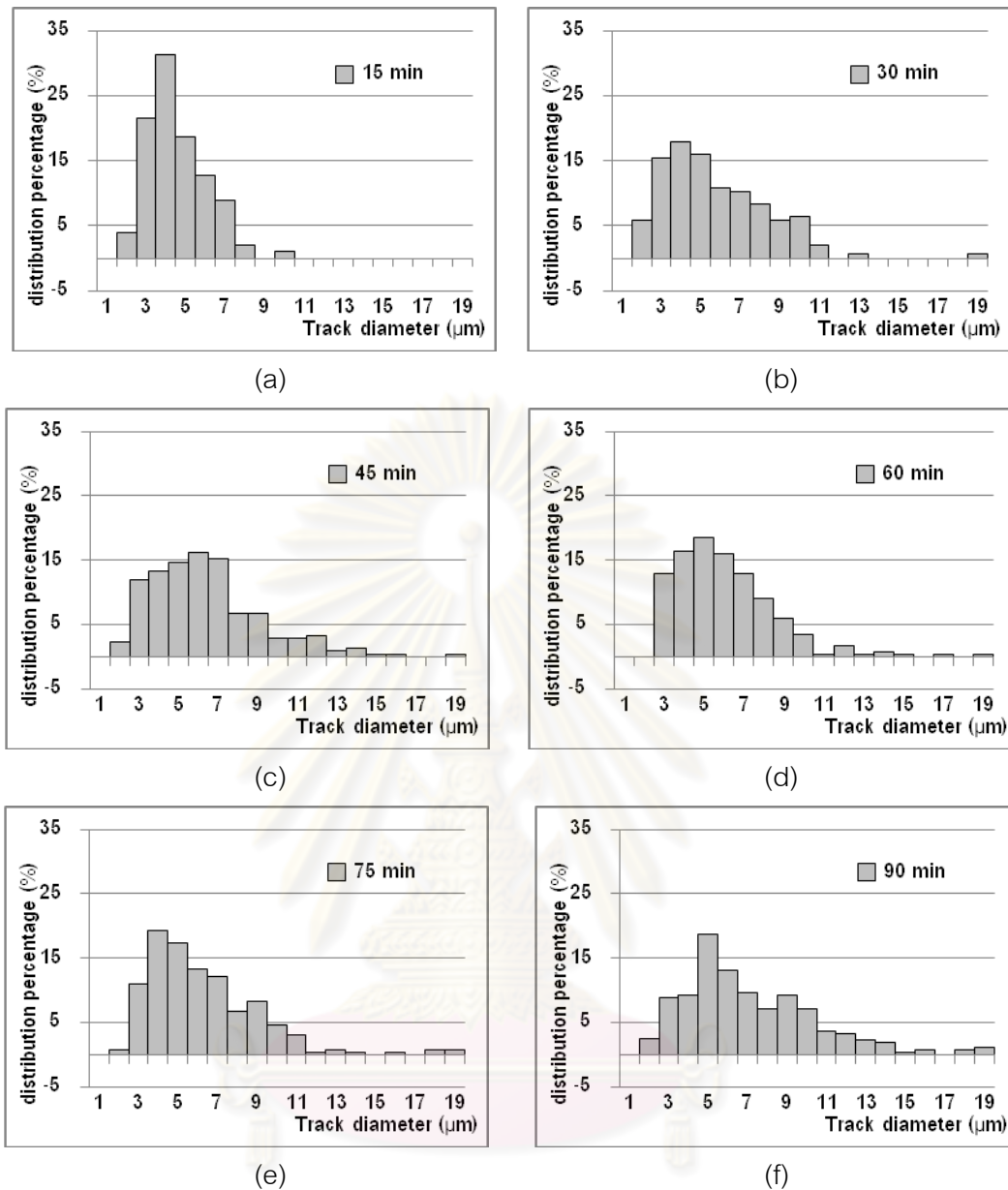
Figure 4.16 Distribution of track diameter at 65°C for different etching times.

Figure 4.16 (a) demonstrated that track diameter in shorter etching time distributed in small diameter. It was a conical phase of etching period. For the etching time 15 min, track diameter distributed in 3-5 μm and no track diameter was larger than 10 μm. When etching time increased, track diameter was larger due to prolonged etching time led to transitional and spherical phase [8].
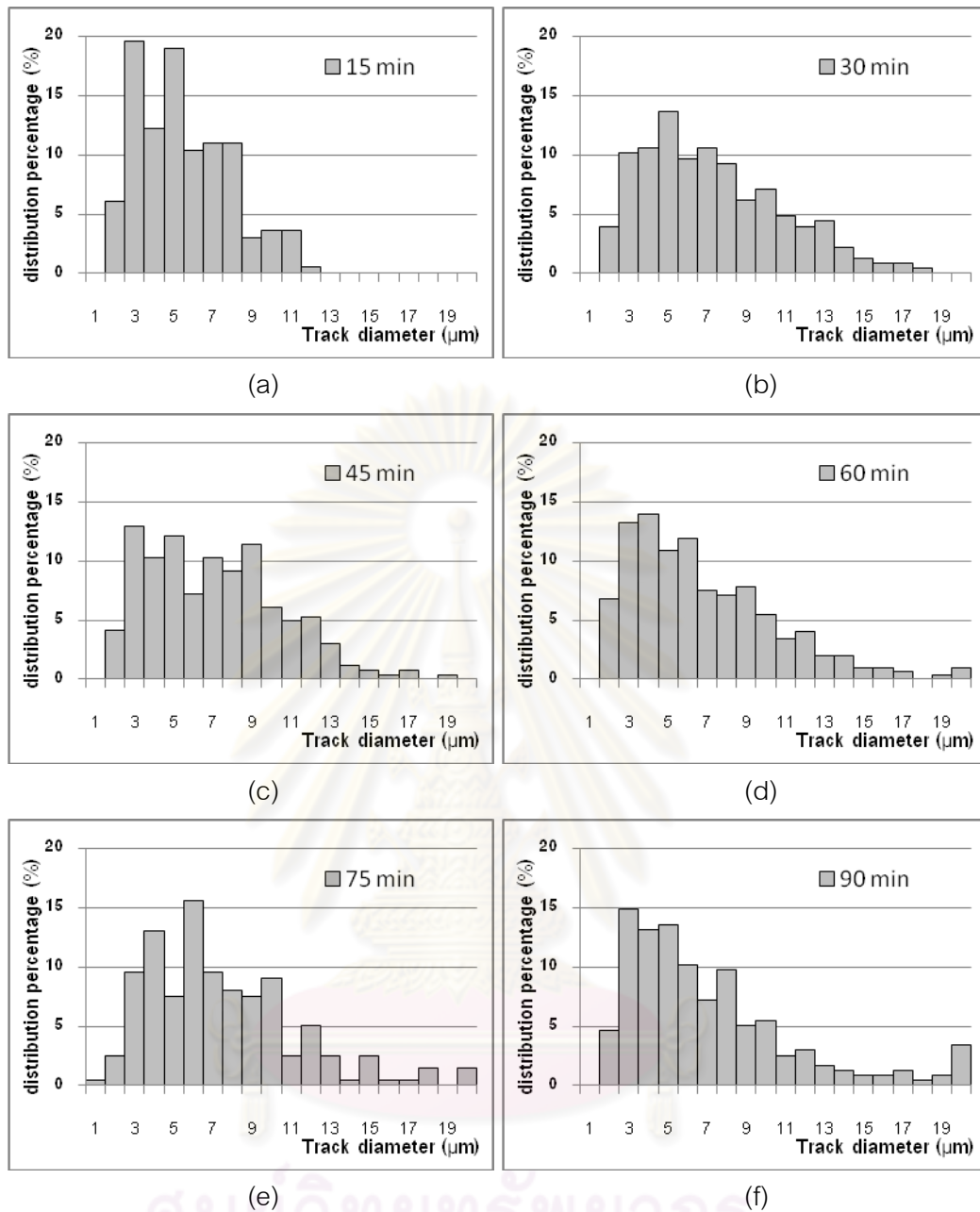
Figure 4.17 Distribution of track diameter at 70°C for different etching times.

At etchant temperature 70°C, etchng time 15 min, track diameter distributed to larger size than etchant temperature 65°C, etchng time 15 min. Mean of track diameter was also larger. The distribution of track diameter in other etching times distributed randomly. When etching time increased, track diameter increased.
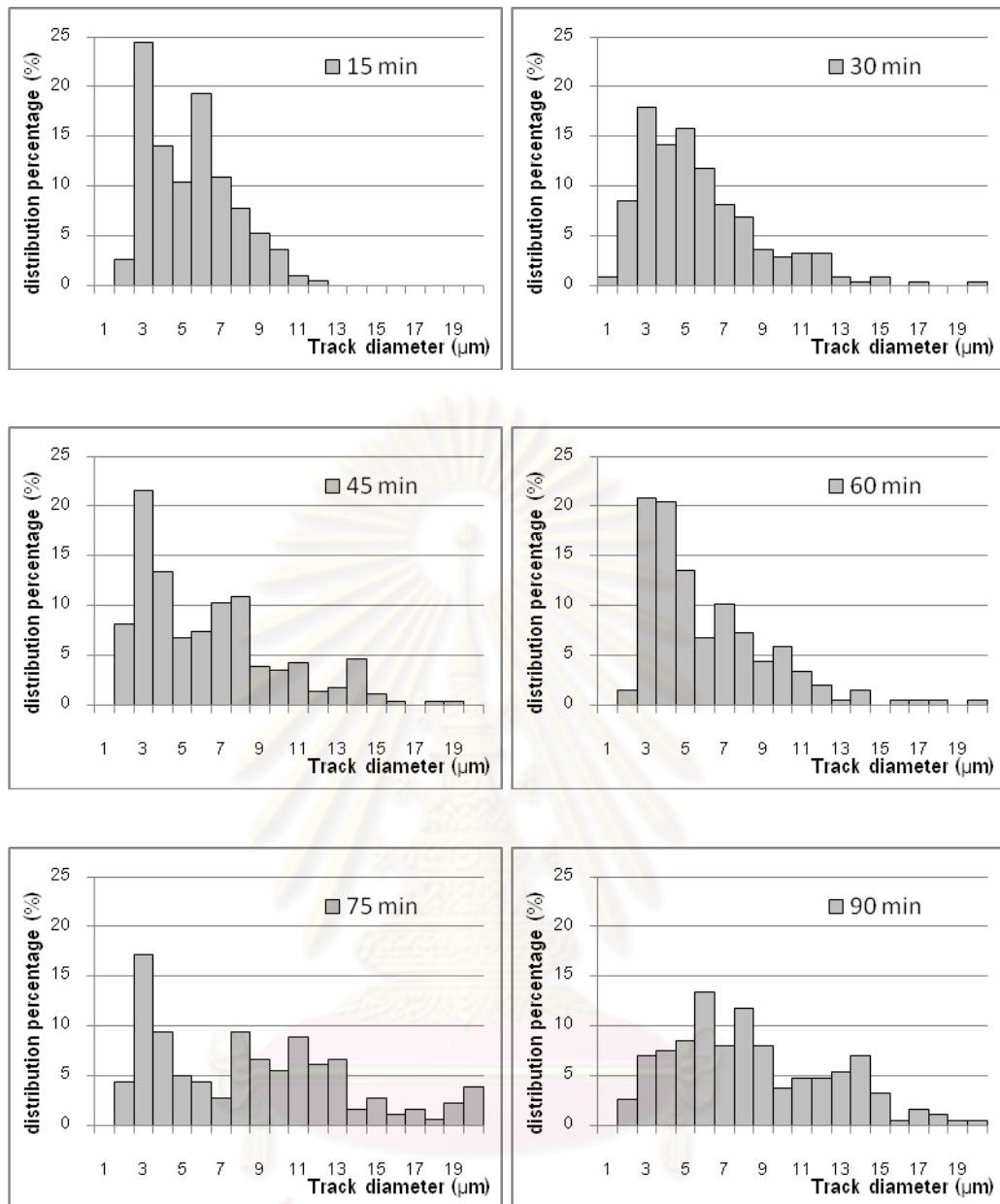
Figure 4.18 Distribution of track diameter at 75°C for different etching times.

Pattern of distribution of track diameter at 75°C at etching time 15 min was same as at 70°C. When etching time increased, track diameter distributed to larger size too. But distribution of track diameter at etching time 45 and 60 min were shifted to the smaller value again due to some of new proton tracks in the PC was observed.

Table 4.9 -4.11 showed the mean, median, standard deviation (SD), minimum and maximum values of track diameter in each etching time at etchant temperature 65, 70 and 75 °C, respectively.

Table 4.9 Statistic values of track diameter in each etching time at 65°C

Etching time (min)	Track diameter (µm)				
	Mean	Median	SD	Minimum	Maximum
15	5.01	4.57	1.49	2.19	10.32
30	6.17	5.69	2.64	2.19	19.75
45	6.92	6.66	3.10	2.31	25.66
60	7.00	6.23	2.57	3.02	19.29
75	6.79	6.08	3.19	2.43	31.63
90	7.57	6.62	3.39	2.19	19.57

Table 4.10 Statistic values of track diameter in each etching time at 70°C

Etching time (min)	Track diameter (µm)				
	Mean	Median	SD	Minimum	Maximum
15	6.02	5.59	2.39	2.31	12.17
30	7.78	7.28	3.53	2.53	18.70
45	7.59	7.28	3.41	2.19	19.72
60	7.32	6.50	3.80	2.19	24.88
75	7.96	7.05	4.74	1.64	23.20
90	7.72	6.35	3.81	2.19	32.13

Table 4.11 Statistic values of track diameter in each etching time at 75°C

Etching time (min)	Track diameter (µm)				
	Mean	Median	SD	Minimum	Maximum
15	5.91	5.71	2.26	2.07	12.33
30	6.20	5.47	3.14	1.94	22.47
45	6.79	6.25	3.19	2.31	19.90
60	6.55	5.47	3.46	2.64	29.76
75	9.12	8.78	5.11	2.31	27.17
90	8.93	8.47	4.03	2.31	22.07

The mean and median of track diameter at 65 and 70°C in each etching time were not different significant. But Mean and median of track diameter at 75°C in each etching time were different significant.

Table 4.12 showed percentage of light transmission at the different temperature. All of track-etched PCs were decreased visible and IR transmissions compare to control PC with etching and control without etching and with neutron irradiation. UV was absorbed by thickness of PC. The transmission of visible light and IR at shorter etching time was less effect than longer etching time. Those mean the distribution of track diameter affect the transmission of visible light and IR. The results showed that PC with variation of distribution of track diameter affect the transmission of light and IR.

Table 4.12 Percentage of light transmission at the different temperature

Etching time condition	Percentage of transmission (%)								
	65°C			70°C			75°C		
	UV	Visible light	IR	UV	Visible light	IR	UV	Visible light	IR
No PC	100	100	100	100	100	100	100	100	100
$C_{no\ etch}$	0	85	92	0	85	92	0	85	92
C_{etch} 90 min	0	84	91	0	84	92	0	84	92
15 min	0	83	91	0	82	89	0	83	91
30 min	0	82	90	0	82	88	0	82	90
45 min	0	81	89	0	82	88	0	81	88
60 min	0	80	88	0	80	87	0	81	89
75 min	0	80	88	0	80	87	0	80	88
90 min	0	80	88	0	80	87	0	80	87

Note: $C_{no\ etch}$ no etch was control PC without etching

C_{etch} was control PC with etching for 90 min

The transmission of UV through all of PCs was totally absorbed by inherent properties of PC. Shorter etching time led to less track density and distribution of smaller track diameter, it will not affect the transmission of visible light and IR. The distribution within larger diameter and larger track density will increase the effect of transmission of visible light and IR. But they were not different significant.

From the above data of track density, distribution percentage of track diameter and percentage of light transmission in each temperature was found that proton track on PC affected percentage of visible light and infrared transmission.

.4.2.2 Variation condition of tracked-etch PC

Track-etched PC was formed in different condition of track density, etching time and etchant temperature in order to correlate with transmission of light. The condition of PC was divided into six conditions following as Table 4.13 to form the different track size, shape (Figure 4.19) and track density (Table 4.14). In this study, track density and size were analyzed only reverse side of PC.

Table 4.13 Condition of neutron irradiation, etchant temperature and etching time

	irradiation time	PEW($^\circ$C)	etching time
condition 1	3 days	75	15 min
condition 2	3 days	70	15 min
condition 3	3 days	65	30 min
condition 4	7 days	70	45 min
condition 5	3 days	70	35 min
condition 6	7 days	70	60 min

Table 4.14 Track densities in various conditions

Condition	Track density on one side (tracks/ cm^2)	Sensitivity in formation of proton tracks [*]
1	3.04×10^5	2.3×10^{-5}
2	3.74×10^5	2.9×10^{-5}
3	3.85×10^5	3.0×10^{-5}
4	5.39×10^5	1.8×10^{-5}
5	5.83×10^5	4.5×10^{-5}
6	1.11×10^6	3.7×10^{-5}

[*] = obtained from track density (tracks/cm^2) divided by neutron fluence (n/cm^2)

Track density on PC condition 4 and 5 was more than condition 1-3 about 1 time and condition 6 was more than condition 1-3 about 2 times .
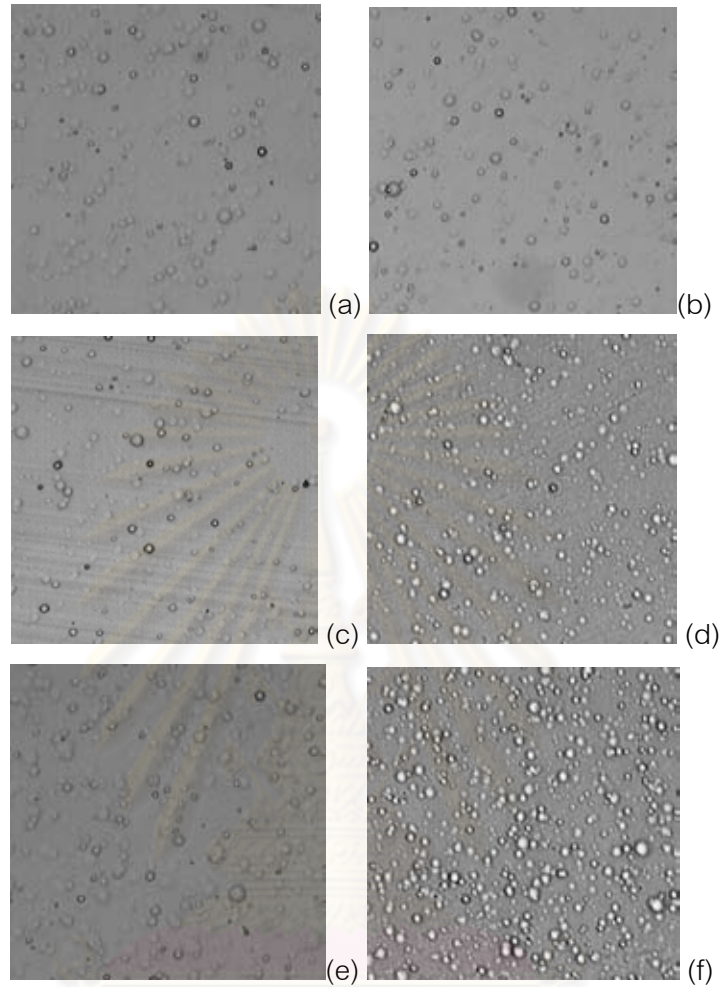
Figure 4.19 Capture track image (400x400 pixels) on the reverse side in various conditions (a) condition 1, (b) condition 2, (c) condition 3, (d) condition 4, (e) condition 5 and (f) condition 6.

The distribution percentage of track diameter was shown in Table 4.15 and plotted curve shown as Figure 4.20. Table 4.16 showed the mean, median, standard deviation (SD), minimum and maximum values of track diameter in each condition.

Table 4.15 Distribution of track diameter at different conditions

Track size	Number of track in percentage (%)					
(µm)	Condition 1	Condition 2	Condition 3	Condition 4	Condition 5	Condition 6
1	0.00	0.00	0.00	0.00	0.00	0.00
2	1.48	4.38	0.78	0.83	3.05	0.00
3	1.48	8.37	5.04	1.94	14.97	0.27
4	6.40	10.76	8.53	4.43	16.50	2.68
5	10.84	14.34	23.26	24.38	16.50	11.54
6	12.32	14.74	21.71	29.92	12.94	27.92
7	14.78	17.13	15.50	18.01	12.18	25.64
8	18.23	14.34	13.57	9.97	11.17	15.44
9	13.79	7.97	8.14	6.37	4.82	8.05
10	8.37	5.58	2.71	2.77	2.79	4.56
11	6.90	1.59	0.78	0.83	3.30	2.55
12	1.48	0.80	0.00	0.55	0.51	0.81
13	1.48	0.00	0.00	0.00	0.51	0.27
14	2.46	0.00	0.00	0.00	0.25	0.00
15	0.00	0.00	0.00	0.00	0.25	0.27
16	0.00	0.00	0.00	0.00	0.25	0.00

Table 4.16 Statistic values of track diameter in each conditions

Condition	Track diameter (µm)				
	Mean	Median	SD	Minimum	Maximum
1	8.13	8.04	2.44	2.74	14.84
2	6.76	6.78	2.21	2.31	12.77
3	6.71	6.58	1,82	1.03	12.52
4	7.81	7.51	1.64	1.03	13.31
5	6.35	5.94	2.46	2.19	16.61
6	7.53	6.50	1.65	3.10	15.97
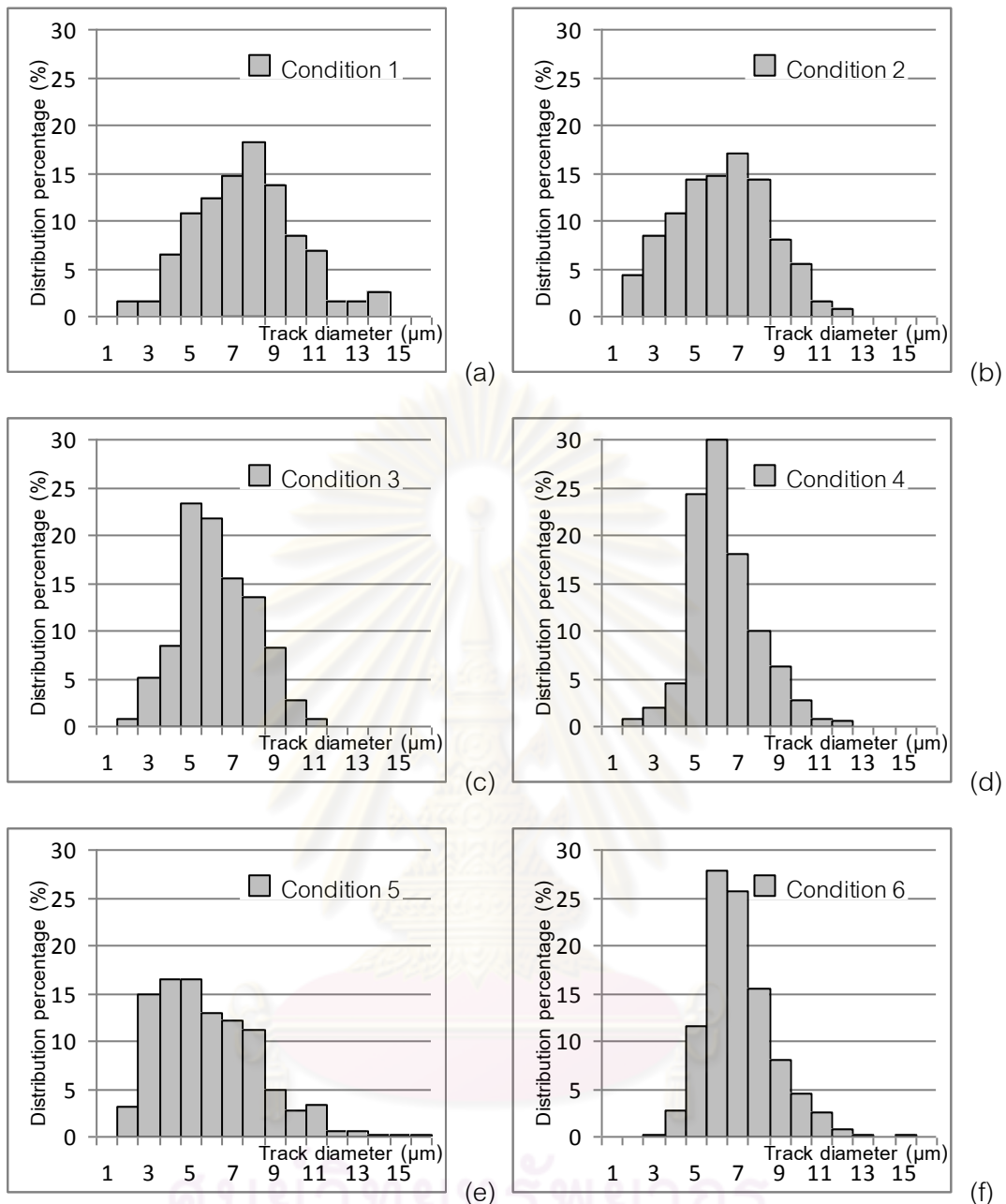
Figure 4.20 Distribution of track diameter for different conditions.

From Table 4.14 and Figure 4.20 showed that track density and distribution of track diameter in each condition were different. The distribution percentage of track diameter can be divided into two patterns. First pattern was condition 1, 2 and 5. Track diameters were distributed randomly in wide range of diameter. Their standard deviations were 2.44, 2.21 and 2.46, respectively. Second pattern was condition 3, 4 and 6. Distribution of diameter in each condition was different from first pattern. It varied within narrow range of track diameter. Their standard deviations were 1.82, 1.64 and 1.65, respectively.

Table 4.17 showed percentage of transmission of UV, visible light and IR through the different track-etched PCs.

Table 4.17 Percentage of light transmission at different conditions

	Percentage of transmission (%)								
	no PC	$C_{no\ etch}$	C_{etch}	#1	#2	#3	#4	#5	#6
UV	100	0	0	0	0	0	0	0	0
Light	100	85	84	81	79	80	81	77	72
IR	100	91	91	88	86	88	90	84	80

The results showed that UV was absorbed by all of PCs. The minimum and maximum effects of track-etched PCs to percentage of light and IR transmission were condition 4 and 6, respectively. This study showed that the different track density and different distribution of track diameter affected percentage of light and IR transmission. Larger of track density and distribution of track diameter within wide range increased the effect of transmission of visible light and IR.

The simplified experiment on transmission of laser pointer beam was set to observe the effect of laser light transmission (Figure 4.21). The wavelenght of laser pointer was 650-670 nanometer (nm). Figure 4.22 displayed the projected image of laser pointer beam transmitted through track-etched PC.
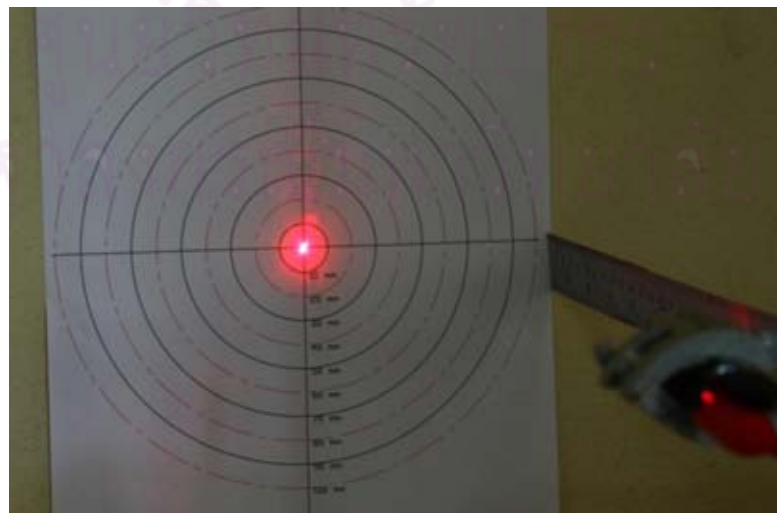
Figure 4.21 Setting of experiment on transmission of laser beam from laser pointer.
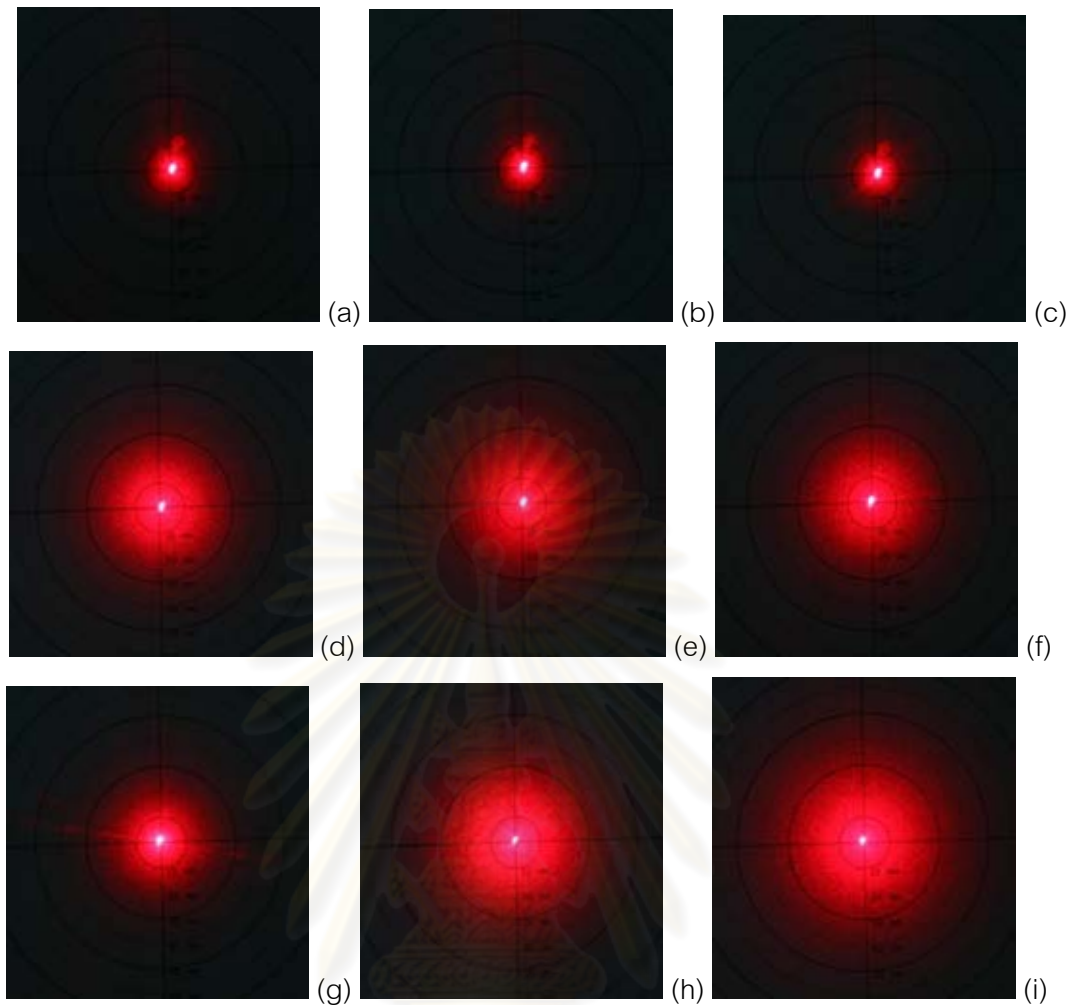
Figure 4.22 Projected image of laser pointer beam transmitted through track-etched PC in various conditions: (a) No PC, (b) PC with etching, (c) PC with neutronirradiation, without etching, (d) condition 1, (e) condition 2, (f) condition 3, (g) condition 4, (h) condition 5 and (i) condition 6.

Projected images of laser pointer beam transmitted through track-etched PC in various conditions were analyzed by using plot profile of ImageJ software in order to change to intensity profile. It was shown as Figure 4.23.
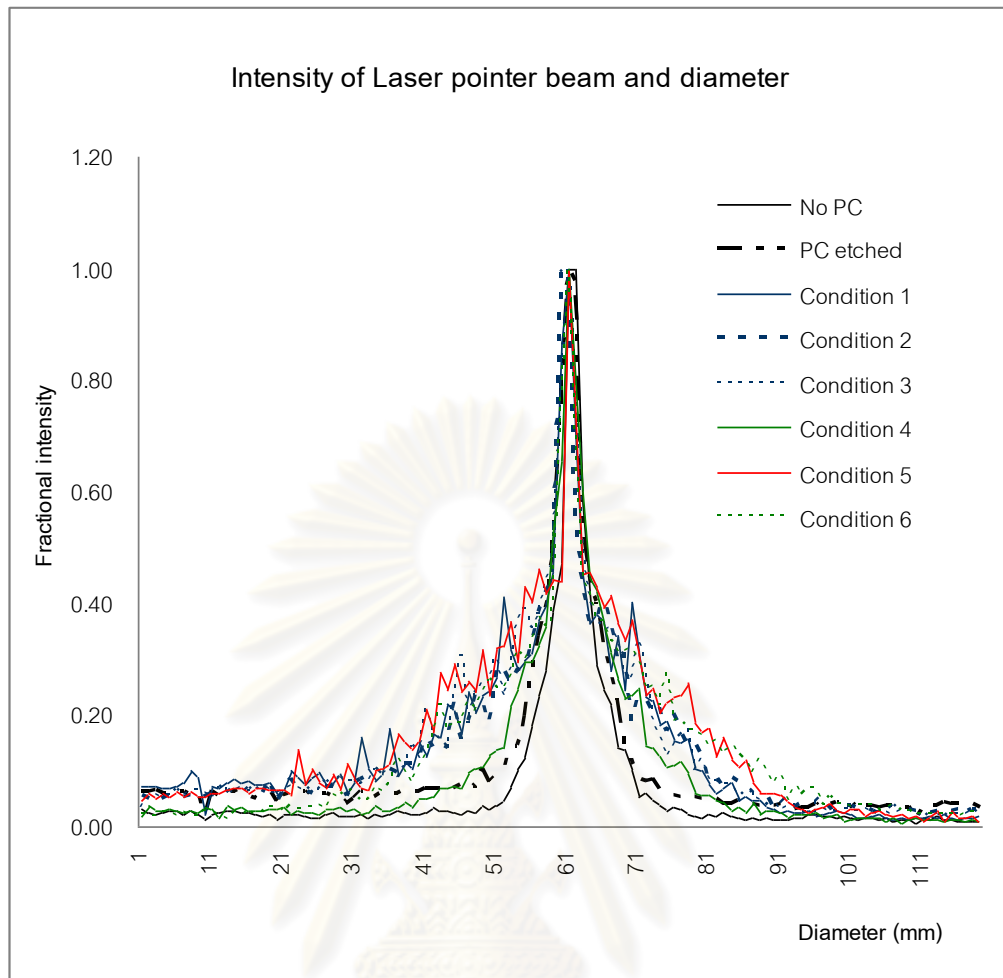
Figure 4.23 Intensity profile of projected image of laser pointer beam transmitted through track-etched PC in various conditions.

The results showed that the projected image of laser beam transmission was related to the percentage of IR transmission in table 4.10. Projected image of laser beam of No PC, PC with etching condition were not different. PC with condition 5 and 6 diffused laser pointer beam more than the condition of No PC and PC with etching about 3 times. The minimum diffusion effect of laser pointer beam was PC in condition 4. The result corresponded with the percentage of IR transmission.

4.2.3 Reproducibility test

The reproducibility test was performed by comparing analysis data of three track-etched PCs irradiated and etched with the same condition in terms of track density, track diameter distribution, mean, median, SD of track diameter and

transmission of UV, visible light and IR. Three pieces of PC chips were irradiated with neutron from Cf-252 source 1day and etched PEW solution at etchant temperature 70°C, 1 hr. The analyzed data were shown in Figure 4.24 and Table 4.18.

Table 4.18 Comparison data of Track density, mean, median, SD and transmission percentage of UV, visible light and IR

	PC no. 1	PC no. 2	PC no. 3
Track density (tracks/cm^2)	3.99×10^5	4.08×10^5	4.11×10^5
Mean (µm)	7.27	7.21	6.97
Median (µm)	6.54	6.33	6.25
SD	3.11	3.33	2.87
Minimum	1.94	2.19	2.83
Maximum	19.56	20.56	19.22
Transmission percentage of			
- Ultraviolet	0	0	0
- visible light	84	84	84
- Infrared	87	86	87

The results showed that track density, the mean and median of track diameter of track-etched PC no. 3 differed from track-etched PC no. 1 and 2 less than 5%. Transmission of UV, visible light and IR of all conditions were not different significant.

Figure 4.24 showed that most probability of track diameter of all track-etched PCs were 5 µm. Distribution of track diameter of track-etched PC no. 1 and 2 were same patterns but track diameter of track-etched PC no. 3 distributed mild differently.
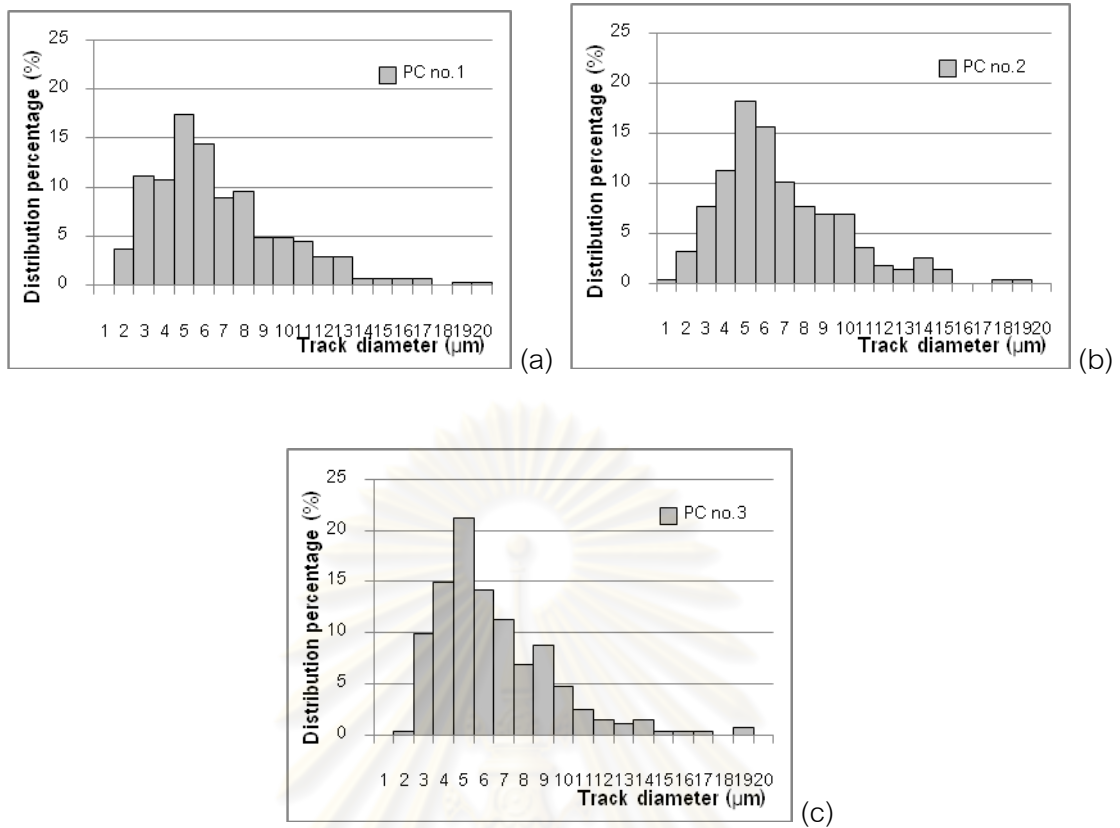
Figure 4.24 Distribution of track diameter of track-etched PC no.1, 2 and 3 with neutron

irradiation time 1 day, etched PEW 70°C, 1 hr.

4.3 Physical properties test of track-etched PC

In this study, two pieces of track-etched PC, PC with etching and original PC chips were tested physical properties in terms of tension and impact strength tests in order to observe the difference. Tension strength was tested by Scientific and Technological Research Equipment Center, Chulalongkorn University and impact strength was done by Department of Science service, Bangkok, Thailand. The test reports were shown in Appendix F. Table 4.19 showed the maximum stress of tensile strength test. The results were not different significant. In part of impact strength test, there was limitation of a hammer load of test at Department of Science service, the maximum load was 22 J. the results showed the impact strength of all of PC conditions were bigger than 22 J or 150 J/cm^{2}.

Table 4.19 Tensile strength test

PC conditions	Tensile strength test: Maximum Stress (kgf/mm^2)
Original PC:	
Piece no. 1	5.15
Piece no. 2	6.41
PC with etched 1 hr:	
Piece no. 1	6.32
Piece no. 2	6.35
PC with neutron irradiated 3 day and etched 1 hr:	
Piece no. 1	6.01
Piece no. 2	5.43

4.4 Design of a Cf-252 neutron irradiation facility

From this investigation, it could be concluded that track-etched polycarbonate can be produced by irradiating PC with thermal neutrons from a Cf-252 source. However, for the source used in this research, the irradiation time about 3 days is practically too long for manufacturing track-etched PC. The source used in this research had originally neutron emission rate of 4.54×10^7 neutrons per second (n/s) on 28th of June 2002 as shown in Figure 3, Appendix A. The emission rate in June 2010 when the experiment was conducted the neutron emission rate was approximately 5×10^6 n/s. The maximum neutron flux in water was therefore only about 5×10^4 n/cm^2.s which was about 100 times lower than that from the research reactor. Therefore, the Cf-252 source strength needs to be increased for production purpose. The sensitivities to neutrons in formation of recoil proton tracks at 1 cm from Cf-252 source were found to be in the range of 1.8×10^{-5} to 4.5×10^{-5} as shown in Table 4.14 which were close to the sensitivity of CR39 track-etched detector in formation of recoil proton tracks of 1.2×10^{-5} as claimed by G. Dajko [31].

The following calculation and design of a Cf-252 neutron irradiation facility is based on 400 μg Cf-252 which gives off 9.2×10^8 neutrons per second. The maximum

neutron flux in water can be obtained from the thermalization factor of Cf-252 which equals 100 [32]. So, the maximum flux equals $9.2 \times 10^8/100 = 9.2 \times 10^6$. It can be also calculated by using a factor obtained from the graph for Cf-252, at a desired distance from the source, in Figure 3 in Appendix B. For example at 1 cm, the factor is 1.1×10^{-2} n/cm^2.s per neutron emitted from the source. Thus the maximum neutron flux is about $9.2 \times 10^8 \times 1.1 \times 10^{-2} \approx 1 \times 10^7$ n/cm^2.s which is about the same as obtained from the graph and about 8 times of the neutron flux from the neutron beam for neutron radiography at the Thai Research Reactor in 4.1 (Formation of proton tracks using thermal neutrons from the Thai Research Reactor). Practically, if the irradiation position is moved further from the source, larger piece of PC can be placed around the source for neutron irradiation but the neutron flux will be decreased. For example, at 10 cm from the source neutron flux will be about $4 \times 10^{-3} \times 9.2 \times 10^8 = 3.68 \times 10^6$ n/cm^2.s which is about 3 times of the neutron flux from the neutron radiography beam port at the Thai Research Reactor. For neutron moderator apart from water (such as transformer oil, low density polyethylene or high density polyethylene), neutron flux can be further increased by a factor of 1.1 to 1.8 [32] as shown in Figure 4, Appendix A.

The irradiation time with 400 μg Cf-252 source will be greatly reduced. For example, irradiation time of 3 days is needed for the source used in this research. The irradiation time with a 400 μg Cf-252 source will be $(5 \times 10^4 \times 3)/3.68 \times 10^6 = 58.6$ minutes which is about 1 hour.

Figures 4.26 and 4.27 illustrate the design of neutron irradiation. Design of neutron irradiation by using Cf-252 source in water, Cf-252 source is placed in the middle of water tank. In this design, four pieces of PC sheets can be placed around the source with the distance 10 cm from the source. The other is design of neutron irradiation by using Cf-252 source in a polyethylene cube in order to increase the neutron flux. The picture shows four pieces of PC sheet are put on the windows, the other two pieces of PC sheets was put on the anterior and posterior windows.
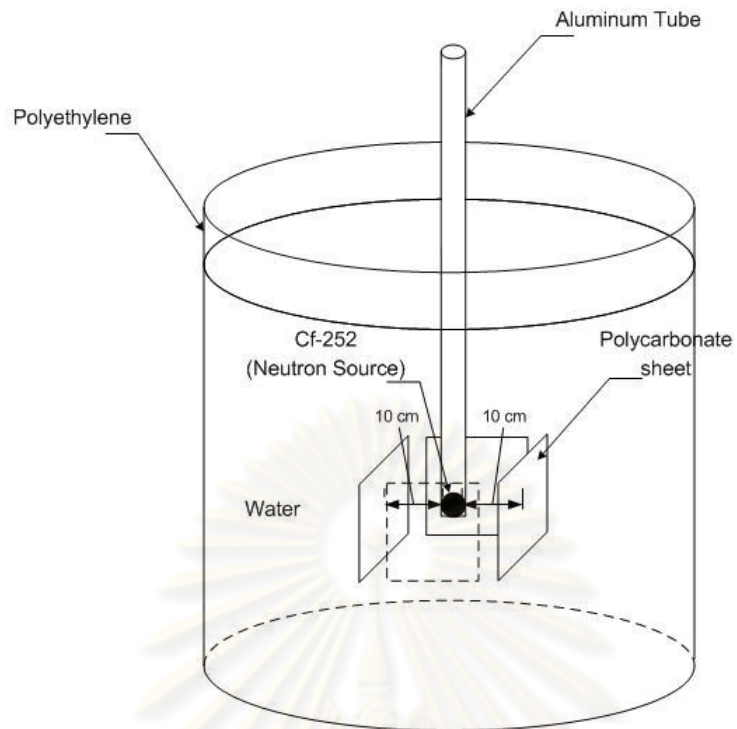
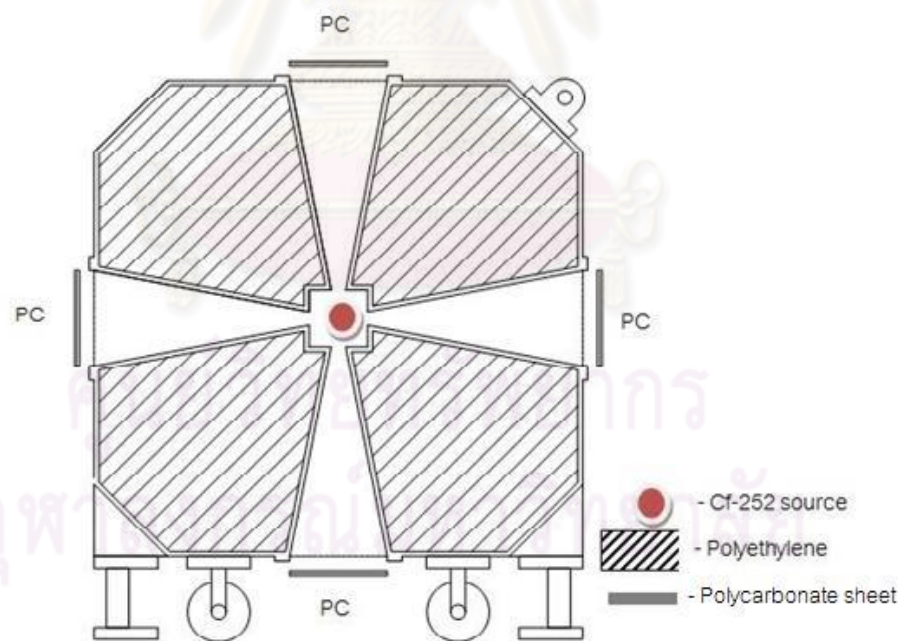Figure 4.25 Design of neutron irradiation by using Cf-252 source in water.

Figure 4.26 Design of neutron irradiation by using Cf-252 source in polyethylene tank.

CHAPTER V

CONCLUSION AND DISCUSSION

5.1 Conclusion and discussion

The applications of nuclear tracks have been developed and applied in a wide variety of technical fields. Recently, one of the most attractive aspects of nuclear track-etch is the investigation of optical properties of nuclear tracks. Many researchers are interested in the investigation of optical properties of nuclear tracks in order to describe the process of track appearance in solid state detectors. The main objective of this dissertation is to create proton tracks in thin sheet of polymer to be used as a light filter or light diffuser. This is based on light scatterings by nuclear tracks which depend mainly upon track density and track size. The track density is directly proportional to the number of neutrons impinging upon the plastic sheet while the track size depends upon the type and energy of charged particles as well as the etching condition.

These studies presented simplified and economical development of light filter film from track-etch polymer. A locally available polycarbonate plastic for sunshade, 1.5 mm thick, was used as a commercial PC because it was inexpensive and available. It is a versatile and tough plastic used for a variety of applications. It is commonly used to make sun shelter and awning. The main advantage of polycarbonate over other types of plastic is the unbeatable strength combined with light weight.

The study could be concluded as follows:

5.1.1 Formation of proton tracks using thermal neutrons from the Thai Research Reactor

The study showed that variation of etching temperature affected track density and distribution of track diameter. Track density at lower temperature of etchant was larger than that at higher temperature of etchant due to lower etching rate corresponding to Figure 2.9, which mentioned that etching rates are typically exponential functions of inverse temperature and increase with concentration [3]. Higher etching rate causes removal of some of tracks on the surface of PC. Track diameters at lower temperature were distributed within small size. When the temperature increased, the distribution of track diameter was shifted to large size due to

etching condition reaching to transitional phase and spherical phase. This was demonstrated in Figures 2.7 and 2.10 in Chapter II. Variation of track density and distribution of track diameter led to variation of transmission of visible light and infrared. The mean and standard deviation of distributions (SD) of track diameters at 65, 70, 75 and 80°C were within 6.47 ± 2.78, 9.27 ± 4.16, 7.58 ± 3.75 and 8.65 ± 3.40 μm, respectively. The most variation of the distribution of track diameter was track-etched PC at 70°C. The minimum diameter was 2.31 μm and the maximum diameter was 24.82 μm.

In case of transmission of UV, PC can totally absorb by itself due to its inherent property. In this study, the maximum effect on the transmission of visible light and infrared were seen in track-etched PC at temperature 65°C. The calculated percentage differences of maximum effect of transmission of visible light and IR through proton track-etched PC chips decreased about 24% and 17% compare to without PC and about 11% and 9% compare to through original control PC, respectively. It can be concluded that temperature of etchant affected track density and distribution of track diameter leading to variation in transmission of visible light and IR.

5.1.2 Formation of proton tracks using neutrons from a Cf-252 source
5.1.2.1 Effects of etching temperature and etching time

The study on variation of etching temperature and etching time with fixed irradiation condition was performed to observe the correlation of etching condition, track density and distribution of track diameter including percentage transmission of light. The results showed that track density at 65°C continuously increased and became constant at etching time of 75 minute, whereas track density at 70°C and 75°C increased to maximum values at etching time of 45 minute and 60 minute, respectively. Then, track density decreased and increased again because some of the tracks were removed, allowing new tracks to be observed. Neutrons from Cf-252 source induced random formation of proton tracks. The productive reactions of recoil-proton can occur anywhere inside the polymer volume along the neutrons trajectories depending upon neutron energy, so new tracks are probably created due to the increasing in etching condition [13].

The study of distribution of track diameter showed that track diameter at 65°C for 15 minutes distributed within small diameter. Mean and SD of track diameter were 5.01 ± 1.49 μm. The minimum and maximum diameters were 2.19 and 10.32 μm, respectively. When etching time increased, some of track diameters distributed to larger size, leading to increased mean and SD of track diameter. The maximum mean and SD of track diameter was found at etching time 90 minute with the value 7.57 ± 3.39 μm. The mean and SD of track diameter at 45, 60 and 75 minutes were not different significantly.

The mean and SD of track diameter at 70°C, etching time of 15 minutes were 6.02 ± 2.39 micrometer. When the etching time increased, the mean of track diameter did not change significantly. But the SD of track diameter was slightly different.

The maximum variation of the mean and SD of track diameter was found in PC with etchant temperature of 75°C and at etching time of 75 minutes. The mean and SD were 9.12 ± 5.11 μm. Figure 4.18 showed that track diameter in each etching time distributed randomly.

Results of transmission of UV, visible light and IR showed that UV was totally absorbed by PC. The calculated percentage difference of maximum effect of transmission of visible light an IR through track-etched PC decreased about 20% and 12% compared to without PC and about 6% and 4% compared to through original PC, respectively. The study found that transmissions of visible light and IR through track-etched PC with etching time longer than 30 minutes at every temperature were not different significantly, leading to no difference in transmission of visible light and IR.

It can be concluded that transmission of visible and IR through track-etched PC with a few track density and small track diameter distribution were not affected, because there was more area with no proton track on PC with a few track density and small track diameter distribution, leading to transmission of visible light and IR can transmit through PC. When the etching time increased, track diameter was distributed within larger size reducing area with no proton track. It also increased the effect of transmission of visible light and IR.

5.1.2.2 Variation condition of tracked-etch PC

Track-etched PCs with different track density and distribution of track diameter were observed for the effect of transmission of light to evaluate the proper condition to create a filter or diffuser film. Neutron irradiation time was varied to form various track density and etching condition was also varied to create the different distribution of track diameter. The results showed that PC with condition 6 (Track density 1.11×10^6 tracks/cm^2, neutron irradiation time 7 days, etched with PEW 70°C, 60 min.) demonstrated the maximum effect of transmission of visible light and IR, and PC with condition 4 (Track density 5.39×10^5 tracks/cm^2, neutron irradiation time 7 days, etched with PEW 70°C, 45 min.) showed the minimum effect. The calculated percentage difference of maximum effect of transmission of visible light and IR through track-etched PC decreased about 28% and 20% when compare to without PC and about 15% and 12% compare to through original PC, respectively. The calculated percentage difference of minimum effect of transmission of visible light and IR through track-etched PC decreased about 19% and 10% when compare to without PC and about 5% and 1% compare to through original PC, respectively.

The results showed that for the same track density such as PC with conditions 2 (Track density 3.74×10^5 tracks/cm^2, neutron irradiation time 3 days, etched with PEW 70°C, 15 min.) and condition 3 (Track density 3.85×10^5 tracks/cm^2, neutron irradiation time 3 days, etched with PEW 65°C, 30 min.) or PC with conditions 4 and 5 (Track density 5.83×10^5 tracks/cm^2, neutron irradiation time 3 days, etched with PEW 70°C, 35 min.), transmission of visible light and IR through PC with higher SD decreased more than that with lower SD. It was demonstrated that at the same track density, PC with wide distribution of track diameter affected transmission of visible light and IR more than narrow distribution of track diameter. For the same distribution of track diameter or same the SD such as PC with conditions 2 and 5 or PC with conditions 4 and 6, transmission of visible light and IR through PC with higher track density decreased more than that lower with track density. It can be concluded that variation of track density and distribution of track diameter affected transmission of visible light and IR.

For the experiment of transmission of laser beam from a laser pointer, the results showed that track-etched PC can diffuse laser pointer beam 1-3 times. PC with conditions 5 and 6 showed the maximum diffusion of laser pointer beam. The minimum diffusion effect was PC with condition 4. The result of transmission of IR was similar. It can be explained by optical model that when light passes through proton track on PC, light will be scattered. Different track sizes and shapes caused different scattering patterns. Groetz et al. [13] performed the scatter pattern in geometries of conical track and oblique track [Figure 2.20-2.21]. The result corresponded with the study of Al-Saad et al., [13] which demonstrated the effect of transmission of He-Ne laser light through proton track-etched PC with varying etching time. The relation was illustrated in Figure 2.23 in Chapter II.

From the above data, it can be concluded that PC with proton track cannot properly be used as a filter because of less effect on transmission of visible light and IR but it can be used as a light diffuser. Recently, PC plastic is widely used as sunshade, skylight and coverway. Track-etched PC can be used instead of normal PC or combined with a lamp in order to diffuse light. IR diffusion decreases or distributes heat.

5.2 Limitation

Limitations of this study are as follows:

5.2.1 Manual evaluation of track properties such as track size, track shape and track density is tedious and may cause human errors. An appropriate track evaluation software is required to obtain a better result and to save time.

5.2.3 This study could not define relation of track shape, track length and transmission of light due to limitation of analysis method and facilities.

5.3 Suggestion

Suggestions are as follows:

5.3.1 More accurate equipment and method for analysis of the track properties should be employed. It will perform appropriate analysis of track characteristics including track length and shape which affect the properties of light transmission.

5.3.2 Use stronger activity of neutron source for irradiation, as the irradiation time will be reduced.

5.3.3 In case of using stirring technique for etching or adding the sensitizer, it will decrease the etching time. The effect of sensitizers on the etching should be studied in laboratory in the future. These factors might play an important role in the quality of proton tracks.

5.3.4 In this study, physical properties in terms of tensile strength and impact strength were evaluated but there was no change between original and track-etched PC. However, other physical properties such as bending strength, impact strength, etc. should also be tested.

5.3.5 It is interesting also to study track etching at low temperature due to high track to bulk etching rate (V_T/V_B). This will take much longer time but it can be performed without a heat source, with no energy consumption. In doing so, track length will be increased and may affect light transmission or diffusion in some extend.

REFERENCES

[1]   Nikezic, D. and Yu, K. N.. Formation and growth of tracks in nuclear track materials. <u>Materials Science and Engineering R 46</u>, 2004: 51–123.

[2]   Hepburn, C. and Windle, A. H.. Review Solid state nuclear track detectors. <u>Journal of Materials Science</u> 15 ,1980: 279-301.

[3]   Fleisher, R. L., Price, P. B. and Walker, R. M.. <u>Nuclear Tracks in Solids Principles & Applications</u>. The regents of the University of California, 1975: 3-118,545.

[4]   Price, P. B.. Recent Applications of Nuclear Tracks in Solids in Opening talk At the 23rd <u>International Conference on Nuclear Tracks in Solids (ICNTS)</u> held in Beijing, 2006: 1-25.

[5]   Nikezic, D. and Yu, K. N.. Analyses of light scattered from etched alpha-particle tracks in PADC. <u>Radiation Measurement</u>, Vol. 43, 2008: 1417-1422.

[6]   Knoll, G. F. Track-etch detectors. <u>Radiation detection and measurement.</u> 3rd edition, New York ,John Wiley & Sons, Inc., 1999: 20, 736-740.

[7]   Nazkhattak, F. Principle of track formation/ revelation in SSNTDs in PhD Thesis: <u>Study of the heavy ion interactions of [14.0MeV/U] ^{208}Pb with ^{208} Pb and ^{197}Au using Mica and CN-85 as solid state nuclear track detectors</u>. 2003: 35-42.

[8]   <u>Nuclear tracked Detectors (NTDs).</u> [Online]. Available from: www.tdx.cesca.es.pdf, [2009, March]

[9]   Jevremovic, T. Interactions of radiation with matter. <u>Nuclear Principles in Engineering.</u> Springer Science and Business Media, Inc, 2005: 173-196.

[10]   Ervin, B. P. Interactions of Charged Particles with Matter. <u>Radiation Physics for Medical physicists.</u> 2nd edition, Springer-Verlag Berlin Heidelberg, 2010: 240.

[11]   Kalsi, P. C., Ramaswami, A. and Manchanda, V. K. <u>Solid State Nuclear Track Detectors and their applications.</u> 2005.

[12]   Lamarsh J. R. and Anthony J. Baratta. <u>Introduction to Nuclear Engineering.</u> 3rd Prentice Hall, Inc., 2001: 52-116.

[13] Rinard, P. Neutron Interactions with Matter. [Online]. Available from: http://www.fas.org/sgp/othergov/doe/lanl/lib-www/la-pubs/00326407.pdf, [2011, March]

[14] Alexander, D. R. Light Measurement Handbook. [Online]. Available from: www.intl-light.com/handbook/, [2011, March]

[15] Mostofizadeh, A., Sun, X. and Kardan, M. R. Application of Optical Methods in Nuclear Track Measurements. Journal of Applied Sciences 7(16), 2007: 2261-2271.

[16] Chankow, N. A study of Uranium exploration by track etch technique. 1975.

[17] Stephens, R. B. Low reflectivity surfaces are formed by particle track etching. United States Patent 4268347, [Online]. Available from: http://www.freepatentsonline.com/4268347.html, [2011, March]

[18] Khan, H. A. and Khan, N. A. Solid State Nuclear Track detection (SSNTD) A useful scientific tool for basic and applied research, 1989.

[19] Michael, A. G. A review- Submicron structures - promising filters in EUV. SPIE Vol. 1549 EUV, X-Ray, and Gamma-Ray Instrumentation for Astronomy II ,1991: 385-394.

[20] Popov, P. C. and Pressyanov, D. S. Track Density Assessment by Obstructed Total Internal Reflection of A Laser Beam. Radiation Measurement, Vol. 27, No. 1, 1997: 27-30.

[21] Chankow, N., Bunchorndhevakul, S. and Ratanatongchai, W. Development of A Technique for Viewing Track-Etch Neutron Radiographs. 2001: 82-92.

[22] Mitrofanov, A. V., Apel P. Y. Ion track filters in imaging X-ray astronomy. Nuclear Instruments and Methods in Physics Research B 245, 2006: 332–336.

[23] Mitrofanov, A. V., Apel, P. Y. and Orelovitch, O. L. Diffraction Filters Based on Polyimide and Poly (Ethylene Naphthalate) Track Membranes. Technical Physics, Vol. 51, No. 9, 2006: 1229–1234.

[24] Nikezic, D. and Yu, K. N. Computer program TRACK_VISION for simulating optical appearance of etched tracks in CR-39 nuclear track detectors. Computer physics Communications 178, 2008: 591-595.

[25]   Polycarbomate. [Online]. Available from:

http://en.wikipedia.org/wiki/Polycarbonate, [2011, March]

[26]   Jaiyen, S. Development of a Prototype for Low Flux Thermal Neutron Radiography system using Californium-252.   Master Degree Thesis, Department of Nuclear Technology, Faculty of Engineering, Chulalongkorn University, 2002: 50-52, 107.

[27]   Pugliesi, F., Sciani, V., Stanojev, P. and Pugliesi, R. Digital System to Characterize Solid state Nuclear Track Detectors. Brazilian Journal of Physics, Vol.37, no.2A, June, 2007: 446-449.

[28]   Souto, E.B. and Campos, L.L. Fast neutron dose response of a commercial polycarbonate. Nuclear Instruments and Methods in Physics Research A 580, 2007: 335-337.

[29]   Mostofizadeh, A., Sun, X. and Kardan, M. R. Improvement of Nuclear Track Density Measurements Using Image Processing Techniques.   American Journal of Applied Sciences 5 (2), 2008:71-76.

[30]   Fungklin, R. Application of Neutron Radiography using Neutron imaging plate for Inspection of Ancient Objects. Master Degree Thesis, Department of Nuclear Technology, Faculty of Engineering, Chulalongkorn University, 2010.

[31]   Dajko, G. The effect of etching solution composition on the response of an electrochemically etched CR-39Detector. Radiation Measurement, Vol 28, Nos 1-6, 1997:133-136.

[32]   International Atomic Energy Agency. Atomic Energy Review. Vol. 15(2), 1977:123-368.

Appendices

Appendix A: Cf-252 Neutron source

Figure 1 Specification of Californium source

Sources

Californium-252

Spontaneous Fission Neutron Sources

Nuclear Data

Californium-252 decays by α-emission and spontaneous fission emitting neutrons.

Half-life (α-decay):	2.73 years
Half-life (spontaneous fission):	85.5 years
Half-life (effective):	2.65 years
Neutron emission:	2.3×10^9 n/sec per mg
Average neutron energy:	~2MeV
Equilibrium γ-exposure rate (from unshielded source):	1.6×10^2 mR/h at 1m per mg ~Air kerma rate at 1m of 1.4mGy/h per mg
Neutron dose rate:	~2.3rem/h at 1m per mg ~23mSv/h at 1m per mg
Specific activity:	~20GBq/mg, ~536mCi/mg

Composition
Californium-252 is incorporated in ceramic material.

Encapsulation
The radioactive material is doubly-encapsulated in welded stainless steel capsules.

Nominal ^{252}Cf content	Nominal ^{252}Cf content activity*	Nominal activity*	Emission n/sec*	Capsule	Code
0.01µg	0.2MBq	5µCi	0.023×10^6	X.1	CVN.101
0.1µg	2MBq	54µCi	0.23×10^6	X.1	CVN.1
0.5µg	10MBq	268µCi	1.15×10^6	X.1	CVN.2
1.0µg	20MBq	536µCi	2.3×10^6	X.1	CVN.3
2.0µg	40MBq	1.07mCi	4.6×10^6	X.1	CVN.4
5µg	100MBq	2.7mCi	1.15×10^7	X.1	CVN.5
10µg	200MBq	5.4mCi	2.3×10^7	X.1	CVN.6
20µg	400MBq	10.7mCi	4.6×10^7	X.1	CVN.7
50µg	1GBq	27mCi	1.15×10^8	X.1	CVN.10
100µg	2GBq	54mCi	2.3×10^8	X.1	CVN.11
200µg	4GBq	107mCi	4.6×10^8	X.1	CVN.12

*Tolerance -10, +20%

Recommended working life: 15 years

Quality Control
Wipe test A
Bubble test D
Immersion test L

Neutron emission measured against standard using BF₃/wax moderator system.

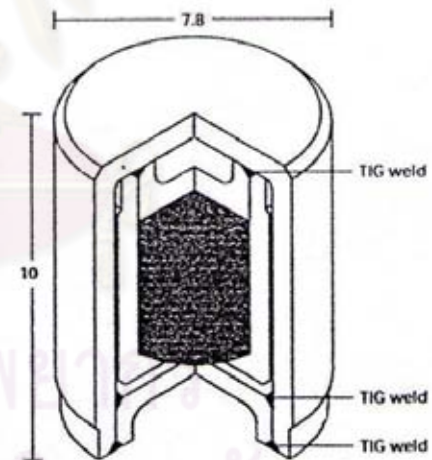The test report includes a statement of the neutron emission.

Neutron spectrum
Americium 241/beryllium source made and measured at AEA Technology using a stilbene crystal and pulse shape discrimination.

Spectrum reproduced by courtesy of: LORCH, E.A. Int. J. Appl. Radiat. Isotopes, 24, 588-9, 1973.
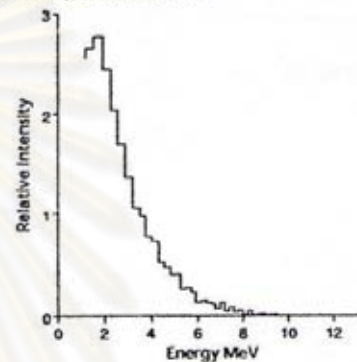
Safety performance testing

ANSI/ISO classification	IAEA special form	Model no.
C66545	GB/007/S-85	CVN CY2

B15

AEA TECHNOLOGY

Figure 2 Thermal neutron flux distributions (experimental) produced by various accelerator neutron source in a water moderator [32].
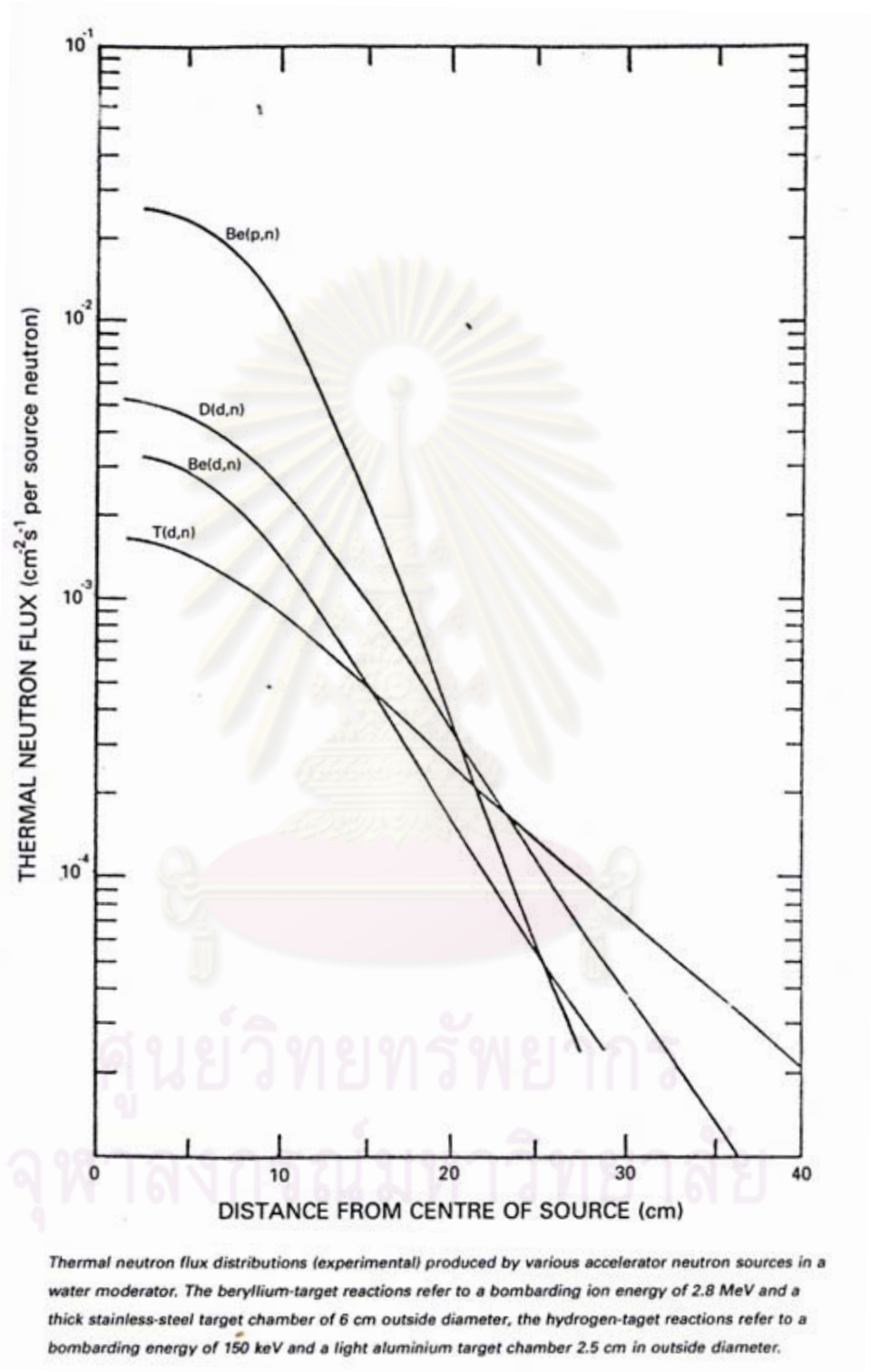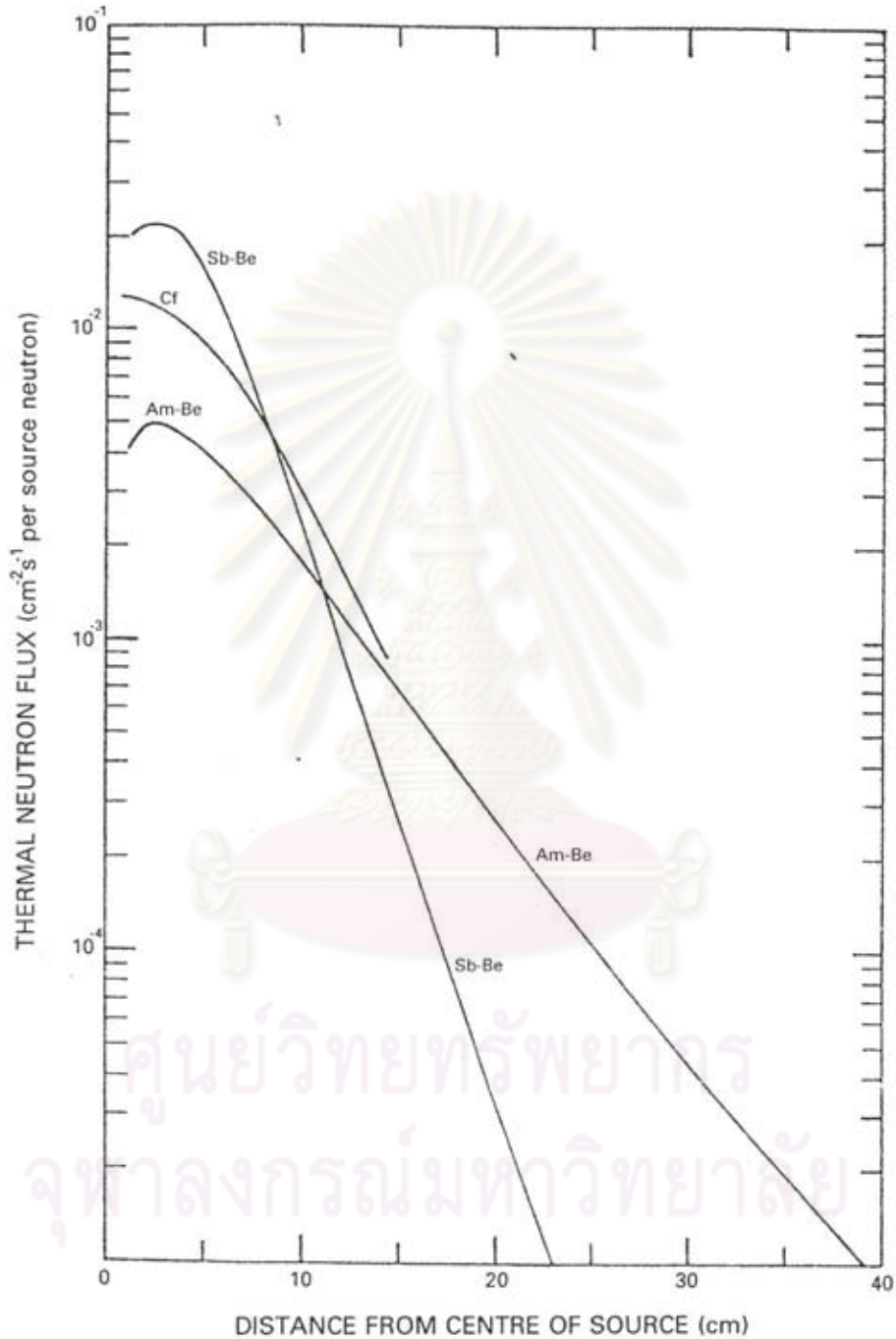

Thermal neutron flux distributions (experimental) produced by various accelerator neutron sources in a water moderator. The beryllium-target reactions refer to a bombarding ion energy of 2.8 MeV and a thick stainless-steel target chamber of 6 cm outside diameter, the hydrogen-taget reactions refer to a bombarding energy of 150 keV and a light aluminium target chamber 2.5 cm in outside diameter.

Figure 3 Thermal neutron flux distributions (experimental) produced by various
radioisotope neutron source in a water moderator [32].

Thermal neutron flux distributions (experimental) produced by various radioisotope neutron sources in a water moderator. The source strengths used were 0.05 Ci (Sb-Be), 10mCi (^{252}Cf), and 1 Ci (Am-Be), the larger source required for neutron radiography will depress the normalized centre flux conciderably in the case of Sb-Be and Am-Be but not in the case of ^{252}Cf.

Figure 4 Peak thermal neutron flux produced and various density of hydrogen
atom
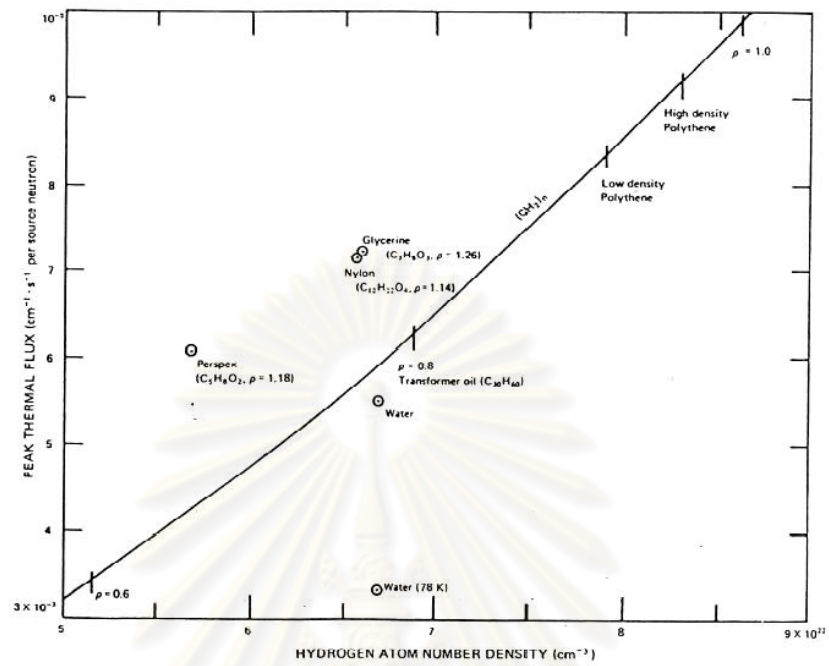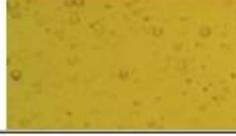
Appendix B: Previous study

Proton track using thermal neutron from Thai research reactor on polycarbonate plastic at different etchant condition

This previous experiment, polycarbonate was irradiated with thermal neutron from Thai research reactor for 60 and 100 min. The etchant conditions were NaOH 6.25N at 70°C and 90°C and PEW at 70°C.

Condition	Irradiated 1 h	Irradiated 2 h
NaOH, 90°C, 40 m		
NaOH, 70°C, 100 m		
PEW, 70°C, 30 m		
PEW, 70°C, 60 m		

The results showed that proton track at PEW solution at 70°C can observed better than both of NaOH conditions.

Appendix C: **Motic MC1000**

1. Before using Motic MC1000, select MC1000Camera.exe from the Settings options.

2. Upon starting MC1000, the Exposure and White Balance operations will be carried out automatically to make the quality and color of images in the Preview window similar to those of actual images. The interface will then

appear as it does on the left 3. Through the Control panel easily alter the quality and effects of the image shown in the Preview window.
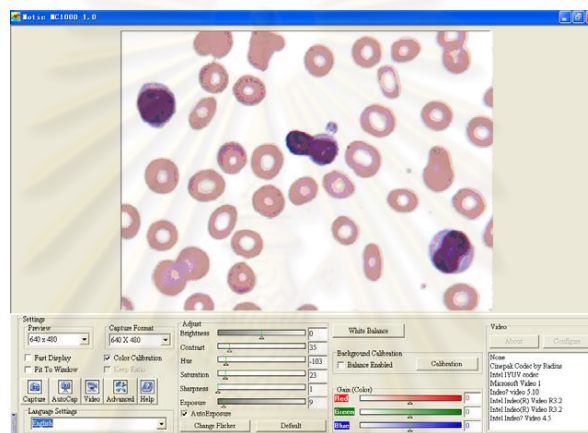
3. Through the Control panel easily alter the quality and effects of the image shown in the Preview window.

4. From the Toolbar, click the Capture button to capture the real-time image shown in the Preview window.
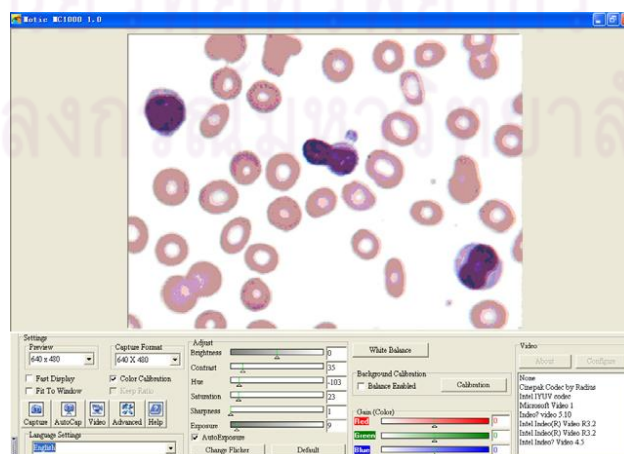
The image captured will be saved in the current user.s Temp folder.

5. Click the Auto Capture button (next to the Capture button) to automatically capture a number of images.

6. Motic MC1000 enables you to record video. From the Toolbar, click the Video button, fill in the name and path and click .OK. to save the video.
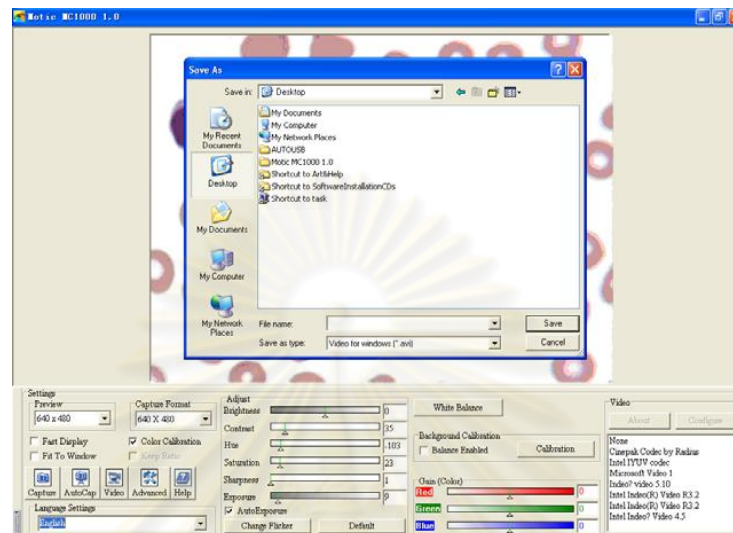
Video will then start recording; click the STOP button to stop recording.
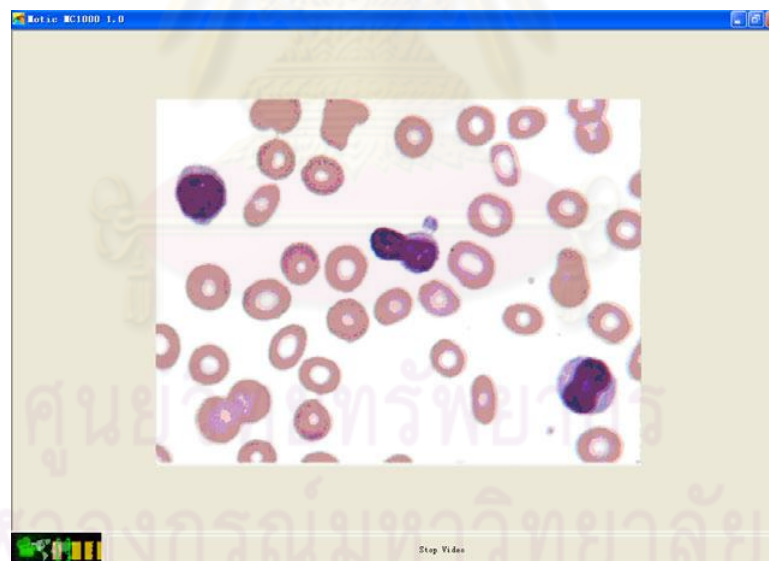
7. Motic MC1000 enables you to adjust Brightness, Contrast and Saturation. If you alter the brightness or switch specimens during observation, use Auto Exposure and White Balance to adjust the image.
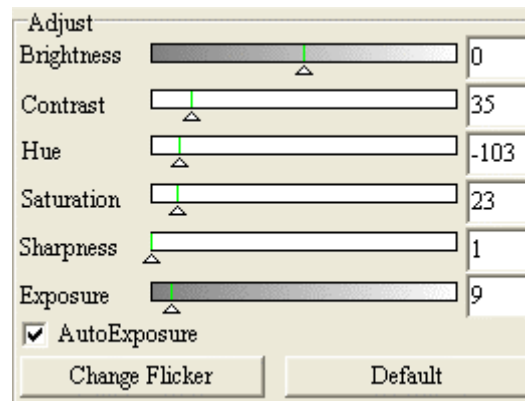
8. The Gain (Color) function may also be adjusted. Move the corresponding scroll bar of the color you wish to adjust and the image will change accordingly.

Appendix D: A Quick Guide to ImageJ

Introduction

ImageJ is a public domain Java image processing software that was developed by Wayne Rasband and others at the National Institutes of Health. Refer to the ImageJ homepage http://rsb.info.nih.gov/ij/ for further information. ImageJ runs with a Java 1.1 (or later) virtual machine and is available for Windows, Mac OS, Mac OS X and Linux.

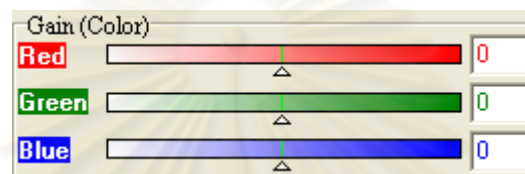ImageJ is designed under aspects of open architecture. It can be extended by user-written Java plugins for special acquisition, analysis and processing tools.

This feature has been used for specific extensions in the practical trainings of the Image Processing master course at the FH-Aachen/Jülich. Therefore, in the context of our Image Processing course we strongly recommend to use our (!) ImageJ Installation Version that includes all the special plugins.

ImageJ can display, edit, analyze, process, save and print images of various formats including TIFF, GIF, JPEG, BMP, DICOM. It supports standard image processing functions such as contrast manipulation, filtering (i.e. sharpening, smoothing), edge detection and others. It can calculate area and pixel value statistics of a user-defined region of interest (ROI). Measurements of distances and angles are ossible. It can create density histograms and line profile plots. It does geometric transformations such as scaling, rotation, flips and zooming. Spatial calibration (in units such as millimeters) as well as density or grey scale calibration is available. The program supports any number of images (display in separate windows) simultaneously.

Starting ImageJ on the PC's of the Medical Informatics Lab.

After starting the computer and booting Windows (please cancel the network login-dialog) you can start ImageJ by double-clicking the ImageJ Symbol on the desktop. The program will start with the ImageJ main window (Fig.1):
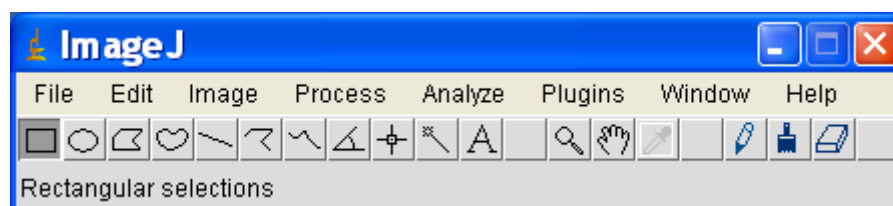

Fig.1: ImageJ main-window

Basic features of ImageJ

Fig.2 shows a typical ImageJ desktop with the ImageJ main-window (top left) together with different image- and result-windows simultaneously opened.
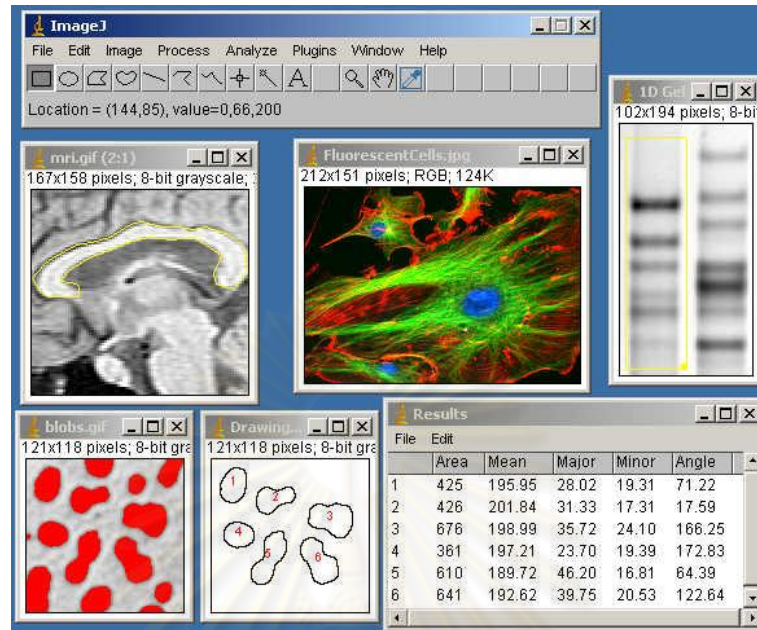
Fig.2: ImageJ desktop example with ImageJ main-window (top left)

The ImageJ main-window - a window that can not be resized or maximized - contains (compare Fig.1):

• menu bar   (at the top) "File", "Edit", "Image", …

• tool bar   (in the middle row)

• status and progress bar   (at the bottom)

Opened images, histograms, measurement results etc. are displayed in additional windows. These windows can be positioned and resized on the screen as usual. They can be copied (to the Windows-Clipboard), edited, printed and saved. In the following some basic operation topics are described which are relevant for all practical studies of the Image Processing course. The more specific tools are explained in the individual practical training manuals. Further information is given in the ImageJ documentation (http://rsb.info.nih.gov/ij/docs/index.html).

Menu Bar: File

File / New: (not used in the course)

Creates a new image window or stack. A dialog box allows you to specify the image title, type, dimensions and initial content.

File / Open:

Opens and displays an image in a separate window.

Remark: All image files for the practical training are stored on the Medical Imaging

master course CD.

File / Close:

Closes the currently active image window.

File / Save:

Saves the active image

Remark: Do NOT save an image to avoid data garbage on our hard disks unless

the practical training manual asks you to do so !!!

File / Print..:

Prints the active image.

Remark: In our Image Processing course we prepared for each topic a special

blank image that can be used as a "print-form". With copy and paste commands

(see below) you can arrange images and other results like histograms together with

text annotations on the print-form for final printout and documentation. Only these

print-forms should be used for printing !

Menu Bar: Edit

Edit / Undo (Strg+Z) :

Reverses the most recent image editing or filtering operation. Only one "undo" step

is possible.

Edit / Copy (Strg+C) :

Copies the contents of the selected region of interest (ROI) of an image or any

other window to the clipboard. If there is no ROI-selection, the entire active

image/window is copied.

Edit / Paste (Strg+V) :

Inserts the contents of the clipboard into the active image. The pasted image is

automatically selected, allowing it to be dragged with the mouse.

Click outside the selection to terminate the paste. Select Edit/Undo to abort the

paste operation.

Remark: With copy and paste you can arrange selected image areas and other

results like histograms on the print-form.

<u>Setting of a ROI (region of interest)</u>

The selection of a well defined section of an image (region of interest, ROI) is a basic operation for image analysis and is very important in our Image Processing course. It can be done in the following ways:

Edit / Selection / Select All (or better: Strg+A):

Creates a rectangular ROI that has the same size as the image.

Edit / Selection / Select None (or better: Strg+Shift+A) :

Deactivates the selection in the active image.

Edit / Selection / Specify … :

This command allows you to position a ROI precisely. The ROI is defined by specifying (in terms of pixels) the size of the ROI box (width and height) and the position of the upper left corner of the ROI (x- and ycoordinates). The values can be selected in the "Specify-window" shown below:
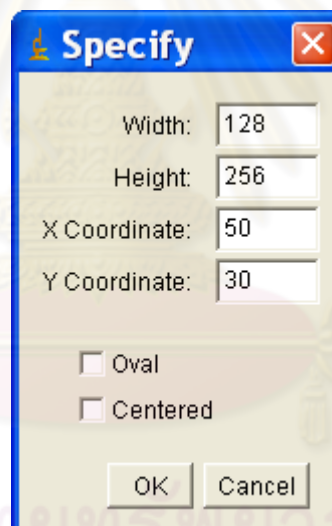
Manual ROI setting (with the button "rectangular selection" on the tool bar):

Manual ROI setting is performed with the „rectangular selection" tool button (left button in tool bar, see Fig. below).

color picker
scrolling tool
magnifying glass
text tool
wand (tracing tool)

freehand line selections
segmented line selections
straight line selections
freehand selections
polygon selections
oval selections
rectangular selections
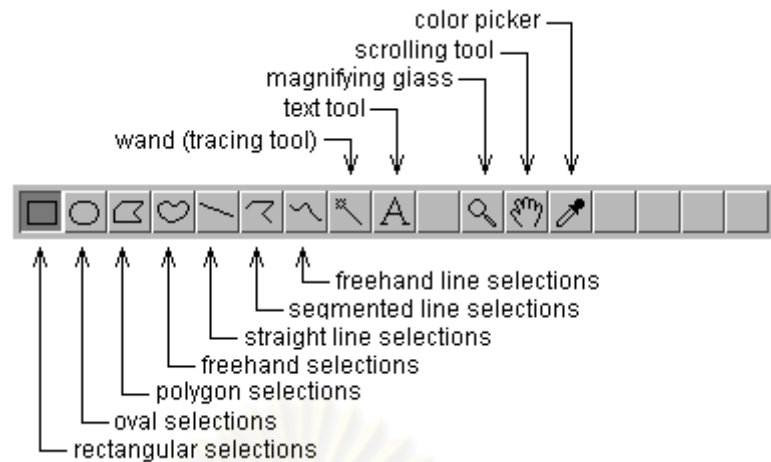
Creating the selection is done by a mouse-drag. After a ROI selection use the points in the corners to resize. With the shift key held down during the drag the ROI is fixed to a square. As a selection is created or resized, its location, width and height are displayed in the status bar.

Using the arrow keys you can move the ROI box. With the arrow keys and the alt key held down you can change the width or the height of the ROI.

**Text Annotations (with the button "text tool" (A) on the tool bar):**

Use the text tool to add text to images. Left mouse click on the text-tool-button and double-click on the image where the text should be positioned creates a rectangular selection containing one or more lines of text. Use the keyboard to write the text and the backspace key to delete characters. The final position of the text can be selected by a mouse drag. Use Edit/Draw (better: Strg+D) to permanently draw the text on the image. Use Edit/Options/Fonts, or double-click on the text tool, to specify the typeface, size and style.

Remark: All images, histograms, LUT-boxes and other results should be labeled by text annotations on the print-form. So, the final print-form contains a clear description of all displayed components and a short specification of the applied analysis or evaluation.

Grey Value Histogram

ImageJ calculates and displays a grey level histogram of the active image respectively an image part defined by the ROI. To display the histogram select Analyze / Histogram (or: Strg+H). In the histogram window the x-axis represents the gray values and the y-axis shows the number of pixels found for each gray value. The total pixel count is also calculated and displayed, as well as the mean, standard deviation

(StdDev) and the minimum / maximum gray value. The Log-button displays an overlay with a logarithmic scaled histogram. The List-button shows a table of the histogram values.
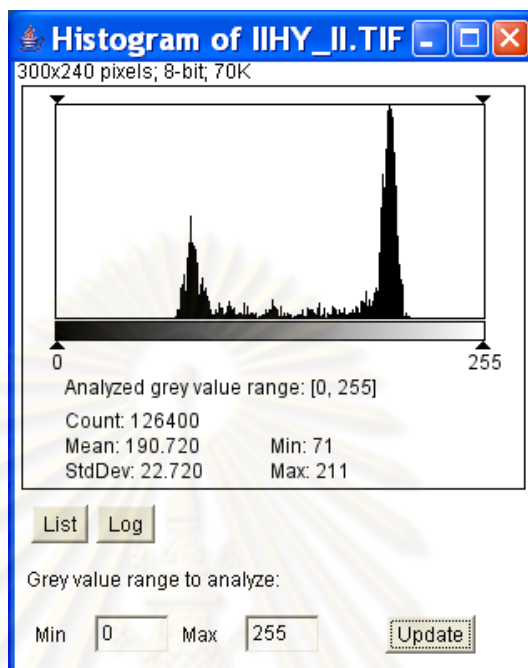
Remark: The histogram and the statistical data are not automatically updated when you alter the ROI. To update the histogram and the statistical calculations press the Update button.

You can define the range that is used to compute the statistical data in the Min and Max fields of "Grey value range to analyse:". After pressing the Update button the selected range is marked in the histogram plot and the statistical data are calculated according to the defined grey value interval between Min and Max.
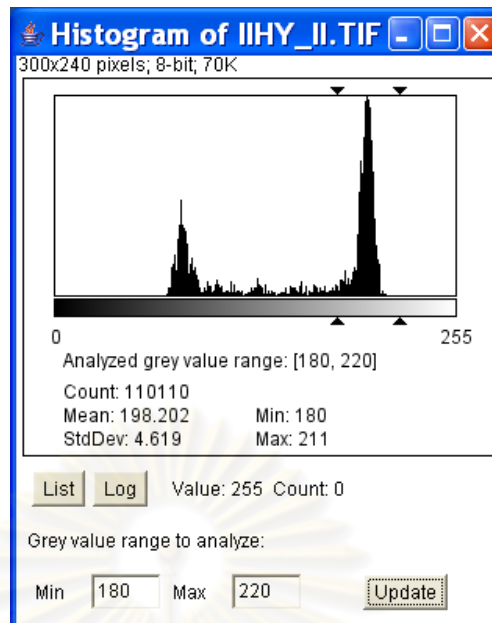
Grey Level Operation

With the tool "LUT Operations" (Image / LUT Operations, or: Strg+L) the brightness and contrast of the active image can be altered. Brightness and contrast are changed by updating the image's look-up table (LUT), so pixel values remain unchanged. Linear and non-linear LUT's can be selected with the LUT Operation window.

<u>Linear LUT's can be modified as follows:</u>

• a- and b-Paramerters can be selected according to the point transformation

 I'(x,y) = (I(x,y) + a) * b.

• The display range can be determined by a min- and max-value.

• A window-width (Window) and the center of the window (Level) is chosen. The individual parameters (a, b, min, max, Window, Level) are selected by six sliders. Each parameter selection may affect the values of other parameters which are modified automatically. The parameter values of a, b, min, max, Window, Level and the resulting LUT are displayed below the histogram. The LUT shows how pixel values are mapped to 8-bit (0- 255) display values. The two numbers at the LUT plot define the display range: Pixels with a value less than the lower number are displayed as black and those with a value greater than the upper number are displayed as white.
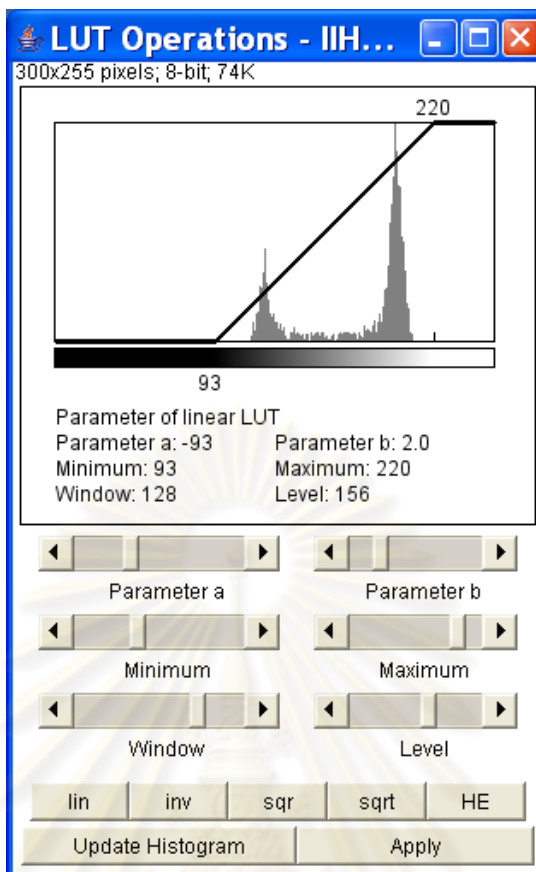
The LUT plot is superimposed on the image's histogram (respectively the histogram of the ROI if a ROI is selected). After modifying the ROI in the active image the displayed histogram in the LUT Operation window can be updated by the button Update Histogram.

Buttons of the LUT Operation window and non linear LUT selection:

lin   Allows the selection of a linear LUT by means of the six sliders as described above. Click on lin also resets the LUT (original brightness of pixel values is displayed).

Inv   LUT for grey level inversion.

sqr   Square LUT.

sqrt   Square root LUT.

HE   Histogram equalization: The histogram equalization is calculated on the basis of the display histogram (if a ROI is selected the ROI's histogram is used for histogram equalization)

Apply   Click on Apply to apply the current LUT mapping function to the pixel data. If there is a ROI selection, only image data within the selection are changed. After modifying the pixel values according to the given LUT a LUT reset takes place.

Thresholds

In the active image lower and upper threshold values can be selected interactively with the threshold tool Image / Adjust / Threshold. The threshold values segments the image into features of interest and background. Pixels with grey values greater than or equal to the lower threshold and less than or equal to the upper threshold are displayed in red.
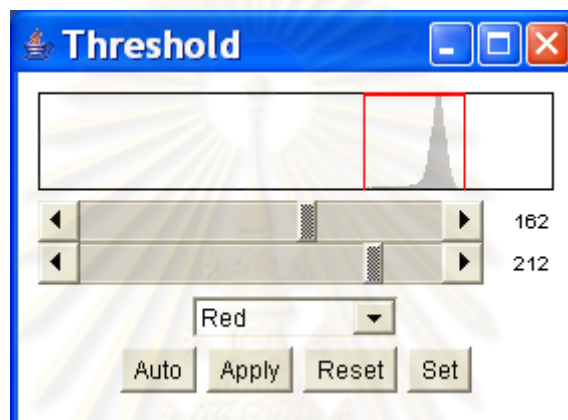
• The Auto button automatically sets the threshold levels based on an analysis of the displayed histogram This is used for **bimodal histogram segmentation**. If a ROI is selected the displayed histogram corresponds to the actual ROI settings (press Reset to update the displayed histogram after changing the ROI).

• Apply sets the thresholded pixels to black (or a given foreground color) and all other pixels to white (or a given background color).

• Reset disables thresholding (removes the red overlay of the thresholded pixels) and updates the displayed histogram (important - especially after changing the ROI selection).

Appendix E: SD2400 Energy Transmission Meter User Manual

General Description

Expanding on our success with sales demonstration tools, our new "Spectrum Detective" product is able to simultaneously display UV, Visible and Infrared transmission values. Being a self-contained syste , there are no additional light sources or power chords necessary, and no adjustments to make. Simply slide the glass sample into the opening and watch the resulting performance data appear on the display. Perform LIVE demonstrations of the performance of your Energy Efficient window products. Simple, fast and convincing; this instrument will take sales demonstrations to a whole new level!

Features

- Three performance values displayed simultaneously

- Single, double or triple pane testing easily accomplished

- Test any sample width up to 2" thick

- Sash/spacer width up to 1.25"

- No additional light sources needed

- Auto-calibration at start-up: NO manual adjustments required

- Battery operated: no power chord required

- Automatic power-off feature for extended battery life

- Replace Battery Indicator

- Continuous measurements

- Professional Image

- Simple operation

- Convenient push-on/push-off power switch

- Small, portable convenient size

- Protective, custom carrying case

Basic Operation

Place the SD2400 on a flat, stationary surface. Turn the instrument on and wait for the system to self-calibrate. After each of the displays show 100%, you can place any sample into the opening to measure the performance characteristics. Here are a few helpful reminders for conducting transmission measurements. Always hold the glass perpendicular to the opening. Do not tilt the glass at angles. For the most accurate transmission measurements, the glass should be held perpendicular to the sensors (as shown in the picture above). It is also recommended that the samples being tested are positioned in the center of the opening. Be aware that fingerprints on the glass can slightly affect the transmission values.

When you slide the glass into position, move the glass all the way into the opening, resting against the stop location. Pay attention to the spacer/sash of your window. Make sure the glass is slid far enough into the opening so the spacer/sash is not blocking one of the sensors.

The instrument will continually monitor its calibration during measurements. If the instrument detects any problems with the calibration, it will reset itself in between measurements. If you mistakenly turn the instrument on with a piece of glass already in position, the displays will calibrate to read 100% with the glass in place. Simply remove the glass sample and wait a few moments. The instrument will re-calibrate itself shortly after the glass is removed. After the displays have returned to 100% after the removal of the glass, you may continue with your measurements.

Spectrum Specifications

The SD2400 displays energy transmission values in three spectrums. The light sources used for each spectrum have a peak response at the following wavelengths:

UV: 365nm

VISIBLE: Full Weighted Spectrum

INFRARED: 950nm

Battery Replacement

The SD2400 is powered by a 9 volt alkaline battery. When the battery voltage is getting too low to operate the meter, the low battery indicator will turn on. The detector can still be used at this point, however it is recommended that the battery be replaced soon. The lights in the meter will begin to grow dim and make it more difficult to conduct easy measurements. Alkaline batteries are recommended for this product.

Auto-Power-Off

The SD2400 instrument is equipped with an automatic power-off feature to extend the life of your battery. The instrument will automatically shut off after approximately 5 minutes.

Warranty

The manufacturer warrants all models of the SD2400 to be free from defects in material and workmanship under normal use and service as specified within the operator's manual. The manufacturer shall repair or replace the unit within twelve (12) months from the original date of shipment after the unit is returned to the manufacturer's factory, prepaid by the user, and the unit is disclosed to the manufacturer's satisfaction, to be thus defective. This warranty shall not apply to any unit that has been repaired or altered other than by the manufacturer. The aforementioned provisions do not extend the original warranty period of the unit which has been repaired or replaced by the manufacturer. Batteries are not covered by warranty. EDTM, Inc. assumes no liability for the consequential damages of any kind through the use or misuse of the SD2400 product by the purchaser or others. No other obligations or liabilities are expressed or implied. All damage or liability claims will be limited to an amount equal to the sale price of the SD2400, as established by EDTM, Inc.

Appendix F: Physical property test report

Tensile test report

SCIENTIFIC AND TECHNOLOGICAL RESEARCH EQUIPMENT CENTRE CHULALONGKORN UNIVERSITY Chulalongkorn Soi 62 Phaya-Thai Rd. Bangkok 10330 Thailand Tel 0-2218-8032 Fax. 0-2254-0211

ศูนย์เครื่องมือวิจัยวิทยาศาสตร์และเทคโนโลยี จุฬาลงกรณ์มหาวิทยาลัย อาคารสถาบัน 3 จุฬาลงกรณ์ซอย 62 พญาไท กรุงเทพฯ 10330 โทร. 0-2218-8032 โทรสาร 0-2254-0211
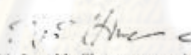
Test Report

Report no. 323/2011   Date of Issue : May 6, 2011   page 1/1

STREC sample code :   MTL/11/172 - 177
Sample type :   Polycarbonate Plastic
Description of specimen : suitable for testing
Sample owner   Miss Sawwance Asavaphatiboon
address :   Department of Nuclear Technology
                 Faculty of Engineering
                 Chulalongkorn University Bangkok Thailand

Objective :   To test mechanical properties
Test method :   ASTM D638 : 1998
Specimen preparation :   ASTM D638 : 1998
Instrument :   Universal testing machine; (Hounsfield H10KM)
Test date :   May 2, 2011
Analyst :   Mr. Somchit Chummuangyen

| Mechanical properties | | | |
Sample name	Ultimate strength (Kgf/mm^2)	Yield strength (Kgf/mm^2)	% Elongation	(Note)
1. No 1	5.43	5.34	112.00	
2. No 2	6.32	0.45	36.88	
3. No 3	6.35	6.35	13.79	
4. No 4	5.15	5.15	52.80	
5. No 5	6.41	6.41	19.12	
6. No 6	6.01	0.49	34.00	

(Mr.Somchit Chummuangyeu)   (Mr. Utai Tiyawisutsri)   (Assoc. Prof. Dr. Amorn Petsom)
Analyst   Technical manager   Acting Director

Remarks : 1. The results are valid exclusively for those samples analysed. 2. The report shall not be reproduced partly, except in full, without written approval of the organization.

ศูนย์วิทยทรัพยากร

จุฬาลงกรณ์มหาวิทยาลัย

Biography

Ms. Sawwanee Asavaphatibon was born on November 9, 1965 at Bangkok province, Thailand. She graduated Bachelor degree of Science in Radiological Technologist from Mahidol University in 1988 and Master degree of Science in Medical Physics from Department of Radiology, Faculty of Medicine, Mahidol University in 1998. She has studied the Doctoral degree of Nuclear Engineering at the Department of Nuclear Technology, Faculty of Engineering, Chulalongkorn University since 2006. At the present time, she works at Department of Radiology, Ramathibodi Hospital, Faculty of Medicine, Mahidol University.